

**Development of high performance vanadium redox flow batteries**

**高性能バナジウム系レドックスフロー電池の開発**

**Zhongxu Tai**

**Saitama Institute of Technology**

**February, 2022**

# Contents

Abstract .....	i
Chapter 1 Introduction .....	1
1.1 Energy storage development and application .....	2
1.2 Energy storage methods .....	3
1.2.1 Potential energy, kinetic energy storage .....	4
1.2.2 Electromagnetic energy storage .....	5
1.2.3 Electrochemical energy storage .....	6
1.3 Several common types of electrochemical energy storage .....	6
1.3.1 Lead acid battery energy storage .....	7
1.3.2 NiCd battery energy storage .....	8
1.3.3 Lithium Battery Energy Storage .....	10
1.3.4 Liquid Flow Battery Energy Storage .....	11
1.4 Development and application of liquid flow battery .....	12
1.4.1 Ferrocrome liquid flow battery .....	12
1.4.2 Zinc-bromine liquid flow battery .....	13
1.4.3 Titanium-manganese liquid flow battery .....	13
1.4.4 All-Vanadium Liquid Flow Battery .....	14
1.5 Development and application of all-vanadium liquid flow batteries .....	14
1.5.1 Development of All-Vanadium Liquid Flow Batteries .....	15
1.5.2 Working Principle of All-Vanadium Liquid Flow Battery .....	15
1.5.3 Composition of an all-vanadium liquid flow battery .....	16
1.5.4 Application of All-Vanadium Liquid Flow Batteries in Energy Storage .....	17
1.6 The purpose of this research .....	20
1.7 References .....	20
Chapter 2 Factors affecting the performance of all-vanadium liquid flow batteries .....	27
2.1 Stack component material properties .....	28
2.1.1 Effect of carbon felt electrodes on battery performance .....	28
2.1.2 Effect of electrolyte on battery performance .....	34
2.1.3 Effect of ion exchange membrane on battery performance .....	35
2.1.4 Effect of bipolar plates on battery performance .....	39
2.2 Impact of stack structure on battery performance .....	40
2.2.1 Effect of electrolyte flow path on battery performance .....	41
2.2.2 Effect of electrolyte flow rate and flow rate on battery performance .....	43
2.2.3 Effect of carbon felt compression ratio on battery performance .....	48
2.3 Impact of external factors on battery performance .....	49
2.3.1 Effect of temperature on battery performance .....	49
2.3.2 Impact of runtime on battery performance .....	51
2.3.3 Effect of overcharging on battery performance .....	52
2.4 Concluding remarks .....	55
2.5 References .....	56
Chapter 3 Research and development of high output vanadium redox flow battery .....	63

3.1 Carbon fiber electrode heat treatment .....	64
3.1.1 Introduction .....	64
3.1.2 Experimental methods .....	64
3.1.3 Experimental results .....	66
3.1.4 Conclusion .....	69
3.2 CNT surface modification of carbon felt.....	70
3.2.1 Introduction .....	70
3.2.2 Experimental methods .....	71
3.2.3 Experimental results .....	73
3.2.4 Conclusion .....	79
3.3 Concluding remarks .....	79
3.4 Nomenclature .....	79
3.5 References .....	80
Chapter 4 Optimal design of battery structure and battery pack test experiment .....	85
4.1 Optimum design of battery frame.....	86
4.1.1 Introduction .....	86
4.1.2 Experimental conditions .....	86
4.1.3 Experimental conditions .....	88
4.1.4 Conclusion .....	92
4.2 Adjustment of electrolyte flow and velocity .....	93
4.2.1 Introduction .....	93
4.2.2 Experimental method.....	93
4.2.3 Experimental results .....	95
4.2.4 Conclusion .....	103
4.3 Evaluation of performance of all-vanadium redox flow battery pack .....	104
4.3.1 Introduction .....	104
4.3.2 experimental method .....	104
4.3.3 Experimental results .....	105
4.3.4 Conclusion .....	108
4.4 Concluding remarks .....	108
4.5 Nomenclature .....	109
4.6 References .....	109
Chapter 5 Conclusions .....	113
Related publications.....	115
Acknowledgements.....	116

## Abstract

In recent years, with the increasing temperature of the earth, people have begun to pay attention to the protection of the environment. The greenhouse effect has brought great challenges to people's survival, so various countries have begun to introduce various policies to control carbon dioxide emissions. The [Paris Agreement] confirmed that carbon dioxide emissions in 2030 will be reduced by 40% compared to 2013. Energy conversion sectors such as power plants are the main sources of higher carbon dioxide emissions. At present, the world's energy structure is dominated by fossil energy, and fossil energy will generate a large amount of dioxide gas when it is converted. Therefore, the main way to solve environmental problems is to change the existing energy structure.

In consideration of practicality, safety, environmental impact and other factors, the development of new renewable clean energy. Renewable clean energy includes solar energy, wind energy, geothermal energy, tidal energy, etc. These energy sources do not produce carbon dioxide when generating electricity, and they are inexhaustible. It is currently the best choice to replace fossil energy. However, these energy sources also have many problems due to factors such as regions, seasons, and weather. For example, in photovoltaic power generation, there is a big difference in the amount of power generated in sunny and rainy days. Wind power generation fluctuates greatly in the windy season and the windless season. Geothermal and tidal power generation are affected by geographic location. In short, it is mainly unstable, fluctuating, and intermittent. So we need to find a way to solve these problems, and power storage is the best way. Through electricity storage, we merge the peak and trough periods of renewable energy power generation. In the case of a large amount of power generation, the battery is used to store electricity, and when the amount of power generation is small, the battery can be used to make up.

As an energy storage battery, vanadium flow battery has many advantages compared with other batteries. For example, it has a long service life, high safety, no waste, no pollution to the environment, etc. The vanadium flow battery has a history of more than 30 years of research and development since 1985, and its technology is very mature. Including Japan's Sumitomo

Electric and other companies, have developed a megawatt-level vanadium flow battery power storage system. However, due to its own characteristics, flow batteries have problems such as low energy density, miniaturization and low cost.

Our current research is mainly to improve the battery output density to achieve miniaturization and low cost. The research method is to modify the electrode of the battery and optimize the design of the battery structure to improve the charge and discharge efficiency of the battery, so that the current density can reach  $200\text{mA}/\text{cm}^2$  with an energy efficiency of 80%.

Electrode modification is mainly to improve the graphitization and specific surface area of the electrode through heat treatment and carbon nanotube coating. At the same time, Raman analysis and charge-discharge experiments are performed on the heat-treated electrode to evaluate its charge-discharge performance. The heat treatment experiment shows that as the heat treatment temperature increases, the graphitization degree of the electrode also increases, but when the temperature reaches  $3000\text{ }^\circ\text{C}$ , the graphitization degree of the electrode is the most complete. However, the charging and discharging performance of the battery has dropped sharply. This is because when the electrode is graphitized, the hydrophilicity of the electrode surface will decrease. Because it is a liquid battery, the electrode needs a certain degree of hydrophilicity, so the charge and discharge performance will decrease as the temperature rises. Carbon nanotube coating is mainly to increase the specific surface area of the electrode and increase the reaction surface of the electrolyte, thereby increasing the charge and discharge performance of the battery. SEM/EDS, Raman, XRD were used to observe and analyze the surface of the treated electrode. At the same time, the electrodes were evaluated by charging and discharging experiments and AC resistance measurement.

The optimal design of the battery structure mainly includes the design of the battery flow path and the optimization of the electrode compression ratio and the electrolysis flow rate. The flow paths of vanadium flow batteries mainly include parallel flow paths, serpentine flow paths and comb-shaped flow paths. The parallel flow path means that the electrolyte flows inside the electrode parallel to the length of the electrode. The serpentine flow path is mainly a flow path that is similar to a sine wave on the surface of the bipolar plate, and the electrolyte flows along the direction of the flow path. The comb-shaped flow path is also processed on the surface of the bipolar plate, similar to the flow path where the teeth of two combs are crossed. The

electrolyte flows in from the inlet, diffuses to both sides, and then flows out from the outlet. The flow direction of the comb-shaped flow path is the flow along the thickness of the electrode. Due to the charge and discharge characteristics of vanadium flow batteries, the vanadium ions involved in the reaction need to flow out of the battery in time, otherwise it will cause excessive local voltage, which will affect the charge and discharge performance of the battery. After the serpentine flow path is enlarged, its flow path becomes very long, which is not conducive to the charging and discharging of the battery, so few people use it. Through simulation experiments and charge-discharge experiments, we verified the uniform fluidity of the electrolytes of the four different flow path batteries, and the charge-discharge test also verified the performance of different flow paths.

The optimization of electrolyte flow rate and electrode compression ratio is mainly to compare the charging and discharging experiments under different electrolyte flow rates through different compression ratios, and to screen the most suitable compression ratio and the most suitable electrolyte flow rate. The compression ratio is mainly achieved by changing the thickness of the battery frame, and the electrolyte flow rate is achieved by changing the voltage of the circulating pump. Increasing the compression ratio can effectively reduce the contact resistance between the carbon dioxide electrode and the bipolar plate. Increasing the electrolyte flow rate can effectively increase the outflow rate of vanadium ions after the reaction. Through our experiments, it is confirmed that the compression ratio is too large, which will cause the ion exchange membrane to rupture and reduce the charge and discharge performance of the battery. After the electrolyte flow rate reaches a certain level, the impact on the battery's charge and discharge performance is gradually reduced.

According to the above research, we assembled a battery pack of 3 groups of single cells. Through charging and discharging experiments on the battery resistance, the highest current density can reach  $800 \text{ mA/cm}^2$ . And when the energy efficiency is 80%, the current density of the battery has also reached  $200 \text{ mA/cm}^2$ . Achieved the research goals we initially set. At the same time, we have continuously charged and discharged the battery pack. Through the comparison of charging and discharging data, we found that after the battery has been running for a period of time, the temperature of the electrolyte will increase, so that the viscosity will decrease, the reaction performance will increase, and the charging and discharging performance

of the battery will also increase. It is often necessary for the battery to maintain a certain operating temperature during operation.

**Keywords:** Secondary battery, Energy storage, Vanadium flow battery, Renewable energy, Accumulator.

## Chapter 1 Introduction

Energy storage or energy storage technology refers to the technology that stores energy and uses it when needed. Energy storage technology converts the energy form that is more difficult to store into a form that is technically easier and cheaper to store. For example, solar water heaters store light energy (radiation) in hot water (heat energy), and batteries store electrical energy in electrochemical energy.

Energy storage has existed since ancient times, but in different eras, according to human dependence on different energy sources, different contradictions endow energy storage with different content. In contemporary times, it is mainly heat storage, hydrogen storage and electricity storage. Since electric energy is currently the most convenient form of energy for production, transmission, distribution and utilization, it has been widely used in modern production and life. In the field of energy storage, electricity storage has become the core content.

Compared with other forms of energy, electric energy itself is not convenient for large-scale storage, so the basic idea of electricity storage is to convert electric energy into other forms of energy, and then convert it back through other forms of energy when needed. With the changes in the world's energy structure and the vigorous development of renewable energy, the electricity storage market will also become larger and larger.

Energy storage has many uses. For example, emergency energy can also be used to store energy when the grid load is low, and output energy when the grid load is high, for peak shaving and valley filling, to reduce grid fluctuations. There are many forms of stored energy, including mechanical energy, thermal energy, electrochemical energy, chemical and electronic. Energy storage involves converting energy in a form that is difficult to store into a more convenient or economically storable form. A large amount of energy storage is currently mainly composed of power generation dams, whether traditional or pumped. The length of time that each technology is suitable for storage varies.

## 1.1 Energy storage development and application

Energy storage technology can be seen everywhere in daily life. The electrochemical energy stored in the battery can be converted into electrical energy for use in electronic products[1]. The reservoir stores the gravitational potential energy of water, which is converted into electrical energy through hydroelectric power generation[2]. The cold storage system uses off-peak electric energy to make ice cubes, and the stored heat energy can be used to reduce cooling electricity during peak times. Living organisms grow by absorbing solar energy, and are buried under the ground for a long time after death, and then transformed into fossil fuels. Food stores chemical energy, which can supply body heat after digestion and absorption.

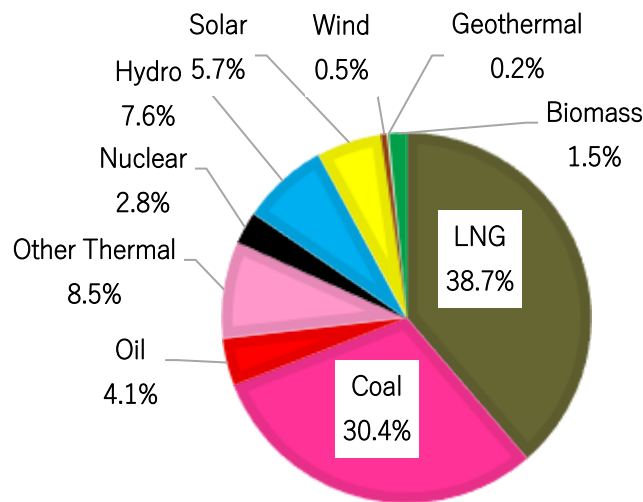


**Fig. 1.1** Share of energy sources in power generation in Japan (2017) [6]

In the 20th century, the power system mainly relied on burning fossil fuels to generate electricity[3]. When electricity consumption changes, the amount of power generation can be adjusted by reducing fuel usage. In recent years, due to issues such as air pollution, dependence on imported energy, and global warming, renewable energy sources (such as wind and solar energy) have developed rapidly [4]. However, wind power cannot be controlled, and power generation is not necessarily when electricity is needed. Solar power generation is affected by the shadow of clouds, and can only generate electricity during the day, and cannot supply peak electricity at night (please refer to the duck curve). Therefore, with the development of renewable energy, the technology that can store intermittent energy has been paid more and more attention[5].

Since the 21st century, the use of mobile devices has increased rapidly, making battery-related use more popular. In remote areas of the world, the use of solar energy is becoming more and more common. Whether there is electric energy is no longer a technical limitation, but an economic and financial problem. With the popularization of electric vehicles, short-distance transportation can no longer rely on fossil fuels, but in the direction of long-distance transportation (such as: air and sea), related technologies are still developing[7].

## 1.2 Energy storage methods

Energy storage methods According to energy storage methods, energy storage can be divided into three categories: physical energy storage, chemical energy storage, and electromagnetic energy storage[8]. Physical energy storage mainly includes pumped water storage, compressed air energy storage, flywheel energy storage, etc., chemical energy storage Mainly include lead-acid batteries, lithium-ion batteries, sodium-sulfur batteries, flow batteries, etc[9]. Electromagnetic energy storage mainly includes supercapacitor energy storage and superconducting energy storage[10]. Lead-acid batteries are generally used in high-power applications, which are mainly used for emergency power supplies, battery cars, and power plants to store surplus energy[11]. Each technology is suitable for storage for different lengths of time. For example, hot water can be stored for several hours, while hydrogen storage can be stored for several days to more than several months. At present, large-scale energy storage systems are mainly hydropower and pumped storage power generation[12]. Grid energy storage refers to large-scale energy storage devices used in the grid.



**Fig. 1.2** Classification of different types of energy storage technologies for stationary applications [13]

### 1.2.1 Potential energy, kinetic energy storage

Mechanical energy storage uses mechanical methods to store energy, such as moving water or heavy objects to a high place (potential energy), moving or rotating objects (kinetic energy), or compressed gas (internal energy). Currently, the more mature technologies are: pumped water energy storage, compressed air energy storage, flywheel energy storage and solid neutral energy storage[14].

Pumped water storage is the use of gravitational potential energy storage to pump water up to the top of a mountain when power demand is low (such as at night), and release water to drive turbines to generate electricity when power demand is high (such as noon or evening) [15]. General turbines can be operated in reverse and can be used as generators or pumps, the most common being Francis turbines. Pumped storage systems can be divided into two types: one is to use two storage reservoirs with a difference in height as energy storage, and the other is to use hydroelectric power generation with downstream storage reservoirs as energy storage. According to statistics in 2012, pumped storage accounts for 99% of the world's total capacity of large-scale energy storage devices, with a capacity of 127,000 megawatts[16]. The actual energy conversion efficiency is between 70% and 80%, up to 87% [17].

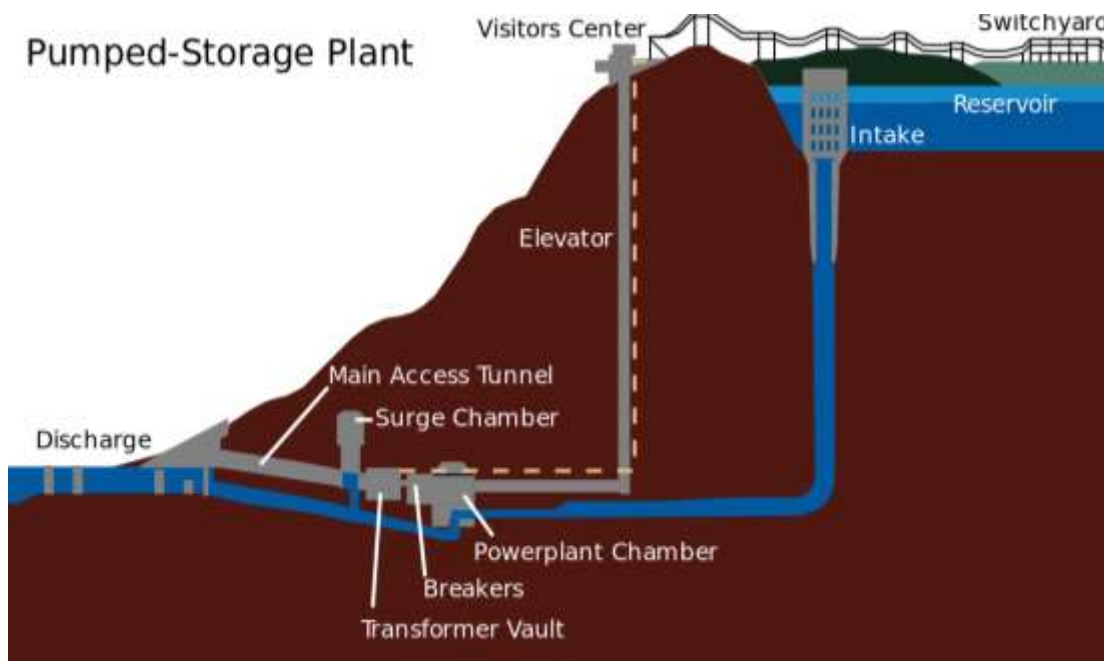


**Fig. 1.3** Diagram of the TVA pumped storage facility at Raccoon Mountain Pumped-Storage Plant in Tennessee, United States [18]

Compressed air energy storage is the use of compressed air to store energy. When electricity is needed, compressed air is used to push the turbine [19]. In large systems, compressed air can be stored in large underground storage spaces, such as underground salt caverns. It can be used to store off-peak electricity and generate electricity when the electricity demand is high [20]. When air is compressed, heat energy is generated, causing its temperature to rise. When the air expands, it will absorb heat. If there is no additional heat supply, its temperature will drop. Compressed air energy storage technology can be divided into three categories according to heat treatment: non-adiabatic, adiabatic and isothermal. Traditional non-adiabatic systems need to burn natural gas when generating electricity to avoid excessively low temperatures. When the adiabatic system saves the heat generated by compression and uses it in expansion, this method can increase efficiency [21].

Compressed air can also be used as a power source for vehicles[22][23]. Small compressed air systems were used as the power source for non-combustion vehicles in the early days, and were used in vehicles operating in coal mines.

Flywheel energy storage uses electrical energy to accelerate a heavy object (flywheel) to rotate quickly, and uses the law of conservation of energy to store energy in the rotational kinetic energy of the object. The stored kinetic energy can be used to generate electricity[24].

Solid gravity energy storage uses an electric motor to raise the height of a solid weight. When the weight is lowered, the electric motor can operate in reverse to become a generator to generate electricity. Studies have pointed out that this technology can start to generate electricity within one second, so it can be used to stabilize the fluctuation of the power grid in a short period of time [25]. Its efficiency can reach 85% [26]. Theoretically, the cost of gravity energy storage should be lower than pumped-storage hydroelectric power generation and battery energy storage [27].

### ***1.2.2 Electromagnetic energy storage***

Electromagnetic energy storage includes: superconducting energy storage, capacitive energy storage, and supercapacitor energy storage[28]. 1. Superconducting energy storage Superconducting energy storage system (SMES) uses coils made of superconductors to store

magnetic field energy, and does not require conversion of energy forms during power transmission, with fast response speed (ms level) and high conversion efficiency ( $\geq 96\%$ ), specific capacity (1-10 Wh/kg)/specific power (104-105kW/kg) and other advantages, can realize real-time large-capacity energy exchange and power compensation with the power system. SMES can fully meet the requirements of transmission and distribution network voltage support, power compensation, frequency regulation, improving system stability and power transmission capacity. 2. Supercapacitor energy storage :Supercapacitor is developed according to the theory of electrochemical double layer, which can provide powerful pulse power[29]. When charging, the electrode surface in an ideal polarization state, the charge will attract the anisotropic ions in the surrounding electrolyte solution, making it It is attached to the surface of the electrode to form an electric double layer, which constitutes an electric double layer capacitor. In the power system, it is mostly used for short-term, high-power load smoothing and power quality peak power occasions, such as the starting support of high-power DC motors, state voltage restorers, etc., to improve the power supply level during voltage dips and transient disturbances.

### ***1.2.3 Electrochemical energy storage***

Energy is stored using electrochemical reactions[30]. It mainly includes battery energy storage, flow battery energy storage, and super capacitor energy storage. Battery: Generally composed of multiple electrochemical cells, which use reversible electrochemical reactions to store electrical energy, also known as secondary batteries because they can be reused. Batteries come in different shapes and sizes, from coin cells to megawatt grid energy storage systems. Compared to disposable (disposable) batteries, the overall energy consumption and environmental impact of batteries are lower. The initial cost of a battery is high, but its average cost of use decreases as the number of uses increases.

## **1.3 Several common types of electrochemical energy storage**

Lead-acid batteries have the highest market share in the past. A single cell has a voltage of 2 volts after charging, and the lead of the negative electrode and the lead sulfate of the positive

electrode are immersed in diluted sulfuric acid (electrolyte). During discharge, the negative electrode produces lead sulfate and produces water in the electrolyte. Lead-acid batteries have lower cost due to their maturity, but their service life and energy density are lower [31].

Nickel-cadmium batteries (NiCd): use nickel oxyhydroxide and metal cadmium as electrodes. Cadmium was banned in the EU in 2004 because of its toxicity and was almost replaced by nickel-metal hydride batteries[32].

Nickel Metal Hydride (NiMH): The first commercial product appeared in 1989 [33]. One of the most common consumer and industrial batteries. The battery's negative electrode is an alloy that can absorb hydrogen, not cadmium.

Lithium-ion battery: It is the battery with the highest energy density and the lowest self-discharge [34] when not in use among the batteries currently used in consumer electronic products. Lithium-Ion Polymer Batteries: Lightweight and can be made in different shapes.

The flow battery utilizes two chemical solutions through the membrane for ion exchange for charging and discharging [35][36]. The voltage of the battery can be calculated from the Nernst equation and is generally between 1.0 and 2.2 volts. The characteristic of this battery is that the amount of stored energy is proportional to the storage capacity of the solution, and the battery power is proportional to the area of the membrane. Technically, flow batteries are similar to fuel cells and electrochemical cells. Can be used in applications that require long-term energy storage, such as grid backup power. Common flow batteries such as all-vanadium redox flow batteries.

### ***1.3.1 Lead acid battery energy storage***

Since the 1970s, lead-acid batteries have been used for backup power in residential solar power installations[37]. While they are similar to traditional car batteries, batteries used in residential energy storage systems are called deep-cycle batteries because they discharge and charge more often than most car batteries.

Traditionally, lead-acid batteries have cost less than lithium-ion batteries, making them more attractive to residential users. However, their operating life is much shorter than that of lithium-ion batteries.

The working life of lead-acid batteries is lower than that of lithium-ion batteries. While some lead-acid batteries can be charged and discharged up to 1,000 times, lithium-ion batteries can be charged and discharged between 1,000 and 4,000 times[38].

Most lead-acid batteries have a lifespan of about 5 years and come with a corresponding warranty. As a result, residential users will have to replace lead-acid batteries many times over the lifetime of a solar power facility.

The energy storage efficiency of lead-acid batteries is lower than other energy storage technologies such as lithium-ion batteries. They also cannot charge or discharge as quickly as lithium battery energy storage systems due to their lower efficiency.

Lead-acid batteries have a low discharge capacity, which means that consuming too much energy can cause their ability to store energy to deteriorate rapidly. Research by the National Renewable Energy Laboratory (NREL) found that releasing 50 percent of the energy in a lead-acid battery could allow it to complete 1,800 charges and discharges before the storage capacity dropped significantly[39]. If discharged to 80% capacity, it can only withstand 600 charges and discharges, after which its capacity will drop significantly.

Since lead-acid batteries have relatively low energy storage efficiency and cannot be fully discharged, lead-acid batteries require more energy storage capacity and space than lithium-ion batteries. Lead-acid batteries are also much heavier than lithium-ion batteries, require a firmer stand to place them, and require more space than lithium-ion battery packs.

Lead is a toxic heavy metal, and although it is recyclable, it can still become contaminated due to improper handling.

### ***1.3.2 NiCd battery energy storage***

Nickel-cadmium battery is a kind of DC power supply battery. Nickel-cadmium battery can be charged and discharged more than 500 times, which is economical and durable[40]. Its internal resistance is small, the internal resistance is small, it can be quickly charged, and it can provide a large current for the load, and the voltage change during discharge is small, it is a very ideal DC power supply battery.

The most fatal disadvantage of nickel-cadmium batteries is that if they are not handled properly during the charging and discharging process, there will be a serious "memory effect"[41], which will greatly shorten the service life. The so-called "memory effect" means that the power of the battery is not completely discharged before the battery is charged, which will cause the battery capacity to decrease over time. The small bubbles accumulated over time reduce the area of the battery plate and indirectly affect the capacity of the battery. Of course, we can alleviate the "memory effect" by mastering reasonable charging and discharging methods. In addition, cadmium is toxic, so nickel-cadmium batteries are not conducive to the protection of the ecological environment. Numerous shortcomings have made nickel-cadmium batteries basically eliminated from the application range of digital equipment batteries.

The nickel-cadmium battery can be charged and discharged more than 500 times, which is economical and durable[42]. Its internal resistance is small, the internal resistance is small, it can be quickly charged, and it can provide a large current for the load, and the voltage change during discharge is small, it is a very ideal DC power supply battery. Compared with other types of batteries, nickel-cadmium batteries can withstand overcharge or overdischarge. The discharge voltage of nickel-cadmium batteries varies according to their discharge devices. Each unit cell (Cell) is about 1.2V, and the battery capacity units are Ah (ampere-hour) and mAh (milliamper-hour). The limit value of the discharge termination voltage is called As "discharge end voltage", the discharge end voltage of nickel-cadmium battery is 1.0/cell (cell is each unit cell). The self-discharge rate is low, and the characteristics of the nickel-cadmium battery will not deteriorate under the condition of long-term storage. After fully charged, the original characteristics can be completely restored. It can be used in the temperature range of 30°C--50°C. Since the unit cell is made of metal container, it is sturdy and durable; it is completely sealed, and there will be no leakage of electrolyte, so there is no need to replenish electrolyte.

The key to improving battery performance and extending battery life is to avoid memory effects and overdischarge[43]. Nickel-cadmium batteries have a memory effect, that is, after a nickel-cadmium battery has been charged and discharged several times at low capacity, if a larger capacity charge and discharge is to be performed, the battery will not work normally. This situation is called memory effect. . Especially in video recorders and video cameras with higher discharge termination voltages, as the working voltage decreases, the battery capacity

also decreases on the surface, but the decrease in discharge voltage may be caused by one or two complete discharges temporarily. Phenomenon. The memory effect makes the performance of the battery unable to be fully utilized, and also brings great inconvenience to the shooting. Therefore, in use, you should pay attention to using a charger with charging and discharging performance, such as Sony's BC-1WDCE, to avoid the memory effect. When using general chargers such as BC-1WA and BC-1WB, one discharge can be performed after about 10 times of charging, and the purpose of preventing memory effect can also be achieved.

### ***1.3.3 Lithium Battery Energy Storage***

Lithium battery is a kind of battery that uses lithium metal or lithium alloy as positive/negative electrode material and uses non-aqueous electrolyte solution. In 1912, the lithium metal battery was first proposed and studied by Gilbert N. Lewis. In the 1970s, M. S. Whittingham proposed and began to study lithium-ion batteries[44]. Due to the very active chemical properties of lithium metal, the processing, storage and use of lithium metal have very high environmental requirements. With the development of science and technology, lithium batteries have become the mainstream[45].

After the lithium battery cell is overcharged to a voltage higher than 4.2V, side effects will begin to occur. The higher the overcharge voltage, the higher the risk[46]. When the voltage of the lithium cell is higher than 4.2V, the number of lithium atoms remaining in the positive electrode material is less than half, and the storage cell often collapses at this time, resulting in a permanent capacity loss of the battery[47]. If charging is continued, since the storage cell of the negative electrode is already full of lithium atoms, subsequent lithium metal will accumulate on the surface of the negative electrode material. These lithium atoms will grow dendrites from the surface of the negative electrode in the direction of the lithium ions[48]. These lithium metal crystals pass through the separator, shorting the positive and negative electrodes. Sometimes the battery explodes before the short circuit occurs. This is because during the overcharge process, the electrolyte and other materials will decompose to generate gas, causing the battery shell or pressure valve to bulge and rupture, allowing oxygen to enter and react with the lithium atoms accumulated on the surface of the negative electrode, and then explode.

Therefore, when charging a lithium battery, an upper voltage limit must be set, so that the battery life, capacity, and safety can be taken into account at the same time. The ideal upper limit of the charging voltage is 4.2V[49]. There is also a lower voltage limit when the lithium battery is discharged[50]. When the cell voltage drops below 2.4V, some of the material begins to break down. And because the battery will self-discharge, the voltage will be lower the longer it is put on, so it is best not to put it at 2.4V to stop when discharging. During the period when the lithium battery is discharged from 3.0V to 2.4V, the energy released only accounts for about 3% of the battery capacity. Therefore, 3.0V is an ideal discharge cut-off voltage. During charging and discharging, in addition to voltage limitation, current limitation is also necessary. When the current is too large, the lithium ions have no time to enter the storage cell and will accumulate on the surface of the material.

After these lithium ions gain electrons, lithium atoms will crystallize on the surface of the material, which is as dangerous as overcharging[51]. If the battery case breaks, it will explode. Therefore, the protection of lithium-ion batteries should include at least three items: the upper limit of the charging voltage, the lower limit of the discharge voltage, and the upper limit of the current. Generally, in the lithium battery pack, in addition to the lithium battery cells, there will be a protective plate, which mainly provides these three protections. However, these three protections of the protective plate are obviously not enough, and the explosion of lithium batteries is still frequent around the world. To ensure the safety of the battery system, the cause of the battery explosion must be analyzed more carefully[52].

### ***1.3.4 Liquid Flow Battery Energy Storage***

A flow battery is a rechargeable fuel cell in which an electrolyte containing one or more dissolved electroactive elements flows through an electrochemical cell that converts chemical energy directly and reversibly into electricity (electroactive elements are "can" Elements in solution participating in the electrode reaction can either be adsorbed on the electrode")[53]. Additional electrolyte is usually stored externally, usually in a water tank, and is usually pumped through the reactor's cell (or cells), although gravity-fed systems are also known. The flow battery can be quickly "recharged" by replacing the electrolyte (in a similar way to refilling

the fuel tank of an internal combustion engine), while recycling the used material to re-energize. Many flow batteries use carbon felt electrodes due to their low cost and sufficient electrical conductivity, although these electrodes limit the charge/discharge power to some extent due to their low intrinsic activity for many redox pairs[54] [55].

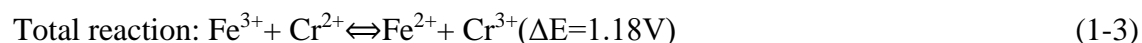
In other words, a flow battery is like an electrochemical battery, except that the ionic solution (electrolyte) is not stored in the battery around the electrodes. Instead, the ionic solution is stored outside the cell and can be fed into the cell to generate electricity. The total amount of electricity that can be generated depends on the size of the storage tank.

## 1.4 Development and application of liquid flow battery

Flow battery is an electrochemical energy storage technology proposed by Thaller in 1974, which is a new battery[56]. The flow battery is composed of a point stack unit, an electrolyte, an electrolyte storage supply unit, and a management control unit. It is a high-performance battery that separates the positive and negative electrolytes and circulates them separately. ) and long cycle life, it is a new energy product.

### 1.4.1 Ferrochrome liquid flow battery

In the 1970s, the Fe-Cr flow battery was first prepared by NASA in the United States, and this research was terminated in the early 1980s[57]. As part of the "moon project", NASA transferred related technology to Japan for continued development, and in 1984. And in 1986, 10kW and 60kW prototype systems were successfully prepared.



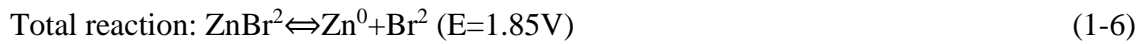
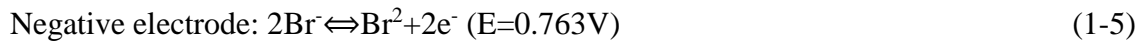
Advantages: low cost and long service life.

Disadvantages: First, the reversibility of the chromium redox couple in the chromium half-cell is poor, which affects the life and performance of the battery[58]; in addition, the positive and negative electrolytes diffuse and penetrate through the diaphragm, resulting in cross-contamination, thereby increasing the self-discharge of the battery[59]. Reduces the coulombic

efficiency of the battery. A large amount of hydrogen is generated during operation, and improper handling is prone to explosion and other dangers.

### 1.4.2 Zinc-bromine liquid flow battery

Since the 1970s, zinc-bromine flow battery technology has received extensive attention[60], and a lot of research and development work has been carried out on how to improve battery performance and life, and ensure its safety and reliability, covering mathematical model analysis, electrodes and separators. Significant progress has been made in materials research, electrolyte optimization, control and operation strategy development.

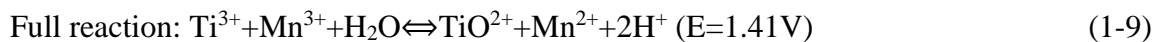
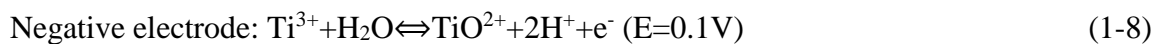


Advantages: low cost, long service life, safety.

Disadvantages: serious self-discharge and zinc dendrite problems, battery performance is greatly affected[61].

### 1.4.3 Titanium-manganese liquid flow battery

Titanium-manganese-based electrolytes consist of titanium and manganese[62]. A cheap and resource-rich sulfuric acid aqueous solution battery is shown in the following reaction equation, the electromotive force of the battery is 1.41 V, and water is used as the system electrolyte, which is expensive and can be expected as an inexpensive electrolyte. However, since  $\text{Mn}^{3+}$  ions are unstable in aqueous solution, the principle of solid deposition of  $\text{MnO}_2$  oxides occurs due to the disproportionation reaction during charging.

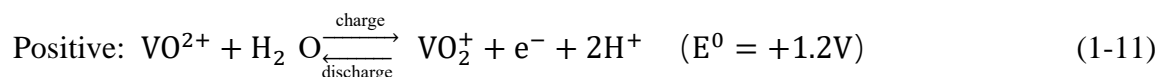


Advantages: low cost, high security.

Disadvantages: There is a self-discharge phenomenon, which affects the battery performance. Unbalanced charge and discharge will produce deposits that block the battery pipeline[63].

#### 1.4.4 All-Vanadium Liquid Flow Battery

An all-vanadium redox battery is a redox battery that uses vanadium as the active material in a circulating liquid state[64]. The electrical energy of vanadium battery is stored in the sulfuric acid electrolyte of different valence vanadium ions in the form of chemical energy, and the electrolytic fluid is injected into the battery stack through an external pump[65]. Circulating flow in a closed loop, using a proton exchange membrane as the separator of the battery pack, the electrolyte solution flows through the electrode surface in parallel and electrochemical reactions occur, and the current is collected and conducted through the double electrode plate, so that the chemical energy stored in the solution is converted into electrical energy .



Advantages: safe, no danger of explosion and fire. long lasting. No self-discharge phenomenon. High energy efficiency, up to 75%~80%, very cost-effective;

Disadvantages: The price of electrolyte is high[66].

### 1.5 Development and application of all-vanadium liquid flow batteries

An all-vanadium redox battery (Vanadium Redox Battery, abbreviation: VRB) is a rechargeable flow battery that uses vanadium ions in different oxidation states to store chemical potential energy[67]. Vanadium redox batteries exploit the ability of vanadium to exist in solution in four different oxidation states, and batteries made using this property have only one electroactive element instead of two[68]. For a number of reasons, including their relatively large size, most vanadium batteries are currently used for grid energy storage, such as connecting to power plants or the grid.

### ***1.5.1 Development of All-Vanadium Liquid Flow Batteries***

The possibility of vanadium flow batteries was explored by researchers in the 1930s by Pissoort, by NASA researchers in the 1970s[69], and by Pellegrini and Spaziante in the 1970s, but none of them successfully demonstrated the technology. In the 1980s, Maria Skyllas-Kazacos of the University of New South Wales first successfully demonstrated an all-vanadium redox flow battery using vanadium in a sulfuric acid solution in each half[70]. Her design, which used a sulfuric acid electrolyte, was patented at the University of New South Wales in Australia in 1986.

The main advantage of an all-vanadium redox flow battery is that it can provide almost unlimited battery capacity simply by using a larger tank and can also be stored in a fully discharged condition for long periods of time without adverse effects. If there is no power available to charge it, it can be recharged simply by changing the electrolyte, and the battery does not suffer permanent damage if the electrolyte is accidentally mixed[71]. The single state of charge between the two electrolytes avoids the capacity reduction due to a single cell in a non-flow battery, the electrolyte is aqueous and intrinsically safe and non-flammable, while a mixed acid developed by the Pacific Northwest National Laboratory is used. The 3rd generation formulation of the solution operates over a wider temperature range and enables passive cooling.

The main disadvantage of vanadium redox technology is the relatively poor energy-to-volume ratio, although recent studies at the Pacific Northwest National Laboratory have doubled the energy density and have more system complexity compared to standard batteries, (although the 3rd generation formulation doubles the energy density of the system), the aqueous electrolyte makes the battery heavy and is therefore only used for stationary applications.

### ***1.5.2 Working Principle of All-Vanadium Liquid Flow Battery***

A vanadium redox battery consists of a battery in which the two electrolytes are separated by a proton exchange membrane. Both electrolytes are vanadium-based, the electrolyte in the positive half-cell contains  $\text{VO}^{2+}$  and  $\text{VO}^{2+}$  ions, and the electrolyte in the negative cell contains  $\text{V}^{3+}$  and  $\text{V}^{2+}$  ions[72]. The electrolyte can be prepared by any of several methods, including

electrolytically dissolving vanadium pentoxide ( $V_2O_5$ ) in sulfuric acid ( $H_2SO_4$ ). The solution remains strongly acidic in use.

In vanadium flow batteries, the two half-cells are additionally connected to tanks and pumps so that very large amounts of electrolyte can be circulated through the battery. Circulation of this liquid electrolyte is somewhat cumbersome and limits the use of vanadium flow batteries in mobile applications, effectively confining them to large stationary installations.

### ***1.5.3 Composition of an all-vanadium liquid flow battery***

The composition of the all-vanadium redox flow battery mainly includes three parts: the stack, the electrolyte and the control system. The composition of the stack mainly includes frame, bipolar plate, collector plate, carbon fiber electrode and ion exchange membrane.

As the overall support of the stack, the frame needs to have a certain strength, and at the same time the electrolyte circulates inside it, and it needs to have high acid resistance. The stack will generate heat during operation, so the thermal expansion coefficient of the frame needs to be minimized, otherwise there will be leakage during long-term operation. At present, the widely used materials are PVC, PP, PPE and PPF.

The main function of the bipolar plate is to transfer electrons to isolate the positive and negative electrolytes, so it needs to have high conductivity and liquid resistance. At the same time, it can also be used as a flow path for the electrolyte to flow. At present, the widely used resin-filled carbon plate and high-density graphite plate.

The main function of the carbon fiber electrode is to provide the electrolyte redox site. As an electrode of a flow battery, a certain degree of hydrophilicity is required, and high conductivity is also required. As the most important part of the battery, the electrode is mainly used PAN carbon fiber felt.

The main function of the ion exchange membrane is to transfer ions and isolate the positive and negative electrolytes, so it needs a certain liquid resistance and ion permeability. The widely used vanadium redox flow batteries are mainly N212 and N211 produced by Nafion. and N117 salt ion exchange membrane.

The main function of the collector plate is to conduct electric charges at the charging and discharging terminals, and the most widely used are high-conductivity metal plates such as gold-plated copper plates.

#### ***1.5.4 Application of All-Vanadium Liquid Flow Batteries in Energy Storage***

In order to meet the needs of different application fields, a variety of energy storage technologies have been researched and developed in the industry, and various energy storage technologies and their applicable scopes have been explored. These energy storage technologies have their own characteristics and applicable fields. Generally speaking, renewable energy power generation systems such as wind energy and solar energy have higher requirements on the power and reversible storage capacity of energy storage technology. Pumped water storage technology, flow battery technology, lithium-ion battery technology, and super lead-acid battery technology have good application prospects in the field of large-scale energy storage technology. The concept of flow battery was proposed by LHThaller (NASA Lewis Research Center, Cleveland, United States) in 1974. This type of battery undergoes a reversible redox reaction (i.e., valence) on the electrode through the active material in the positive and negative electrolyte solutions. The reversible change of state realizes the mutual conversion of electrical and chemical energy. During charging, the positive electrode undergoes an oxidation reaction, and the valence state of the active material increases; the negative electrode undergoes a reduction reaction, and the valence state of the active material decreases; the discharge process is the opposite. The positive and negative electrolyte solutions of the flow battery are stored in external storage tanks, and are transported to the inside of the battery through pumps and pipelines for reaction. In theory, different redox stacks can form a variety of flow batteries. The all-vanadium redox flow battery uses vanadium ions in different valence states as active materials, and realizes the mutual conversion of chemical energy and electrical energy through the change of the valence state of vanadium ions. Compared with other large-scale energy storage technologies, all-vanadium flow battery technology has many advantages.

##### **1. Main advantages and characteristics**

First, the all-vanadium redox flow battery energy storage system is safe and reliable in operation, can be recycled, and has a small environmental load in the life cycle and is environmentally friendly. The energy storage medium of the all-vanadium redox flow battery energy storage system is an electrolyte aqueous solution, which has high safety.

Second, the output power and energy storage capacity of the all-vanadium redox flow battery energy storage system are independent of each other, and the design and placement are flexible. The output power is determined by the size and quantity of the stack, while the energy storage capacity is determined by the concentration and volume of vanadium ions in the electrolyte solution. The output power of the all-vanadium redox flow battery system is in the range of hundreds of kilowatts to hundreds of megawatts, and the energy storage capacity is in the range of hundreds of kilowatt hours to hundreds of megawatt hours.

Third, the working principle of the all-vanadium redox flow battery is to realize the storage and release of electric energy through the change of the valence state of vanadium ions in the electrolyte. The reversibility of the reaction is good, there is no phase change, the electrolyte flows continuously in the electrodes inside the battery, and the charge-discharge state switching response is rapid. The number of charge and discharge cycles is more than 15,000 times, and the service life is 15 to 20 years. The life cycle is cost-effective.

Fourth, the positive and negative electrolyte solutions in the all-vanadium redox flow battery are of the same element, and the electrolyte solution can be used repeatedly through online regeneration. The stack and battery energy storage system are mainly composed of carbon materials, plastics and metal materials. When the all-vanadium redox flow battery system is discarded, the metal materials can be used continuously, and the carbon materials and plastics can be used as fuels. Therefore, the environmental load of the all-vanadium redox flow battery system in the whole life cycle is small and the environment is very friendly.

Fifth, the price is cheap. In recent years, with the continuous progress of all-vanadium redox flow battery material technology and battery structure design and manufacturing technology, the battery performance has been continuously improved, the energy efficiency of the stack can be maintained above 80%, and the working current density has increased from the original 60-80mA/cm<sup>2</sup> increased to 150mA/cm<sup>2</sup>. The power density of the battery is doubled, and under this condition, the cost is greatly reduced. Although the research and development cycle is very

short and the state's investment is very low, the 1MW/5MW scale of the all-vanadium redox flow battery energy storage system has dropped from 7,000 yuan/kWh in 2013 to 3,500 yuan/kWh in 2016. Moreover, the number of charge and discharge cycles is more than 16,000 times, so the cost of its life cycle is very low.

Sixth, the all-vanadium flow battery energy storage system adopts a modular design, which is convenient for system integration and scale expansion. The all-vanadium redox flow battery stack is formed by stacking a plurality of single cells in a filter press method. The rated output power of a single stack of an all-vanadium flow battery is generally between 20 kW and 40 kW; an all-vanadium flow battery energy storage system is usually composed of multiple unit energy storage system modules, and the rated output power of the unit energy storage system module is generally between 100 kW and 300 kW. Compared with other types of batteries, the rated output power of the all-vanadium flow battery stack and battery cell energy storage system module is large, which is convenient for the integration and scale expansion of the all-vanadium flow battery energy storage system.

Seventh, it has strong overload capacity and deep discharge capacity. When the all-vanadium redox flow battery energy storage system is running, the electrolyte solution is circulated in the stack through the circulating pump, and the influence of the diffusion of active substances in the electrolyte solution is small; moreover, the electrode reactivity is high, and the activation polarization is small. Therefore, the all-vanadium redox flow battery energy storage system has a good overload capacity. Moreover, the all-vanadium redox flow battery has no memory effect and has a good deep discharge capability.

Eighth, the energy density of flow batteries is low, and all-vanadium flow batteries are more suitable for stationary large-scale energy storage power stations.

## 2. Promising industrial applications

Large-scale battery energy storage technology needs to meet some basic requirements, namely, high safety; high cost performance in the life cycle; good economy; low environmental load in the life cycle and environmental friendliness, etc. In contrast, among many energy storage technologies, flow battery energy storage technology has the advantages of high energy conversion efficiency, large storage capacity, free site selection, deep discharge, safety and environmental protection, etc., and has become a large-scale and efficient energy storage

technology. Among many flow batteries, the all-vanadium flow battery energy storage technology is the most industrialized flow battery energy storage technology. Pu Neng Century predicts that by 2023, the entire market of flow batteries will reach a scale of one hundred billion.

## 1.6 The purpose of this research

Although all-vanadium flow battery technology has matured after more than 30 years of development, there is still no way to solve the shortcoming of low energy density because it is a flow battery. Due to this disadvantage, the output density of the stack is low, the volume is large and the cost is high. Due to these shortcomings, the mass production and large-scale installation of batteries are difficult. This research mainly improves the charging and discharging performance of the battery by improving the structure of the battery flow path and the modification of the battery carbon fiber battery, thereby reducing the manufacturing cost of the stack and reducing the volume of the stack.

## 1.7 References

1. XingLuo,JihongWang,Mark Dooner,Jonathan Clarke. Overview of current development in electrical energy storage technologies and the application potential in power system operation, *Applied Energy*, Volume 137, 1 January 2015, Pages 511-536.
2. Kamil Kaygusuz,Sustainable Development of Hydroelectric Power, *Energy Sources* Volume 24, 2002 - Issue 9.
3. Mikael Höök,Xu Tang. Depletion of fossil fuels and anthropogenic climate change—A review, *Energy Policy*,Volume 52, January 2013, Pages 797-809.
4. M. Asif T,Muneer. Energy supply, its demand and security issues for developed and emerging economies, *Renewable and Sustainable Energy Reviews*, Volume 11, Issue 7, September 2007, Pages 1388-1413.
- 5.DolfGielen,FranciscoBoshell,DegerSaygin,MorganD.Bazilian,NicholasWagner,RicardoGorini. The role of renewable energy in the global energy transformation, *Energy Strategy Reviews*,Volume 24, April 2019, Pages 38-50.

6. ISEP, based on METI's energy statistics and other information.
7. L. Situ, "Electric Vehicle development: The past, present & future," 2009 3rd International Conference on Power Electronics Systems and Applications (PESA), 2009, pp. 1-3.
8. T.M.I. Mahlia, T.J. Saktisahdan, A. Jannifar, M.H. Hasan, H.S.C. Matseelar, A review of available methods and development on energy storage; technology update, Renewable and Sustainable Energy Reviews, Volume 33, 2014, Pages 532-545.
9. John B. Goodenough. Electrochemical energy storage in a sustainable modern society, Energy Environ. Sci., 2014, 7, 14-18.
10. J.M. Zhao, Z.M. Zhang, Electromagnetic energy storage and power dissipation in nanostructures, Journal of Quantitative Spectroscopy and Radiative Transfer, Volume 151, 2015, Pages 49-57.
11. Bode, H. Lead-acid batteries. United States: N. p., 1977. Web.
12. Yigang Kong, Zhigang Kong, Zhiqi Liu, Congmei Wei, Jingfang Zhang, Gaocheng An, Pumped storage power stations in China: The past, the present, and the future, Renewable and Sustainable Energy Reviews, Volume 71, 2017, Pages 720-731.
13. Jilei Liu, Jin Wang, Chaohe Xu, Hao Jiang, Chunzhong Li, Lili Zhang, Jianyi Lin, Ze Xiang Shen. Advanced Energy Storage Devices: Basic Principles, Analytical Methods, and Rational Materials Design, Adv. Sci. 2018, 5, 1700322.
14. Amiryar, Mustafa E., and Keith R. Pullen. 2017. "A Review of Flywheel Energy Storage System Technologies and Their Applications" Applied Sciences 7, no. 3: 286.
15. Hunt, J.D., Byers, E., Wada, Y. et al. Global resource potential of seasonal pumped hydropower storage for energy and water storage. Nat Commun 11, 947 (2020).
16. Energy storage - Packing some power. The Economist. March 3, 2011 [March 11, 2012].
17. Energy Storage - Hawaiian Electric Company. Accessed: February 13, 2012.
18. dkins, F.E., TVA Report "Raccoon Mountain pumped storage plant; Ten years operating experience," IEEE Transactions on Energy Conversion, Volume EC-2, Issue 3 (September 1987), pages 361 - 368. 1987.
19. Wild, Matthew, L. Wind Drives Growing Use of Batteries, The New York Times, July 28, 2010, p. B1.

20. Keles, Dogan; Hartel, Rupert; Möst, Dominik; Fichtner, Wolf. Compressed-air energy storage power plant investments under uncertain electricity prices: an evaluation of compressed-air energy storage plants in liberalized energy markets. *The Journal of Energy Markets*. Spring 2012, 5 (1): 54.
21. Gies, Erica. Global Clean Energy: A Storage Solution Is in the Air , *International Herald Tribune* online website, October 1, 2012, and in print on October 2, 2012, in *The International Herald Tribune*. Retrieved from NYTimes.com website, March 19, 2013.
22. Diem, William. Experimental car is powered by air: French developer works on making it practical for real-world driving, *Auto.com*, March 18, 2004. Retrieved from *Archive.org* on March 19, 2013.
23. Slashdot: Car Powered by Compressed Air , *Freep.com* website, 2004.03.18.
24. R. Sebastián, R. Peña Alzola, Flywheel energy storage systems: Review and simulation for an isolated wind power system, *Renewable and Sustainable Energy Reviews*, Volume 16, Issue 9, 2012.
25. Fraser, Douglas. Edinburgh company generates electricity from gravity. *BBC News*. BBC. 14 January 2020.
26. Akshat Rathi. Stacking concrete blocks is a surprisingly efficient way to store energy. *Quartz*. August 18, 2018 .
27. Gravity energy storage finally dawns . *TechNews*. [2021-06-13] (Chinese (Taiwan)).
28. S. Ould Amrouche, D. Rekioua, T. Rekioua, S. Bacha, Overview of energy storage in renewable energy systems, *International Journal of Hydrogen Energy*, Volume 41, Issue 45, 2016, Pages 20914-20927.
29. C. Abbey and G. Joos, "Supercapacitor Energy Storage for Wind Energy Applications," in *IEEE Transactions on Industry Applications*, vol. 43, no. 3, pp. 769-776, May-june 2007.
30. José H. Zagal, Metallophthalocyanines as catalysts in electrochemical reactions, *Coordination Chemistry Reviews*, Volume 119, 1992, Pages 89-136.
31. Paul Ruetschi, Aging mechanisms and service life of lead–acid batteries, *Journal of Power Sources*, Volume 127, Issues 1–2, 2004, Pages 33-44.

32. Carl Johan Rydh, Magnus Karlström, Life cycle inventory of recycling portable nickel–cadmium batteries, *Resources, Conservation and Recycling*, Volume 34, Issue 4, 2002, Pages 289-309.
33. Robert C. Stempel, Stanford R. Ovshinsky, Electric Cars and Lead, *Science*, 269, 5225, (741-742), (1995).
34. Arumugam Manthiram. An Outlook on Lithium Ion Battery Technology, *ACS Central Science* **2017** 3 (10), 1063-1069.
35. Badwal, Sukhvinder P. S.; Giddey, Sarbjit S.; Munnings, Christopher; Bhatt, Anand I.; Hollenkamp, Anthony F. Emerging electrochemical energy conversion and storage technologies. *Frontiers in Chemistry*. 24 September 2014, 2.
36. Alotto, P.; Guarnieri, M.; Moro, F. Redox Flow Batteries for the storage of renewable energy: a review. *Renewable & Sustainable Energy Reviews*. 2014, 29: 325–335.
37. "Lead Acid Battery History". Lead-Acid.com. Archived from the original on 2015-09-29. Retrieved 2019-12-25.
38. Matthew Li, Jun Lu, Zhongwei Chen, Khalil Amine. 30 Years of Lithium-Ion Batteries, *Adv. Mater.* 2018, 30, 1800561.
39. Camm, Frederick James. "Lead–acid battery". *Wireless Constructor's Encyclopaedia* (third ed.).
40. "Batteries - Environment - European Commission". ec.europa.eu. Retrieved 18 October 2014.
41. Bergveld, H.J.; Kruijt, W.S.; Notten, Peter H. L. (2002-09-30). *Battery Management Systems: Design by Modelling*. Springer. pp. 38–. ISBN 9781402008320. Retrieved 5 June 2013.
42. General Electric, "Nickel–Cadmium Battery Application Engineering Handbook", 1971.
43. Marathon Battery Company, "Care and Maintenance of Nickel–Cadmium Batteries".
44. J.-H. Shin, W.A. Henderson, G.B. Appetecchi, F. Alessandrini, S. Passerini, Recent developments in the ENEA lithium metal battery project, *Electrochimica Acta*, Volume 50, Issue 19, 2005, Pages 3859-3865.
45. Quan Li, Tiancheng Yi, Xuelong Wang, Hongyi Pan, Baogang Quan, Tianjiao Liang, Xiangxin Guo, Xiqian Yu, Howard Wang, Xuejie Huang, Liquan Chen, Hong Li, In-situ

- visualization of lithium plating in all-solid-state lithium-metal battery, *Nano Energy*, Volume 63, 2019, 103895.
46. Siyuan Li, Lei Fan, Yingying Lu, Rational design of robust-flexible protective layer for safe lithium metal battery, *Energy Storage Materials*, Volume 18, 2019, Pages 205-212.
47. Yinquan Hu, Heping Liu, Yi, Liu, Kaifeng Zhang. Capacity Loss Analysis of Lithium Iron Phosphate Power Batteries Group, *Journal of Wu Han University of Technology*, Vol.33 No.9 Sep.2011.
48. FENG Shanshan, LIU Xiaobin, GUO Shilin, HE Bingbing, GAO Zhenguang, CHEN Mingyang, GONG Junbo. Nucleation, growth and inhibition of lithium dendrites[J]. *CIESC Journal*, 2022, 73(1): 97-109.
49. S.S. Zhang, K. Xu, T.R. Jow, Study of the charging process of a LiCoO<sub>2</sub>-based Li-ion battery, *Journal of Power Sources*, Volume 160, Issue 2, 2006, Pages 1349-1354.
50. Sheng Shui Zhang, The effect of the charging protocol on the cycle life of a Li-ion battery, *Journal of Power Sources*, Volume 161, Issue 2, 2006, Pages 1385-1391.
51. J.-M. Tarascon, M. Armand. Issues and challenges facing rechargeable lithium batteries. *Materials for Sustainable Energy*, pp. 171-179 (2010).
52. Xuning Feng, Dongsheng Ren, Xiangming He, Minggao Ouyang, Mitigating Thermal Runaway of Lithium-Ion Batteries, *Joule*, Volume 4, Issue 4, 2020, Pages 743-770.
53. Park, M., Ryu, J., Wang, W. et al. Material design and engineering of next-generation flow-battery technologies. *Nat Rev Mater* 2, 16080 (2017).
54. Aaron, Douglas. In Situ Kinetics Studies in All-Vanadium Redox Flow Batteries. *ECS Electrochemistry Letters*: A29–A31.
55. McCreery, Richard L. Advanced Carbon Electrode Materials for Molecular Electrochemistry. *Chemical Reviews*. July 2008, 108 (7): 2646–2687.
56. Arenas, L.F.; Ponce de León, C.; Walsh, F.C. Engineering aspects of the design, construction and performance of modular redox flow batteries for energy storage. *Journal of Energy Storage*. June 2017, 11: 119–153.
57. M. Lopez-Atalaya, G. Codina, J.R. Perez, J.L. Vazquez, A. Aldaz, Optimization studies on a Fe/Cr redox flow battery, *Journal of Power Sources*, Volume 39, Issue 2, 1992, Pages 147-154.

58. Codina, G., Aldaz, A. Scale-up studies of an Fe/Cr redox flow battery based on shunt current analysis. *J Appl Electrochem* 22, 668–674 (1992).
59. Huan Zhang, Yi Tan, Jiayan Li, Bing Xue, Studies on properties of rayon- and polyacrylonitrile-based graphite felt electrodes affecting Fe/Cr redox flow battery performance, *Electrochimica Acta*, Volume 248, 2017, Pages 603-613.
60. M.C. Wu, T.S. Zhao, H.R. Jiang, Y.K. Zeng, Y.X. Ren, High-performance zinc bromine flow battery via improved design of electrolyte and electrode, *Journal of Power Sources*, Volume 355, 2017, Pages 62-68.
61. Qinzhi Lai, Huamin Zhang, Xianfeng Li, Liqun Zhang, Yuanhui Cheng, A novel single flow zinc–bromine battery with improved energy density, *Journal of Power Sources*, Volume 235, 2013, Pages 1-4.
62. Yong-Rong Dong, Hirokazu Kaku, Kei Hanafusa, Kiyooki Moriuchi and Toshio Shigematsu. A Novel Titanium/Manganese Redox Flow Battery *ECS Trans.* 2015, 69 ,59.
63. Mingjun Nan, Lin Qiao, Yuqin Liu, Huamin Zhang, Xiangkun Ma, Improved titanium-manganese flow battery with high capacity and high stability, *Journal of Power Sources*, Volume 522, 2022, 230995,
64. Skyllas-Kazacos, M. Rychcik, M. Robins, R. G. Fane, A. G. Green, M. A. New All-Vanadium Redox Flow Cell, *Journal of the Electrochemical Society*, Volume 133, Issue 5, pp. 1057 (1986).
65. M. Rychcik, M. Skyllas-Kazacos, Characteristics of a new all-vanadium redox flow battery, *Journal of Power Sources*, Volume 22, Issue 1, 1988, Pages 59-67.
66. A.A. Shah, H. Al-Fetlawi, F.C. Walsh, Dynamic modelling of hydrogen evolution effects in the all-vanadium redox flow battery, *Electrochimica Acta*, Volume 55, Issue 3, 2010, Pages 1125-1139.
67. Maria Skyllas-Kazacos, Leesean Goh, Modeling of vanadium ion diffusion across the ion exchange membrane in the vanadium redox battery, *Journal of Membrane Science*, Volumes 399–400, 2012, Pages 43-48.

68. Theresa Sukkar, Maria Skyllas-Kazacos, Water transfer behaviour across cation exchange membranes in the vanadium redox battery, *Journal of Membrane Science*, Volume 222, Issues 1–2, 2003, Pages 235-247.
69. Kale, Mayank. "Modeling and Simulation of Vanadium Redox Flow Batteries."
70. Maria Skyllas-Kazacos, Barry J. Welch, Reduction of sulphur in  $\text{PbS}$   $\text{PbCl}_2$   $\text{NaCl}$  melts, *Electrochimica Acta*, Volume 25, Issue 2, 1980, Pages 179-182,
71. Ao Tang, Simon Ting, Jie Bao, Maria Skyllas-Kazacos, Thermal modelling and simulation of the all-vanadium redox flow battery, *Journal of Power Sources*, Volume 203, 2012, Pages 165-176,
72. Dixuan Cheng, Yuehua Li, Chao Han, Zhangxing He, Jing Zhu, Lei Dai, Wei Meng, Ling Wang, Endowing electrospun carbon fiber with excellent electrocatalytic properties towards  $\text{VO}_2^+/\text{VO}^{2+}$  redox reaction for vanadium redox flow battery by in situ iridium decoration, *Colloids and Surfaces A: Physicochemical and Engineering Aspects*, Volume 586, 2020, 124137,

## Chapter 2 Factors affecting the performance of all-vanadium liquid flow batteries

Since the composition of the all-vanadium redox flow battery system mainly includes three parts (Fig. 2.1): the stack body, the electrolyte and the control system, there are three main factors affecting the performance of the all-vanadium redox flow battery. They are the stack body, electrolyte and external factors. The current research on all-vanadium redox flow batteries is also mainly aimed at these three aspects. Among them, the most important thing is the research of the stack body.

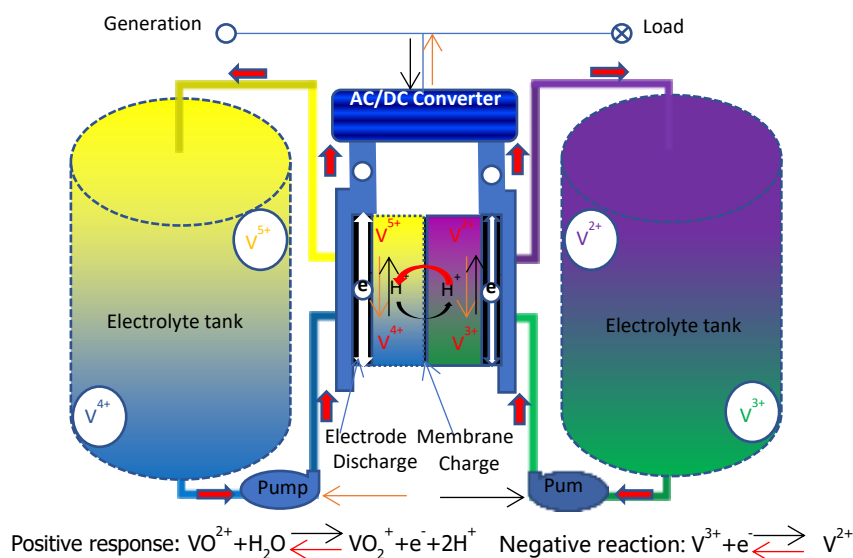


**Fig. 2.1.** The VRFB charge and discharge principle diagram

The research on the body of the stack mainly includes two aspects, one is the aspect of the composition of the stack. The second is the electrolyte flow path inside the stack. The composition of the stack has been described in detail above. Among them, the main materials include carbon fiber electrodes, bipolar plates and separators. Carbon fiber electrodes, as a battery charging and discharging site, have attracted the attention of researchers. The charge-discharge performance of the electrode is improved by various methods. With the deepening of research, the charge-discharge current density of all-vanadium redox flow batteries has been increased from  $30\text{mA}/\text{cm}^2$  at the beginning to  $80\text{-}100\text{mA}/\text{cm}^2$ . In terms of current density alone,

the improvement of the charge-discharge performance of the all-vanadium redox flow battery is the fastest compared to other batteries.

Regarding the electrolyte, it is mainly the concentration of the electrolyte and the method of adding other active substances to improve the battery capacity. Since the viscosity of the electrolyte is about 3 times that of water (for example, 1.6mol electrolyte), the viscosity of the electrolyte needs to be considered while increasing the concentration of the electrolyte. As the viscosity increases, the load of the pump increases and the uniform fluidity of the electrolyte inside the stack will also be greatly affected. In addition, the concentration of the electrolyte increases as the temperature increases, and the precipitation of vanadium is also a very important problem that needs to be solved.

In terms of external factors, the main one is temperature. The effect of temperature on battery performance is critical. One is the impact on the electrolyte mentioned above, and the other is the impact on the stack body. Since the stack shell needs to be corrosion-resistant, PCV, PP and other materials are widely used. These materials will thermally deform when the temperature increases, which will affect the battery's charge and discharge performance while affecting the battery's sealing.

## **2.1 Stack component material properties**

The factors affecting the battery performance have been briefly introduced in the previous section, and the following three factors will be explained one by one. The first is the material of the stack body. Through the literature survey, the important components of the stack are introduced.

### ***2.1.1 Effect of carbon felt electrodes on battery performance***

Carbon fiber is a fiber made by carbonizing acrylic fiber or pitch (a by-product of petroleum, coal, coal tar, etc.) at high temperatures(**Fig. 2.2**). A fiber obtained by thermally carbonizing an organic fiber precursor contains 90% or more carbon in a mass ratio. As an important advanced reinforcement material, carbon fiber has the advantage of being "light and strong." Compared with iron, its specific gravity is 1/4, its specific strength is 10 times, and its specific elastic

modulus is 7 times [1-4]. In addition, it has excellent wear resistance, heat resistance, thermoelasticity, acid resistance and electrical conductivity. Disadvantages include high manufacturing cost [5-8], difficulty in processing and difficulty in recycling. In addition, the material itself is anisotropic.

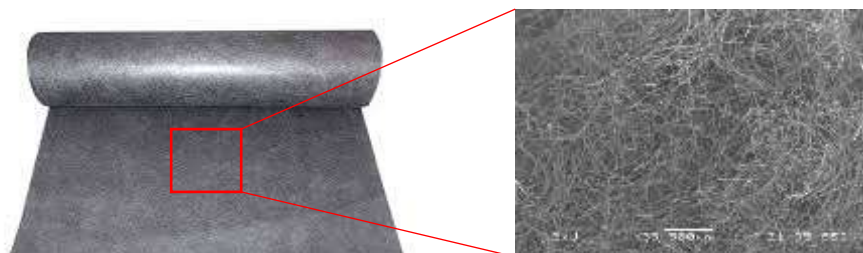


**Fig. 2.2** Commercially available carbon felt electrodes

Currently, carbon fiber is rarely used as a single material, but is mainly used as a composite material in combination with a base material such as synthetic resin. Its composite materials have been widely used in the fields of aerospace, sporting goods, automobile manufacturing, energy development, and civil engineering [9-11]. Carbon fiber can be divided into polyacrylonitrile-based carbon fiber, pitch-based carbon fiber, viscose-based carbon fiber, phenolic-based carbon fiber, and vapor-grown carbon fiber according to the source of raw materials. At present, the largest amount is polyacrylonitrile PAN-based carbon fiber. Over 90% of the carbon fibers on the market are mainly PAN-based carbon fibers[12-16].

In the face of such a huge market demand, more and more researches on PAN-based carbon fibers have been conducted. Among them, the surface treatment is mainly used to increase the mechanical properties of carbon fiber, to ensure that there is an ideal fiber/matrix interface, to ensure that the effective load is transferred from one fiber to another through the matrix [17,18]. The interface performance largely depends on the surface of the carbon fiber. Therefore, the surface treatment of carbon fiber can be used to obtain a good interface and a composite material with perfect mechanical properties [19, 20]. Carbon fiber surface oxidation is currently the main surface treatment technology. Surface oxidation can increase the number of functional groups on the surface of the fiber, thereby enhancing interfacial bonding. However, strong interface bonding is not necessarily conducive to the mechanical properties of composite materials,

especially ceramic matrix composite materials [21, 22]. Heat treatment is another treatment technology of carbon fiber, which has been applied to the preparation of carbon fiber reinforced ceramic matrix composites [23-25].

As a key component of the VRFB, the electrode not only provides the site for the redox reaction of vanadium ions but also plays an important role in the performance of the battery. The performance of the electrode directly affects the charging and discharging performance of the VRFB. Carbon felt is a widely used electrode material due to its good stability, high conductivity and low cost. However, carbon felt electrodes also have some disadvantages, such as poor electrochemical activity and a small specific surface area. These problems need to be solved by surface modification.

With the gradual attention of energy storage, the research on all-vanadium redox flow batteries is also increasing. Since 1992 Maria Skayllas-Kazakos published paper[26]. It is mentioned in the text that heat treatment can increase the functional groups on the electrode surface and increase the hydrophilicity and specific surface area of the electrode. There were relatively few papers published in 1989-2009, and a lot more after 2010. Most of them pursue the hydrophilization of the electrode surface and enlarge the specific surface area.

In 2016, Venkata Yarlagadda et al. published a paper [27,28] showing studies which increased the specific surface area of the electrode to 29 times the original one by producing multi-walled carbon nanotubes directly on the electrode surface by the electrical deposition method (**Fig. 2.3**). The efficiency of the H<sub>2</sub>-Br<sub>2</sub> fuel cell was 16% higher than that using a triple-layer fuel cell at an 80% discharge voltage. In 2019, H.R. Jiang et al. published a paper [29,30] in which a two-hole graphite felt electrode was prepared by a simple and effective catalytic etching method with seven times the specific surface area of the original stone carbon felt, current densities of 300 and 400 mA/cm<sup>2</sup> and energy efficiencies of 82.47% and 77.69%. The performance of the carbon felt electrode was effectively improved.

In the same year, Igor Derr and others in Germany published a paper comparing the performance of positive and negative electrodes under different conditions through charge and discharge experiments[31-33]. Analysis of the electrodes after continuous charge and discharge shows that both positive and negative electrodes are oxidized to generate functional groups, but

the number of negative electrodes is increased. Therefore, increasing the functional group may not necessarily improve the performance of the battery.

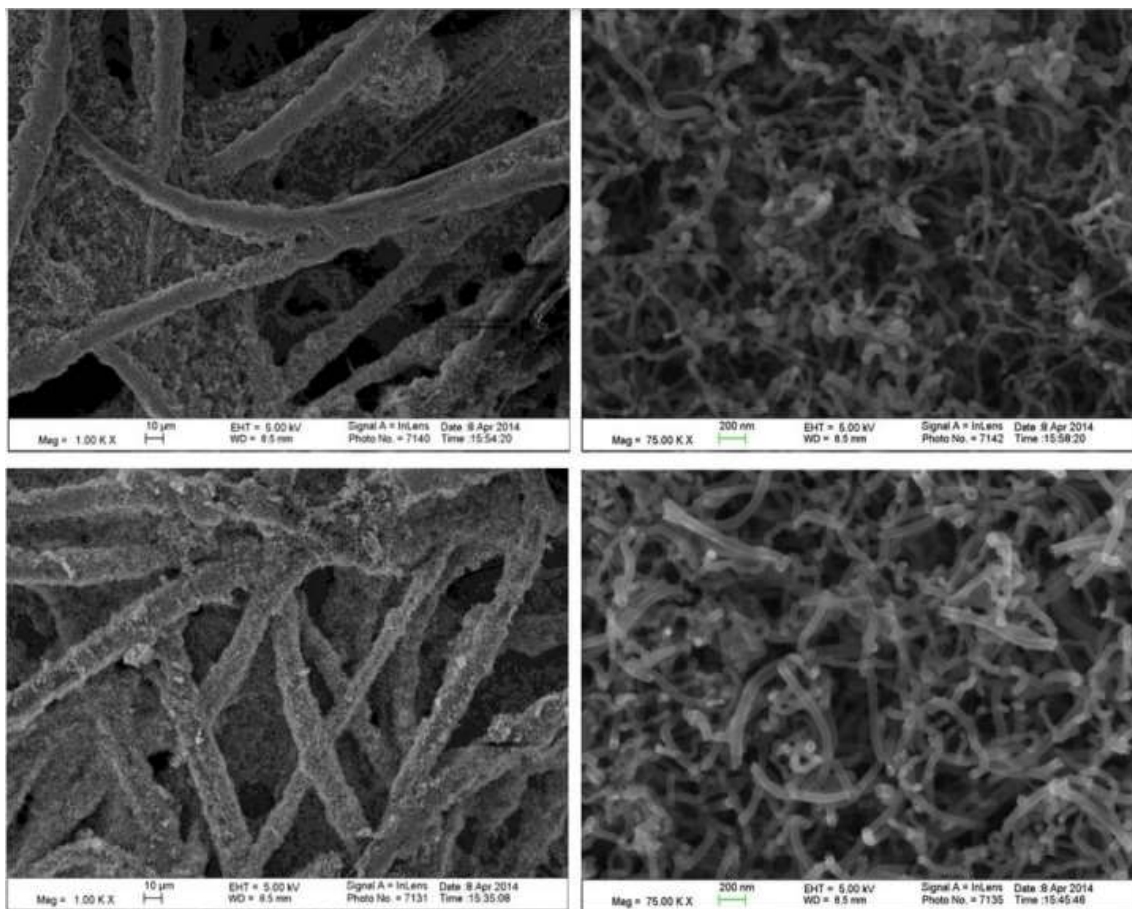


**Fig. 2.3** Pre-soaked carbon electrodes (in  $\text{CoSO}_4$  and  $\text{H}_3\text{BO}_3$ ) after MWCNT growth a) sample 4 (resynthesized) and b) sample 5. [27]

In 2019, the T.S. Zhao team of Hong Kong University of Science and Technology published a paper [34]. The reasons indicated by the voltage were studied, the design of the battery was adjusted, the charge-discharge resistance of the battery was reduced, and the surface activity of the electrode was improved. Unprecedented improvements in VRFB performance through these experiments. At current densities of 200, 400, and 600  $\text{mAcm}^2$ , the energy efficiencies of the cells were 91.98%, 86.45%, and 80.83%, and the electrolyte utilization rates were 87.97%, 85.21%, and 76.98%, respectively. Even at an ultra-high current density of 1000  $\text{mA cm}^2$ , the battery still maintains an energy efficiency of up to 70.40%. At room temperature, the cell achieves a peak power density of 2.78  $\text{W cm}^2$  and a limiting current density of  $\sim 7$   $\text{A cm}^2$ . Furthermore, the cell can be cycled stably for more than 20,000 cycles at a high current density of 600  $\text{mAcm}^2$  (Fig. 2.4- Fig. 2.5)

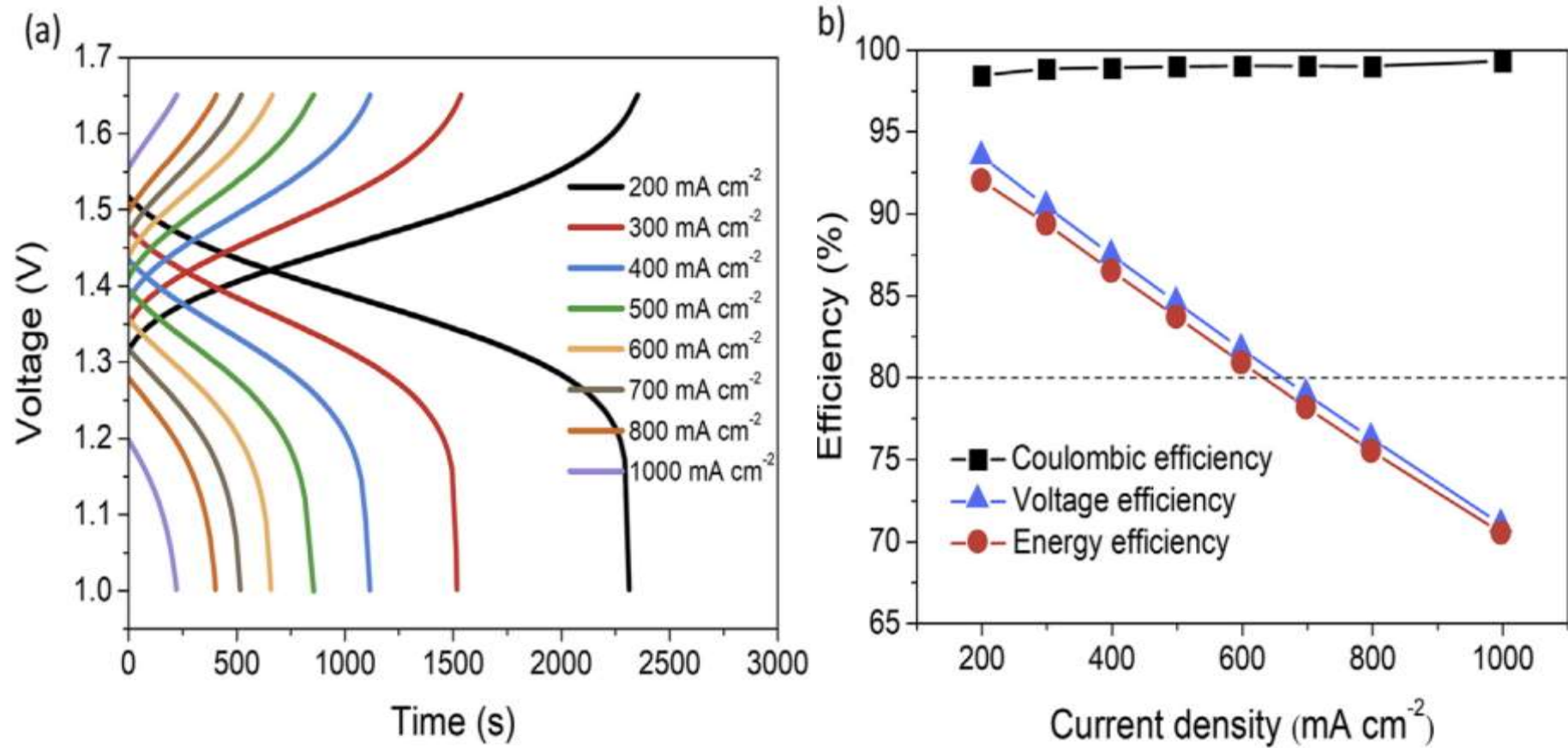


**Fig. 2.4.** (a) The charge-discharge curves of the designed high-performance VRFB at the current densities ranging from 200 to 1000 mAcm<sup>2</sup>. (b) The coulombic, voltage and energy efficiencies of the designed high-performance VRFB[34].

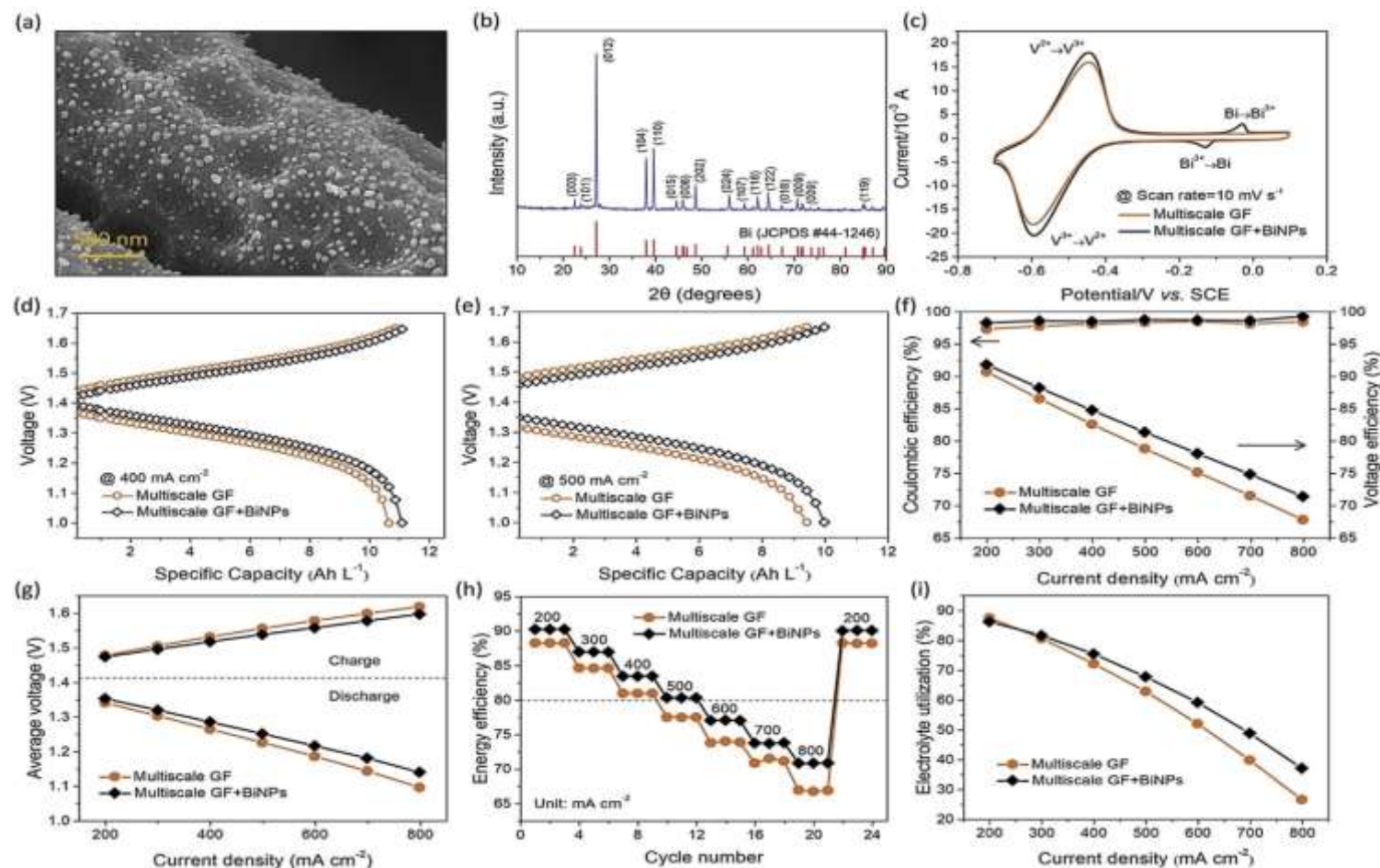


**Fig. 2.5.** (a) SEM image and (b) XRD pattern of multiscale GF + BiNPs. (c) CV curves of multiscale GF in solutions with and without Bi<sup>3+</sup> with the potential windows of -0.7 to 0.1 V vs. SCE at the scan rate of 10 mV s<sup>-1</sup>. The charge-discharge curves of VRFBs with multiscale GF and multiscale GF+ BiNPs at the current densities of (d) 400 and (e) 500 mA cm<sup>2</sup>. The (f) coulombic and voltage efficiencies, (g) average voltage, (h) energy efficiency changes as cycle numbers, and (i) electrolyte utilization of VRFBs with multiscale GF and multiscale GF+BiNPs[34]

### ***2.1.2 Effect of electrolyte on battery performance***

There are two main methods for preparing electrolyte: mixed heating preparation method and electrolysis method. Among them, the mixed heating method is suitable for preparing 1mol/L electrolyte solution, and the electrolysis method can prepare 3~5mol/L electrolyte solution. The electrolyte of all-vanadium redox flow battery was initially prepared by mixing and heating to directly dissolve  $\text{VOSO}_4$  in  $\text{H}_2\text{SO}_4$ , but due to the high price of  $\text{VOSO}_4$ , it is not suitable for large-scale application. Therefore, people began to turn their attention to other vanadium compounds such as  $\text{V}_2\text{O}_3$ ,  $\text{V}_2\text{O}_5$ ,  $\text{NH}_4\text{VO}_3$ [35]. Although the cost is reduced, these compounds have poor solubility in sulfuric acid, so it is difficult to obtain high-concentration electrolytes by mixing heating.

The electrolysis method is based on  $\text{V}_2\text{O}_5$  or  $\text{NH}_4\text{VO}_3$  as raw materials, adding the same concentration of  $\text{H}_2\text{SO}_4$  and  $\text{H}_2\text{SO}_4$  solution containing  $\text{V}_2\text{O}_5$  to the positive and negative electrodes of the electrolytic cell, and then adding appropriate direct current to the positive and negative electrodes to generate divalent and Trivalent vanadium. This method can prepare high-concentration vanadium electrolytes in large quantities. At the same time, the operation is relatively simple, and it is easier to realize industrial production. The disadvantage is that the speed is slow, the equipment requirements are higher, and the energy consumption is high.

At present, the widely used electrolytes for all-vanadium redox flow batteries are mainly low-concentration and high-concentration electrolytes. The concentration of the electrolyte directly affects the capacity of the battery. Theoretically, with the same volume of electrolyte, using a high concentration of electrolyte, the capacity of the battery will be doubled. But this is only considering capacity. As a battery, its charge-discharge performance is also an important evaluation index. Using high-concentration electrolyte, the resistance of the electrolyte will increase, the viscosity of the fluid will be greatly increased, and the flow rate of the electrolyte will be reduced, which increases the load of the pump and increases the internal consumption of the entire system. Therefore, to improve the stability of the electrolyte, a lot of experiments are needed.

Skyllas-Kazaco's research group found through research that the concentration of vanadium ions is below 3mol/L and the concentration of sulfuric acid is 3-4mol/L is more stable than the solution of 2mol/L, and the charge-discharge performance of the electrolyte is better [36]. At the same time, they also studied the solubility of  $\text{VOSO}_4$  in  $\text{H}_2\text{SO}_4$ , and the results showed that the solubility decreased with the increase of sulfuric acid concentration. While studying the effect of electrolysis and concentration on battery performance, mixed acid electrolytes have also been proposed. Hydrochloric acid or organic substances are added to the electrolyte as a new supporting electrolyte. Liu et al. used tetrabutylamine tetrafluoroborate as the supporting electrolyte and vanadium acetylacetonate as the electrolyte to assemble a flow battery, and obtained a coulombic efficiency close to 50(**Fig. 2.6.**)[37]. Kim et al. utilized hydrochloric acid as the electrolyte. It can dissolve 3mol/L vanadium ions of various valence states without precipitation[38].

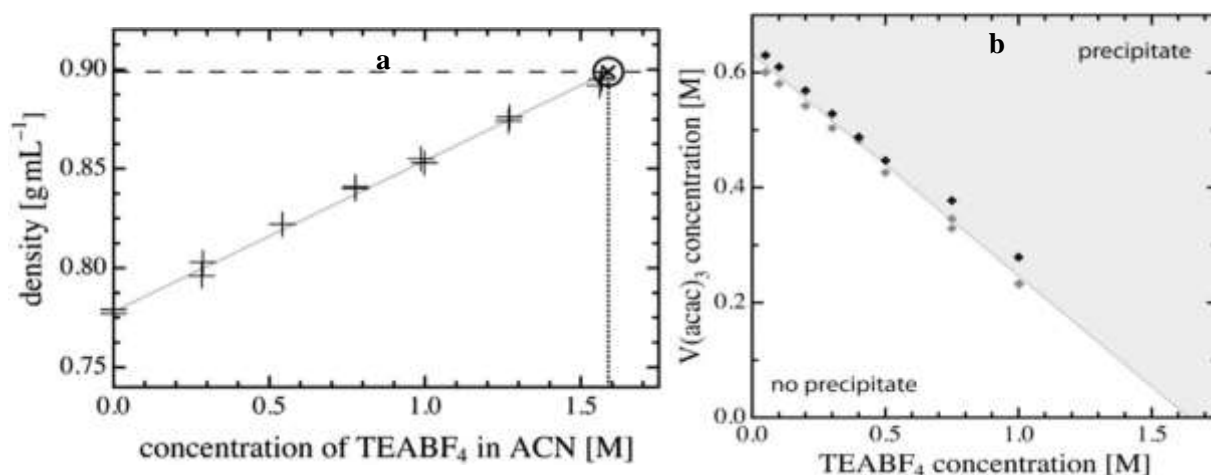


**Fig. 2.6. a:** . Densities of binary solutions of TEABF<sub>4</sub> in ACN vary with solute concentration. **b:**Phase diagram that establishes the maximum solubility of V(acac)<sub>3</sub> active species as a function of TEABF<sub>4</sub> concentration in ACN at room temperature[37].

### 2.1.3 Effect of ion exchange membrane on battery performance

Ion exchange membranes are thin films made of polymer materials with ion exchange properties (inorganic ion exchange strands are also available, but their use is not yet common). It is similar to ion exchange resin in that an active group is attached to the polymer backbone,

but the mechanism, method and effect are different. There are many types of ion exchange membranes on the market, and there is no uniform classification method. Generally, it is divided into three categories according to the macroscopic structure of the film:

1. Heterogeneous ion-exchange membrane is made of powdered ion-exchange resin and binder, kneading, pulling tabs, and hot-pressing with mesh. The resin is dispersed in the binder, so its chemical structure is not uniform.

2. Homogeneous ion exchange membrane Homogeneous ion exchange membrane is made by introducing active groups into an inert support. It has no heterogeneous structure and is homogeneous by itself. Its chemical structure is uniform, the pores are small, the membrane resistance is small, it is not easy to leak, and the electrochemical performance is excellent, and it is widely used in production. But the production is complicated and the mechanical strength is low.

3. Semi-homogeneous ion exchange membranes are also made by introducing active groups into polymer supports. But the two do not form a chemical combination, and their performance is between the homogeneous ion exchange membrane and the heterogeneous ion exchange membrane.

In addition, ion exchange membranes can be divided into five types according to their functions and structures: cation exchange membrane, anion exchange membrane, amphoteric exchange membrane, mosaic ion exchange membrane, and polyelectrolyte composite membrane. The construction of the ion exchange membrane is the same as that of the ion exchange resin, but in the form of a membrane.

Cation exchange membranes are widely used in vanadium redox flow batteries. Mainly with Nafion exchange membrane. According to different thickness, it is divided into N212(Fig. 2.7), N211, N117 and other models. When the battery is charged, the trivalent vanadium of the negative electrode loses electrons and becomes divalent vanadium. According to energy conservation,  $H^+$  passes through the exchange membrane to the positive electrode, so the positive electrode changes from tetravalent vanadium to pentavalent vanadium.

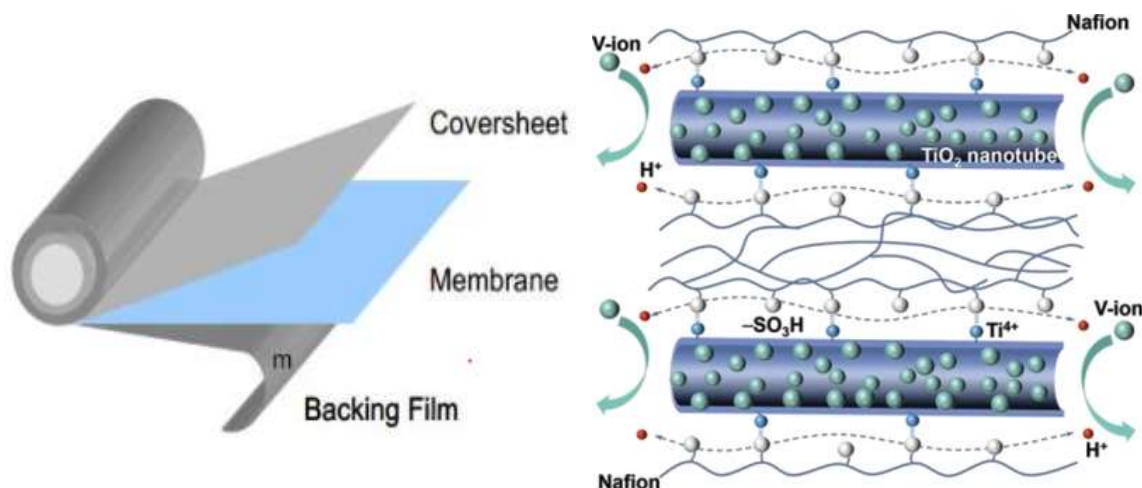


**Fig. 2.7** Ion exchange membranes and how they work

With the increase of research efforts, people have conducted comparative experiments on various exchanges to find and develop ion exchange membranes that are more suitable for all-vanadium redox flow batteries. In 2005, Zhang Huamin and others published a paper, using anion exchange membrane JAM-10 and cation exchange membrane Nafion-117 for all-vanadium redox flow batteries[39]. The research on its physical and electrochemical properties showed that the mechanical strength of perfluorinated Nafion-117 membrane and The chemical stability is better than that of the JAM-10 film, and the Nafion-117 film has good electrical conductivity and is suitable for high current charge and discharge, but the positive and negative vanadium solutions are easier to penetrate each other, the transfer of water is fast, and the coulombic efficiency of the battery is lower than that with JAM -10 membrane battery. The JAM-10 membrane has a repulsive effect on cations, which can effectively inhibit the cross-contamination of the positive and negative solutions, but the water transfer slows down and the electrode resistance increases; the coulombic efficiency of the JAM-10 membrane battery is high, but the voltage efficiency is low and the current is large. It is more obvious when charging and discharging.

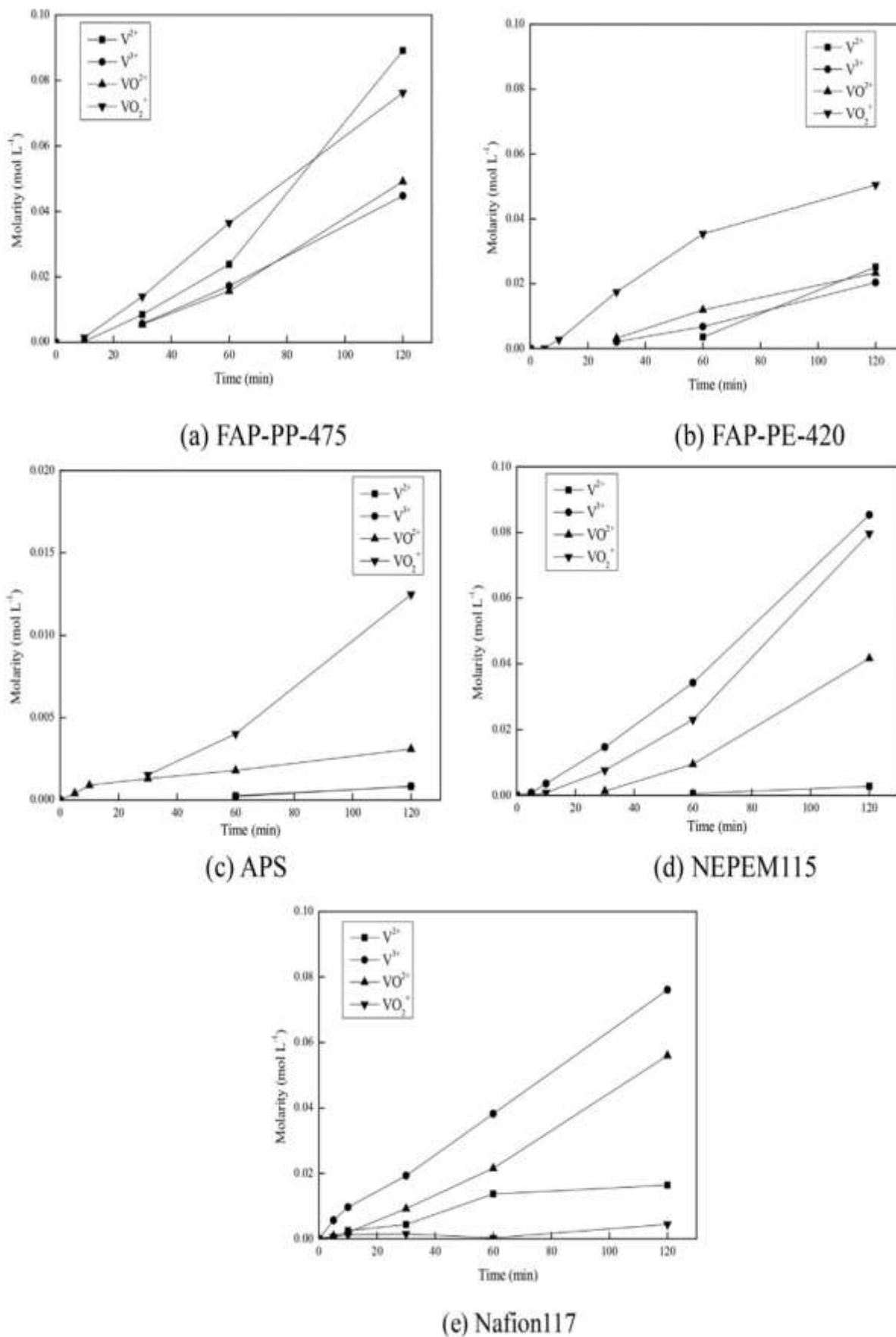


Fig. 2.8. Performance comparison of different ionic membranes[40].

In 2018, Gab-JinHwang et al. tested three commercial anion exchange membranes and two commercial cation exchange membranes as separators for all-vanadium redox flow batteries (VRFBs) [40]. Membrane properties such as ionic conductivity and permeability of each vanadium ion were evaluated. The ionic conductivity decreased sequentially: Nafion117  $\approx$  APS > NEPEM115 > FAP-PP-475 > FAP-PE-420 (**Fig. 2.8**). Anion exchange membranes have low permeability to vanadium ions compared to cation exchange membranes. The energy efficiencies of VRFBs using commercial ion exchange membranes are almost identical in the range of 76.0-78.7%.

### ***2.1.4 Effect of bipolar plates on battery performance***

The bipolar plate, also known as the collector plate, is one of the important components of the battery. It has the following functions and properties: separates the positive and negative electrodes, prevents the cross-mixing of the positive and negative electrolytes; collects and conducts current, with high conductivity; designed and processed flow channels can provide flow space for the electrolyte; corrosion resistance; impact resistance and vibration; thin thickness; light weight; at the same time low cost, easy machining, suitable for mass production, etc.

At present, the materials used in battery bipolar plates can be roughly divided into three categories: carbon materials, metal materials and composite materials of metal and carbon.

(1) Carbon materials. Carbonaceous materials include graphite, molded carbon materials, and expanded (flexible) graphite. Conventional bipolar plates use dense graphite that is machined to form gas flow channels. Graphite bipolar plate has stable chemical properties and low contact resistance with MEA.

(2) Metal materials. Metal materials such as aluminum, nickel, titanium and stainless steel can be used to make bipolar plates. The metal bipolar plate is easy to process, can be manufactured in batches, has low cost, thin thickness, and has high volume specific power and specific energy of the battery.

(3) Composite materials. If the contact resistance between the bipolar plate and the MEA is large, the polarization loss caused by the ohmic resistance is large, and the operation

efficiency is reduced. Among the commonly used bipolar plate materials, graphite material has the smallest contact resistance, and non-conductive oxide films are formed on the surfaces of stainless steel and titanium to increase the contact resistance.

The all-vanadium redox flow battery is the first one that is widely used due to the corrosiveness of the electrolyte. For the research on the bipolar plate of vanadium redox flow battery, it is mainly to add some elements on the basis of carbon plate to change the original chemical and physical properties. For example, adding resin to increase airtightness, adding graphene to increase conductivity, etc.

In the 1980s, Maria Skyllas-Kazacos first published a battery using vanadium ions for both positive and negative electrodes, and successfully conducted a charge-discharge experiment. At that time, they used artificial graphite plates, the current density was only  $3\text{mA}/\text{cm}^2$  (**Fig. 2.9A**), and the impedance was very large, because they only used bipolar plates and didn't use carbon ion, which led to the voltage exceeding 2V and corrosion at the positive electrode [41].

In 1987, they used carbon felt and bipolar plates to assemble batteries for the first time (**Fig. 2.9B**) [42]. The structure is the same as that of NASA, and it is also the most widely used assembly method. In this way, the current density reaches  $40\text{mA}/\text{cm}^2$  and the energy efficiency is 73% [43]. In 1989, they used carbon felt, graphite powder and polymethylene bipolar plate for the first time, and the energy density reached 86% under the current density of  $30\text{mA}/\text{cm}^2$  [44]. At the same time, the corrosion of the bipolar plate disappeared after using the carbon felt. From 1991 to 1995, they published papers successively. By adjusting the ratio of bipolar plates, they obtained the best preparation method of bipolar plates.

## **2.2 Impact of stack structure on battery performance**

Due to the complexity of the internal structure of the all-vanadium redox flow battery, the influence of the internal structure of the stack on the performance of the battery is also very critical. At the same time as the design and development of the stack, some key points affecting the battery performance that need to be considered are introduced in detail below.

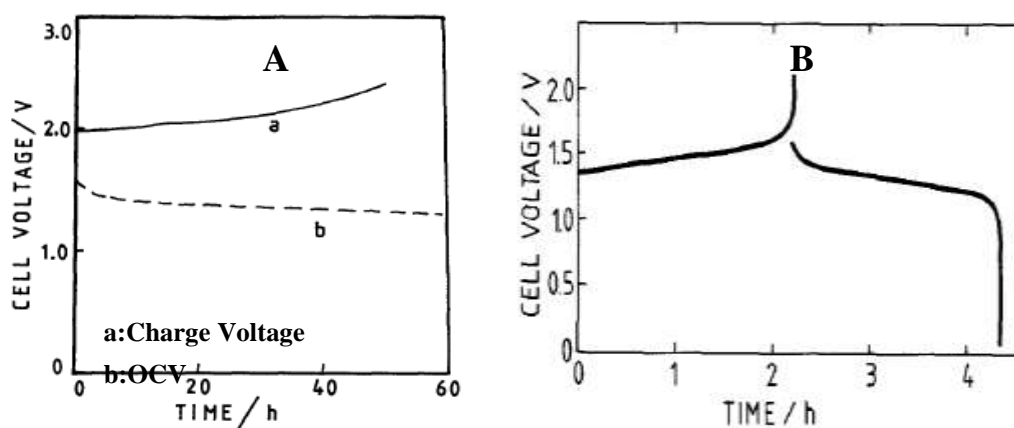


Fig. 2.9 Charge-discharge curve.[41.42]

### 2.2.1 Effect of electrolyte flow path on battery performance

The electrolyte flow channel refers to the flow mode of the electrolyte inside the stack. By processing the bipolar plate, the electrolyte flows along the processing route. At present, there are three types of flow channels used in all-vanadium redox flow batteries, namely DC type, serpentine type and comb type (Fig. 2.10).

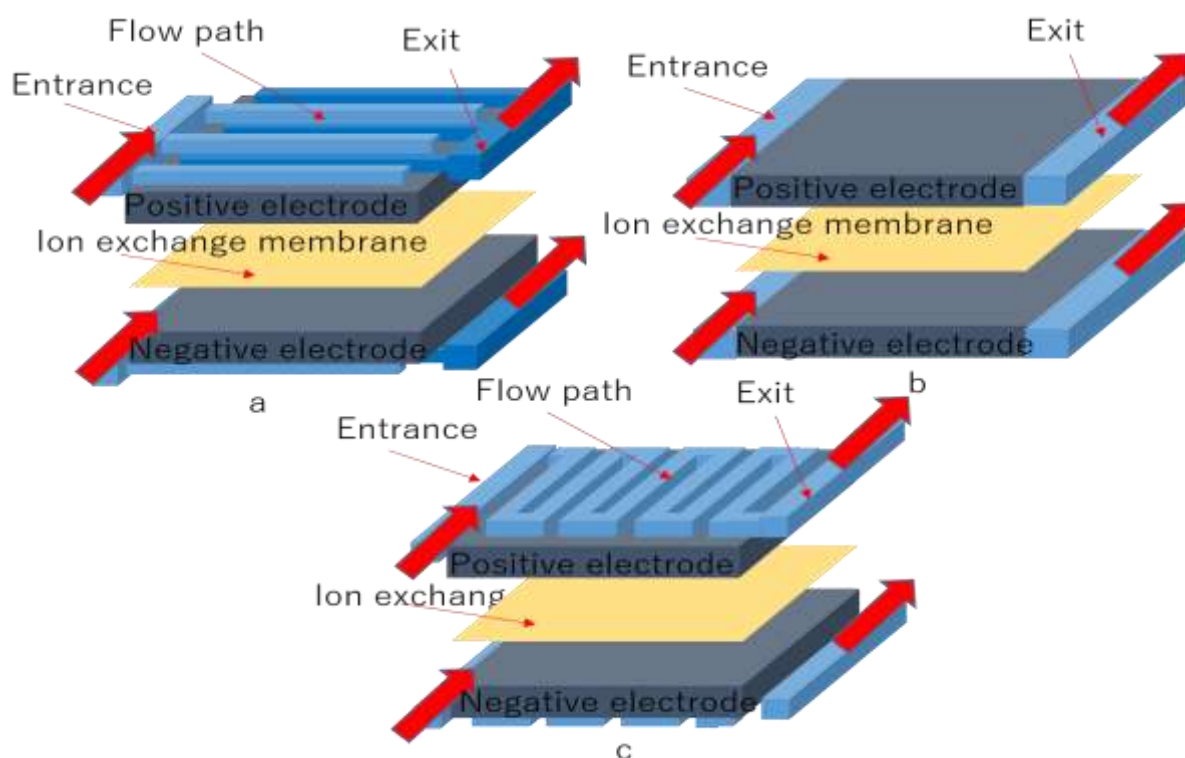
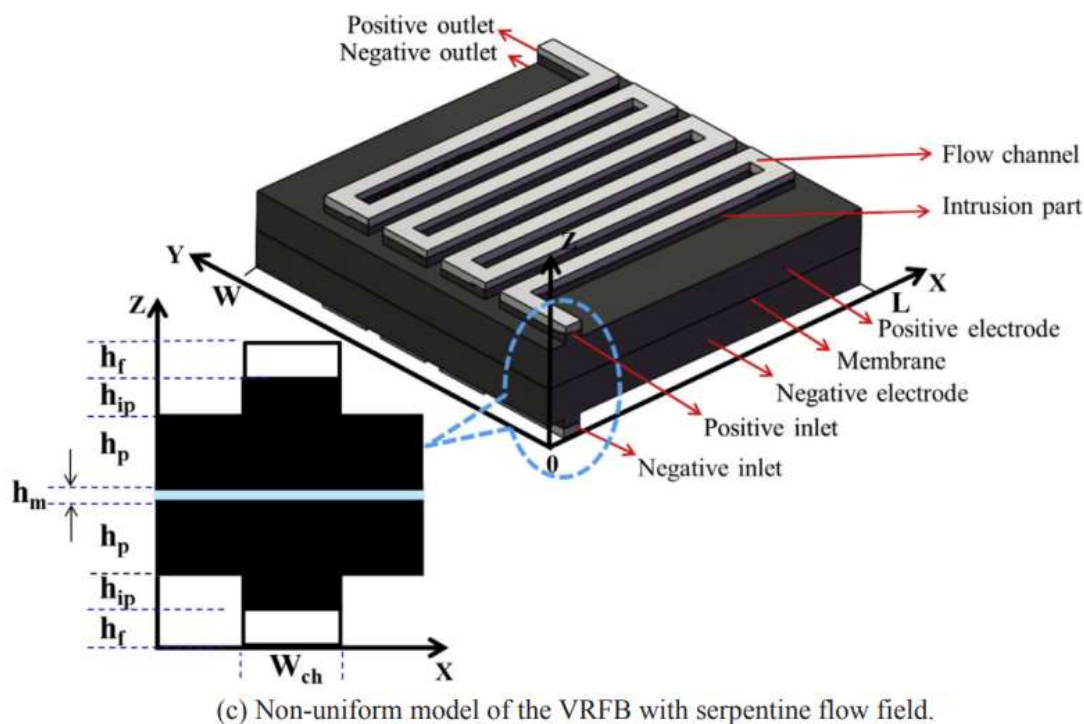


Fig. 2.10 Three different electrolyte flow paths

Among them, the DC type (**Fig. 2.10b**) is a common type, which does not need to process the flow channel, so that the electrolyte flows freely from bottom to top in the carbon felt under the action of the pump. The advantage of this method is that there is no need to process the bipolar plate, and the cost is low. The serpentine flow channel is processed by processing the flow channel as shown in **Fig. 2.10c**, and the electrolyte flows from the inlet to the outlet in the flow channel. This kind of flow channel is proved by experiments that it is not very conducive to the charging and discharging of the vanadium redox flow battery after the size of the stack is enlarged. Because the electrolyte of the battery is charged and discharged inside the stack, the reacted electrolyte needs to flow out of the stack in time, otherwise it will cause the imagination of the local voltage inside the stack to be too high, which will affect the charge and discharge performance of the battery. The comb-shaped flow path is shown in **Fig. 2.10a**. The electrolyte enters from the inlet and then diffuses to the outlet flow channels on both sides perpendicular to the direction of the carbon felt. with liquidity.

While the battery materials are continuously improved the research on the optimization of the battery frame is also gradually paid attention by researchers. In 2018 Q. Wang et al. published a paper [45] to investigate the performance of VRFB under non-uniform compression electrode and serpentine flow field with different compression ratios (CR). The maximum concentration uniformity and the minimum current density and overpotential were obtained by optimization for a CR of 55.7% (**Fig. 2.11.**). This study is a guideline for the design of VRFBs considering compression electrodes. In the same year Ravendra Gundlapalli et al. published a paper [46]. The charge and discharge performance parameters of large VRFBs were investigated experimentally and through simulations, and the results showed that increasing the cell size increased the weight efficiency and volumetric efficiency of the stack for the same local electrochemical performance. Although the cell pressure drop increases with increasing cell size, the pressure drop in the manifold decreases as the number of channels decreases. For large VRFBs, the pressure drop can be further reduced by creating deeper recesses in the serpentine channels. 2013 Q. Xu et al. published a paper [47]. presented a three-dimensional numerical model and investigated the flow field design for three vanadium redox flow control batteries (VRFBs). The results show that for each flow field, there exists an optimal flow rate at which the optimal flow field has the highest efficiency.



**Fig. 2.11.** Geometric model for the non-uniformly compressed electrode.[45]

### 2.2.2 Effect of electrolyte flow rate and flow rate on battery performance

Due to the charge-discharge characteristics of the all-vanadium redox flow battery, as mentioned above, the reacted vanadium ions need to flow out of the stack in time, otherwise the local voltage inside the stack will be too high, thereby reducing the charge-discharge performance of the stack. At the same time, the flow rate and flow of the electrolyte will also affect the internal consumption of the battery system. If the flow rate is too large, the load of the pump will also increase accordingly. If the flow rate is too small, the electrolyte inside the battery will be overcharged. In view of the above problems, the flow rate and flow of the electrolyte have gradually been paid more attention by researchers.

In 2011, Doug Aaron of Tennessee University in the United States published a paper using a small all-vanadium redox flow battery to test the electrolyte flow [48]. The results show that when the electrolyte flow rate is  $0.5\text{mlmin}^{-1}$ , the highest current density is  $40\text{mA/cm}^2$ . When the electrolyte flow is increased to  $25\text{mlmin}^{-1}$ , the highest current density can reach  $330\text{mA/cm}^2$  (**Fig. 2.12**). Therefore, the maximum current density is increased by the increase of the flow rate of the electrode solution.

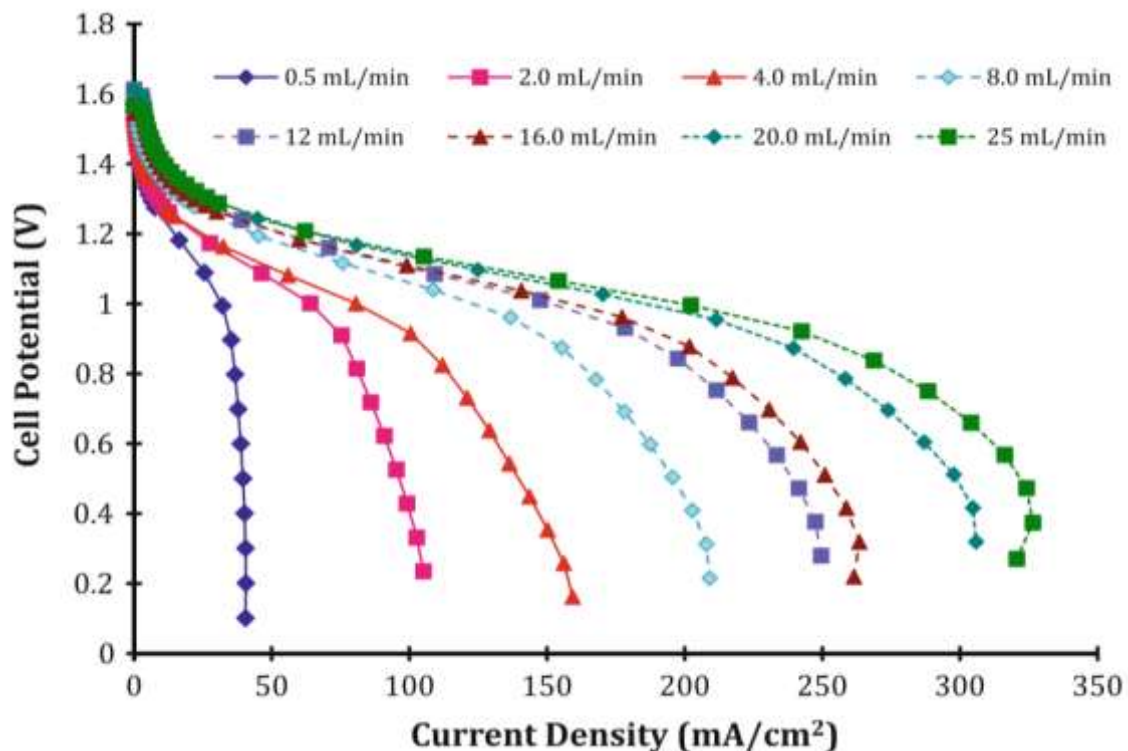


**Fig. 2.12.** Polarization curves of batteries at different electrolyte flow rates [48].

In 2012, Zhang Huamin from the Dalian Institute of Chemical Physics, Chinese Academy of Sciences published a flow rate optimization strategy for vanadium redox flow batteries [49]. In the experiment, a battery pack of 875cm<sup>2</sup> 15 cells was used to determine the effect of different flow rates on the charge and discharge of the battery pack. Experiments show that the power of the battery and the charging and discharging efficiency of the battery pack increase with the increase of the flow rate of the electrolyte, but the efficiency of the entire energy storage system decreases with the increase of the flow rate (Fig. 2.13- Fig. 2.15).

In 2014, AoTang and Maria Skyllas-Kszacos of UNSW in Australia published on the influence of vanadium redox flow battery electrolyte flow rate on batteries and battery systems [50]. In the later stage of discharge, increase the flow rate to reduce the concentration difference and improve the charge-discharge efficiency and battery capacity.

In 2016, S. Kumar of IIT-Madras in India published a paper [51] on the effect of electrolyte flow rate on battery charge and discharge power density. The experimental results show that the cell voltage is affected by the concentration potential in the high current density region, and the highest current density increases with the increase of the electrolyte flow rate. The highest power density also increases with increasing electrolyte flow rate.

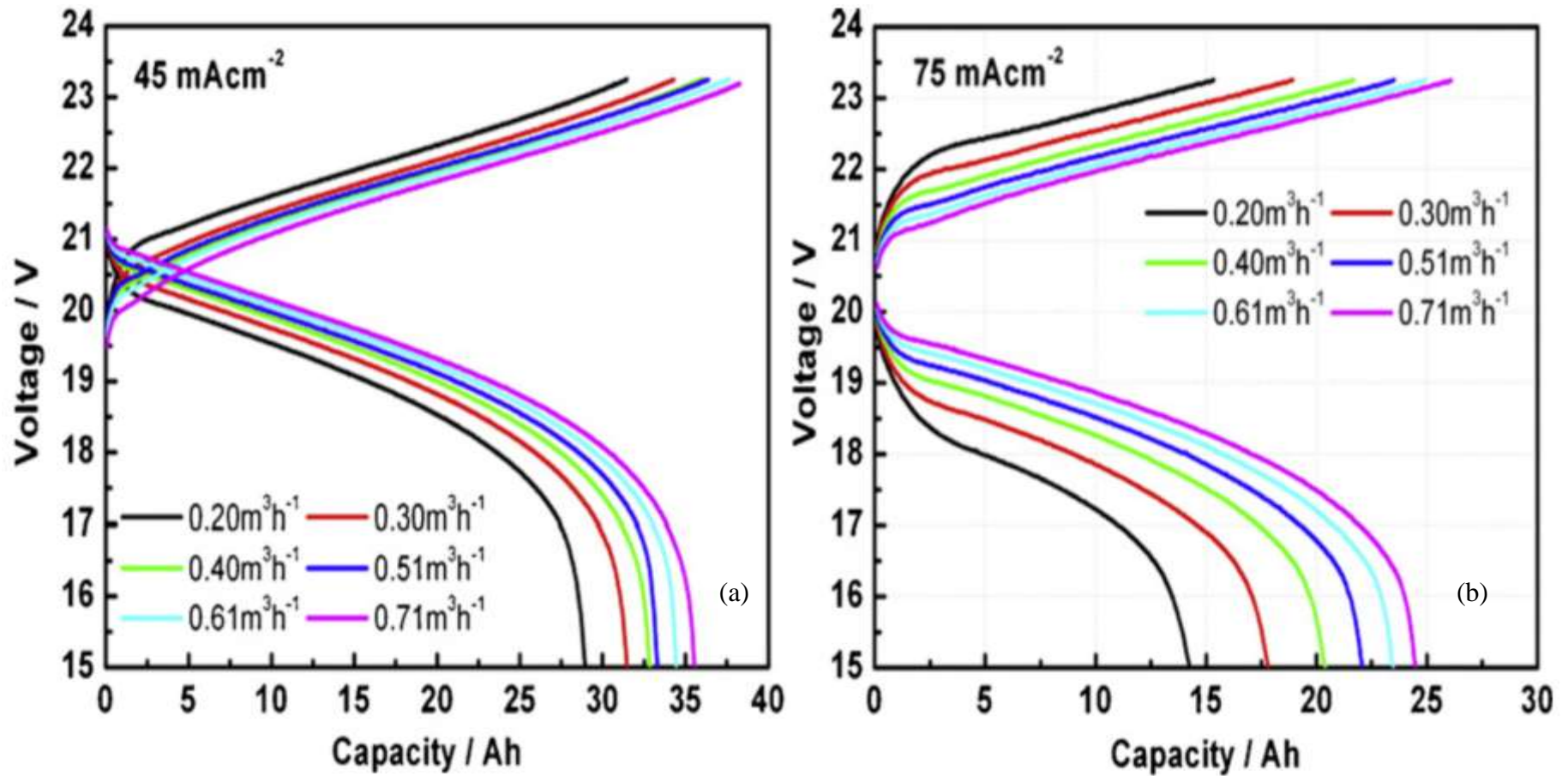


**Fig. 2.13.** The charge-discharge curves of the battery pack under different electrolyte flow rates. (a) at a charge-discharge current density of 45 mA cm<sup>-2</sup>, (b) at a charge-discharge current density of 75 mA cm<sup>-2</sup>[49].

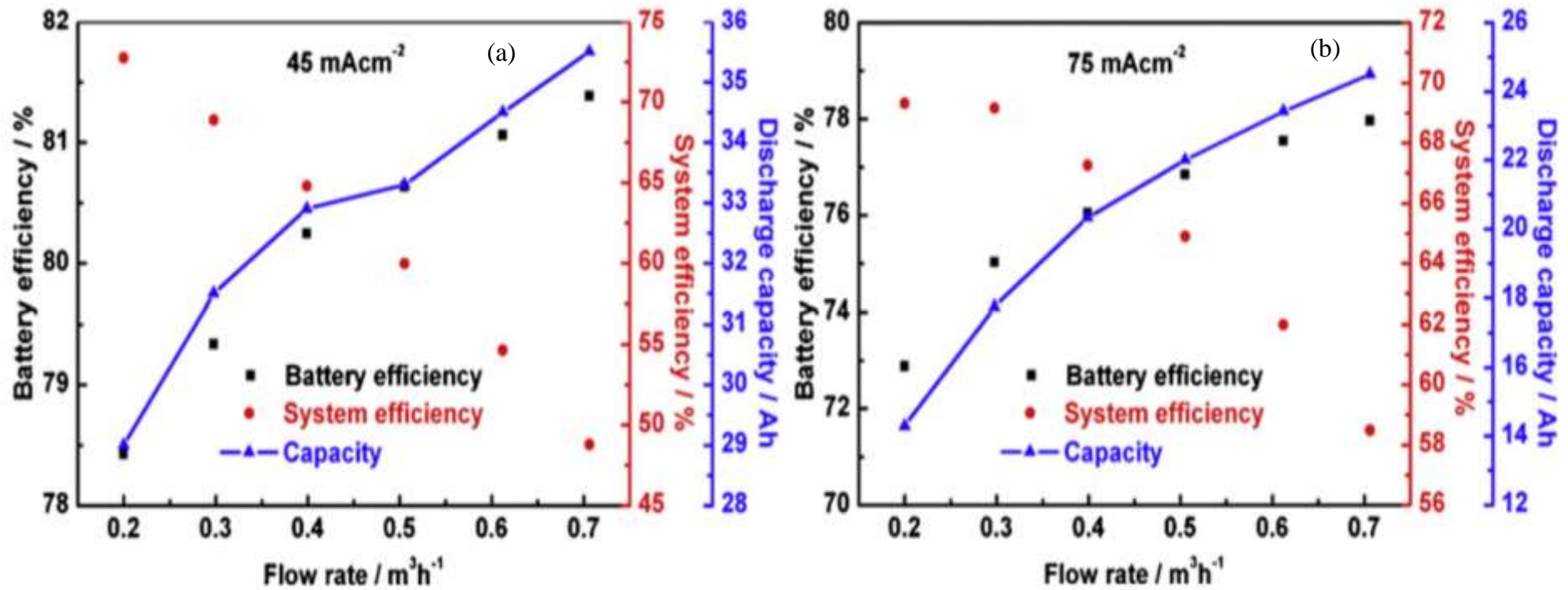


**Fig. 2.14.** The charging and discharging efficiency of the battery pack, the battery power, and the charging and discharging efficiency of the power storage system under different electrolyte flow rates. (a) at a charge-discharge current density of  $45 \text{ mA cm}^{-2}$ , (b) at a charge-discharge current density of  $75 \text{ mA cm}^{-2}$ [49]

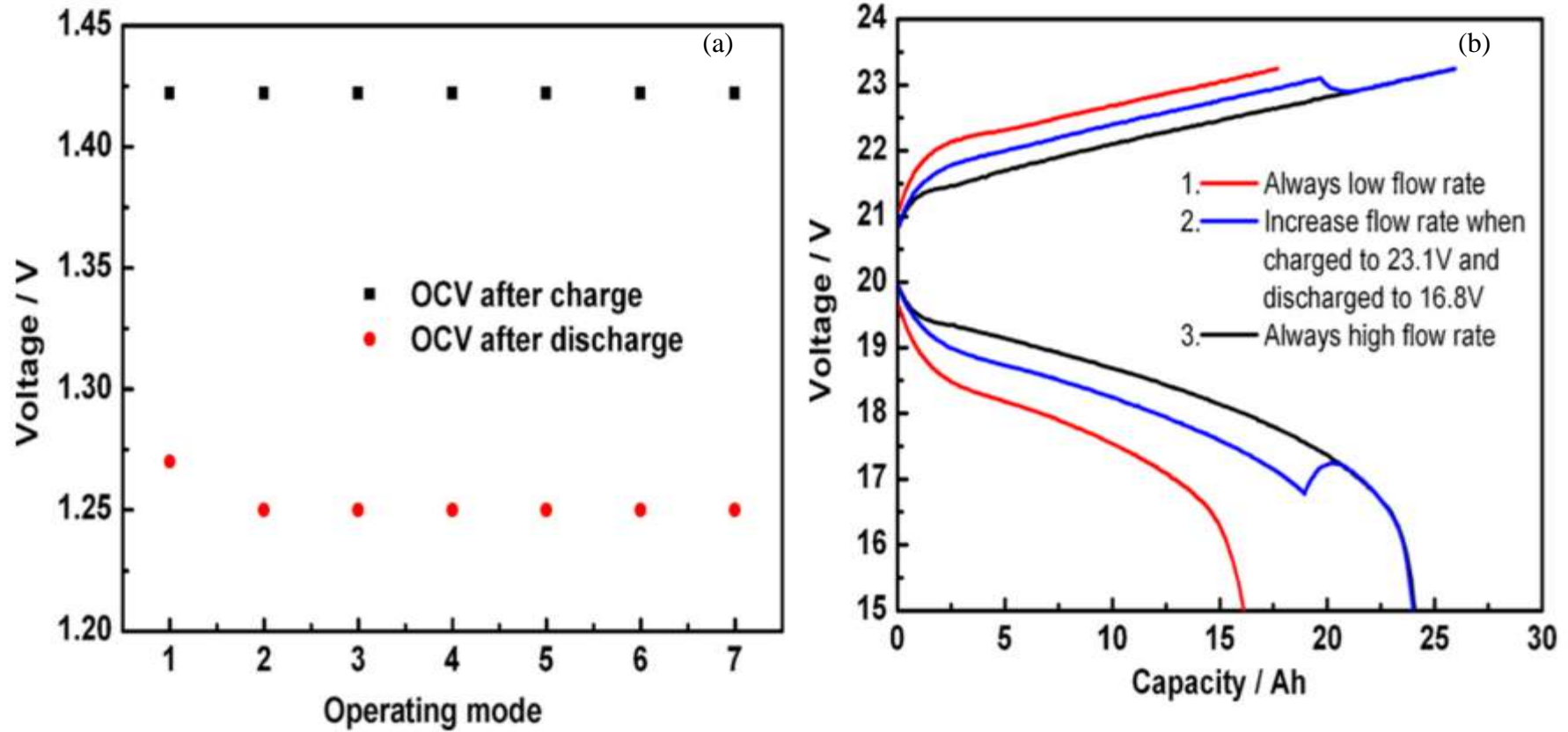


**Fig. 2.15.**(a) OCVs after charge process and discharge process at different operating modes when using an optimal strategy of flow rate for charge process. (b) Charge–discharge curves at different operating modes when using an optimal strategy of flow rate for discharge process[49]

### ***2.2.3 Effect of carbon felt compression ratio on battery performance***

As an important part of the all-vanadium redox flow battery, the carbon felt electrode not only affects the charge and discharge performance of the battery from the material, but also has a certain impact on the battery performance in terms of structure. Due to the structure of the battery, the carbon felt is between the separator and the bipolar plate, and the contact resistance between the carbon felt and the bipolar plate during charging and discharging will reduce the charging and discharging performance of the battery. How to reduce the contact resistance is also an important part of the current research. There are two ways to reduce the contact resistance, one is to add highly conductive materials, and the other is to compress the carbon felt.

In 2014, Kim et al. from South Korea published a paper. In order to reduce the contact resistance between the bipolar plate and the carbon felt, they inserted soft graphene sheets. The results showed that the energy efficiency of the battery was increased from 80% to 85% [52]. In 2015, Zhang from Sichuan University published a paper in which a bipolar plate was obtained by copolymerizing vinyl monomers. It was verified by experiments that the voltage efficiency was 80% when the current density was 50mA/cm<sup>2</sup>, and the voltage efficiency was 85% when the current density was 70mA/cm<sup>2</sup>[53].

In 2014, Se-KookPark et al. published a paper, and the results showed that the specific resistance and porosity of the electrode decreased with the increase of the electrode compression percentage[54]. Furthermore, with the increase of the electrode compression percentage, the discharge time and maximum power of VRFB cells gradually increased due to the increase of electron transfer. The energy efficiency of the battery increases with increasing electrode compression percentage, up to 20%. When the electrode compression percentage is greater than 20%, the energy efficiency decreases due to the combined effects of reduced cell resistance, poor electrolyte transport, and prolonged charge/discharge time. From our results, it can be concluded that compressing the electrodes has a positive effect on battery performance

In 2019, Chin-Lung Hsieh et al published a paper to study the effect of graphite felts with different compression ratios (CR) on the performance and efficiency of VRFBs[55]. The

impedance of a single VRFB under different graphite felt CR was measured under different working conditions. The results show that the performance of VRFB increases with the increase of CR due to the decrease of areal resistance and concentration overpotential. When the electrolyte flow rate was  $100 \text{ mL min}^{-1}$  and the current density was  $80 \text{ mA cm}^{-2}$ , the optimal energy efficiency of the porous electrode was 73% ( **Fig. 2.16**).

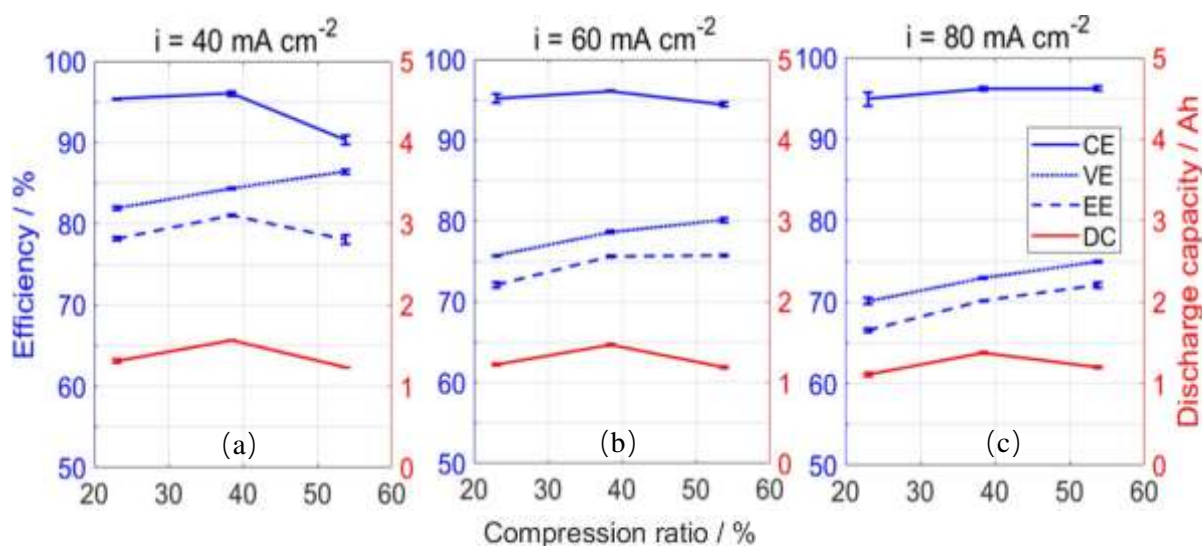


**Fig. 2.16.** Effect of CR on the coulombic, voltage and energy efficiency and discharge capacity of the VRFB operating at  $100 \text{ mL min}^{-1}$  under various current density levels: (a)  $40 \text{ mA cm}^{-2}$ ; (b)  $60 \text{ mA cm}^{-2}$ ; (c)  $80 \text{ mA cm}^{-2}$ [55].

## 2.3 Impact of external factors on battery performance

For the external factors affecting the battery performance, the main temperature is the temperature, which has a great influence on the battery body and the electrolyte. The second is the operating time of the battery. As the operating time of the battery becomes longer, the performance of the components inside the battery will be greatly changed. Finally, the effect of overcharge and discharge on the battery is irreversible. The following describes in detail the effects of various external factors on the battery.

### 2.3.1 Effect of temperature on battery performance

In the early stage of research on all-vanadium redox flow batteries, people began to pay attention to the effect of temperature changes on the performance of all-vanadium redox flow

batteries. The effect of temperature is mainly divided into two aspects, which are also mentioned above, that is, the effect on the electrolyte and the effect on the internal resistance of the battery charge and discharge. When the temperature rises, the pentavalent vanadium in the electrolyte will precipitate. At the same time, the viscosity of the electrolyte will decrease, the flow rate will increase, and the internal resistance of battery charge and discharge will be reduced.

In order to study the specific temperature at which the positive electrolyte is more likely to be precipitated. In 2009, Faizur Rahman and Maria Skyllas-Kazacos published a paper on 1000h long-term experiments on electrolytes with different sulfuric acid concentrations and different temperatures[56]. The results show that when the temperature is 50°C, the electrolyte of 3M  $V^{5+}$  6M sulfuric acid is easy to precipitate after 50h. However, the electrolyte of 2M  $V^{5+}$  6M did not precipitate at various temperatures.

In 2016, Maria Skyllas-Kazacos published a paper showing that  $V^{3+}$  is easy to precipitate at low temperature, while  $V^{5+}$  is the opposite, and the higher the temperature, the easier it is to precipitate[57]. At the same time, with the change of sulfuric acid concentration, the precipitation of positive and negative electrolytes will also change. The higher the sulfuric acid concentration, the easier the precipitation of negative electrode  $V^{3+}$ . The lower the sulfuric acid concentration is, the easier the positive electrode  $V^{5+}$  is to precipitate. So it is important to control the temperature and the concentration of sulfuric acid. Because the  $V^{5+}$  of the positive electrode will become  $V_2O_5$  after precipitation and will not be dissolved again(**Fig. 2.17**).

In 2016, Shuibo Xiao of Tsinghua University published a paper, 1.5M3.875H<sub>2</sub>SO<sub>4</sub> has been precipitated for 80h at 35°C[58]. Each paper has a different view on the electrolyte measurement and precipitation. There is currently no specific precipitation limit. At the same time, the paper also discusses the effect of temperature on charge and discharge. The higher the temperature, the higher the conductivity and the lower the viscosity. So the higher the temperature, the better the battery performance.

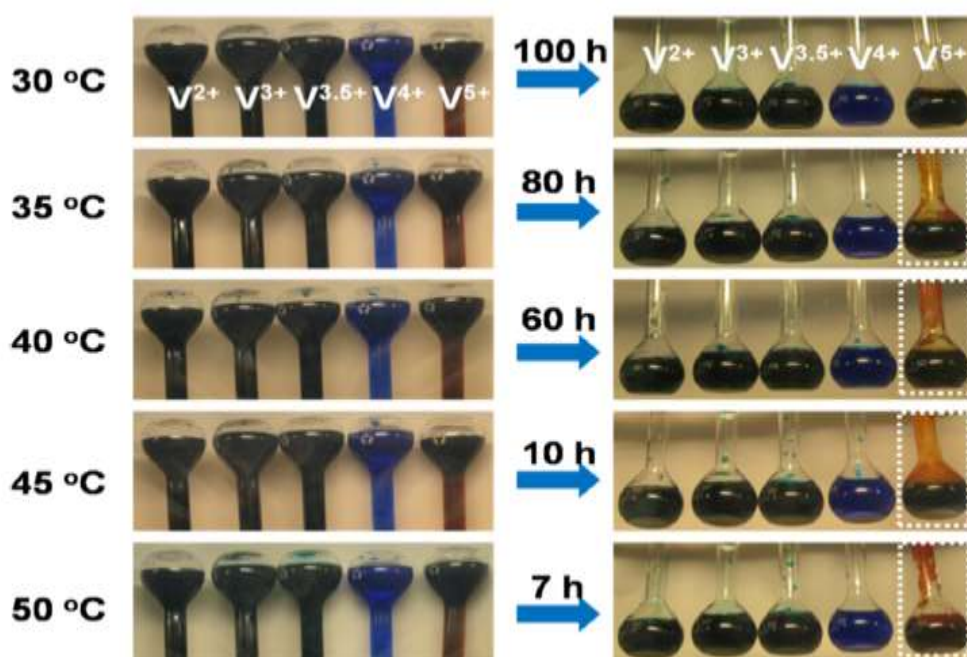
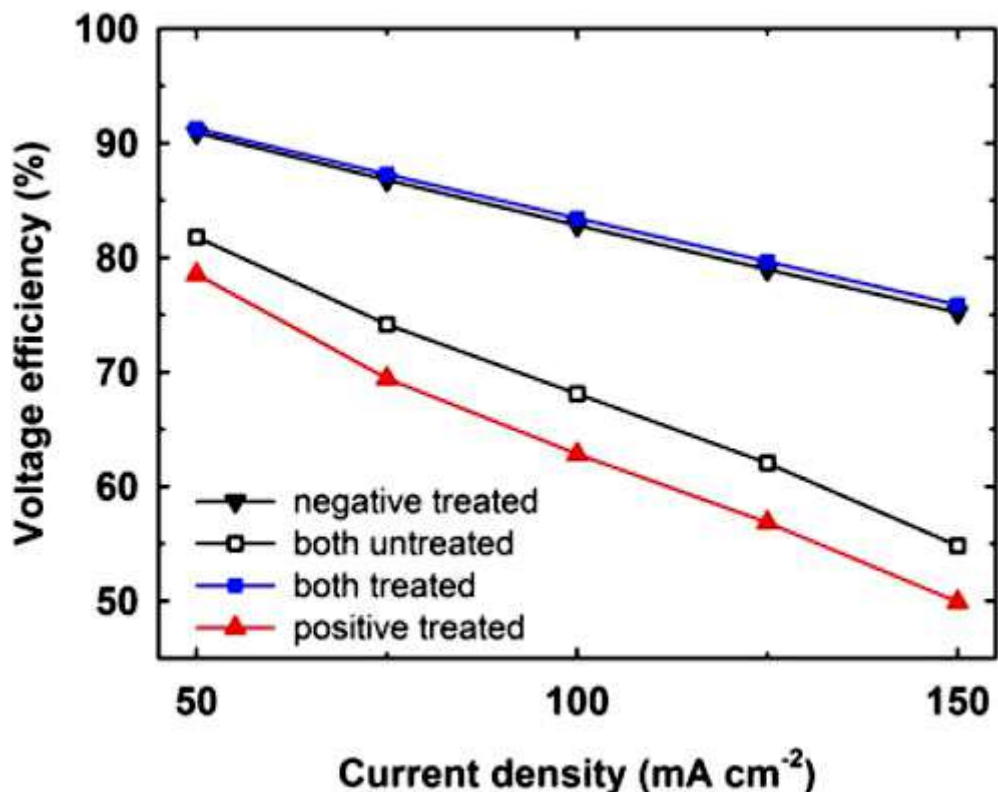


Fig. 2.17. Photographs of five types of electrolytes at high temperature[57].

### 2.3.2 Impact of runtime on battery performance

The biggest advantage of the all-vanadium redox battery is its long service life. As an energy storage battery, its designed service life is more than 20 years. The most important effect of the operating time on the battery is the valence balance of the electrolyte. Due to the long-term operation, the electrolyte is shifted, and the valence state of the electrolyte needs to be adjusted by flushing. The second is that as the running time becomes longer, the system temperature will increase accordingly. The impact of temperature on battery performance has been described above. In addition, long-term continuous charging and discharging of the electrolyte will cause redox reactions on the surface of the electrodes, which will also cause certain degradation of the electrodes.

From 2018 to 2019, P. Mazur of the Czech Republic published a paper. By conducting multiple continuous charge and discharge experiments on the battery, the changes of carbon felt were compared without considering the electrolyte[59,60]. The results show that the carbon radon impedance of the negative electrode increases by 5 times after 2000 times of charge and discharge. The impedance of the positive electrode does not change(**Fig. 2.18**).



**Fig. 2.18.** Dependence of voltage efficiency on current density of charge-discharge cycles [59].

In 2019, shuaizhou Liu et al. published a paper to investigate the changes in the total amount of vanadium ions in the negative electrolyte and the actual discharge of the battery during the multiple charge-discharge cycles of the all-vanadium redox flow battery[61]. The total amount of vanadium ions in the negative electrolyte was obtained. The theoretical discharge capacity was calculated, and the utilization rate of the electrolyte after different charging and discharging cycles was calculated. However, the theoretical utilization rate of the electrolyte is not significantly reduced, indicating that the main factor affecting the capacity decay of vanadium batteries is the transmembrane migration of the electrolyte. It will also accelerate the decay of battery capacity to a certain extent. At the same time, other factors that may accelerate the decay of battery capacity such as temperature and materials are analyzed.

### **2.3.3 Effect of overcharging on battery performance**

The safe charging and discharging voltage of the all-vanadium redox flow battery is below 1.65V. If the voltage exceeds this voltage, the positive electrode of the electrolyte will precipitate hydrogen, which will cause potential safety hazards. At the same time, excessive

charging and discharging will also cause irreversible damage to the carbon fiber electrodes. Burning the electrode can also cause corrosion to the bipolar plate. Greatly reduce the charge and discharge performance of the battery.

In 2017, Igor Derr et al. published a paper, comparing them with different charge-discharge cut-off voltages of 1.6V and 1.8V(Fig. 2.19- Fig. 2.21). The results show that the higher the charge termination voltage, the more severe the performance degradation[62].

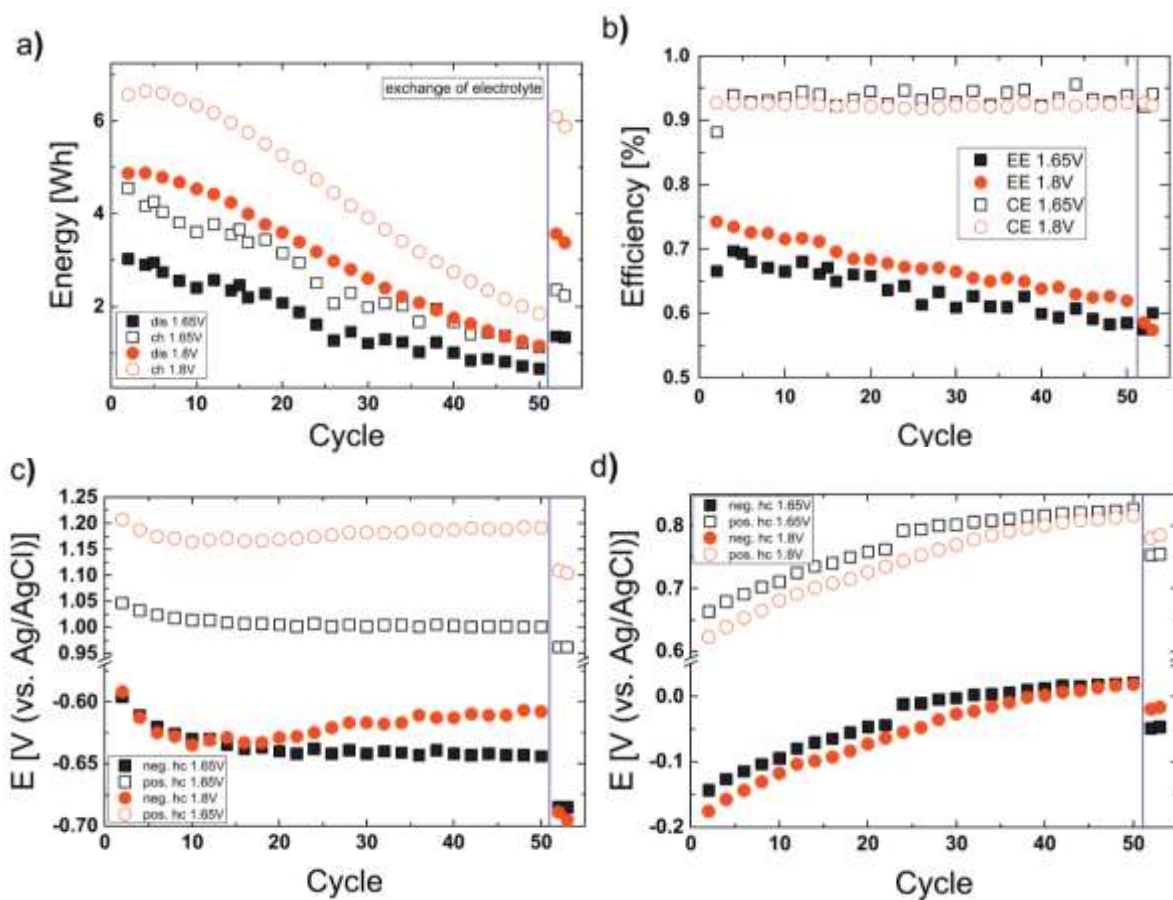


**Fig. 2.19.** Comparison of two long term experiments with 50 cycles and different cut-off voltages. After 50 cycles the electrolyte was exchanged and three additional cycles were recorded. The squares represent the experiment with 1.65 V and the circles represent the experiment with 1.8 V cut-off voltage. a) Input and output Energy plotted against the cycles. b) The energy efficiency (EE) and the coulomb efficiency (CE). c) Maximum half-cell potentials that were reached during the charge process. d) Maximum half-cell potentials that were reached during the discharge process[62].

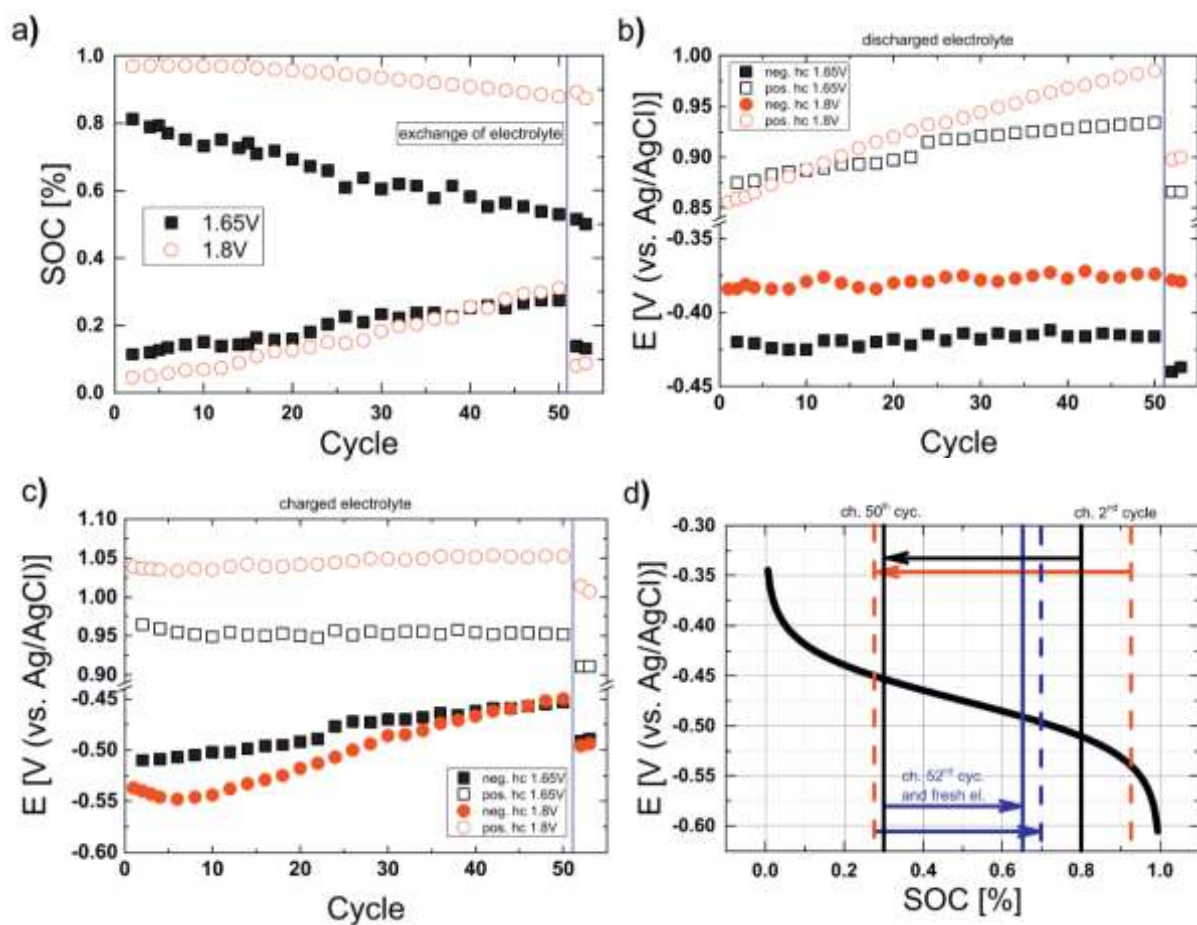


**Fig. 2.20.** Open circuit measurements and the calculated theoretical states of charge after each charge and discharge process. a) The state of charge (SOC) that was calculated from the open circuit voltages (OCV) for the according cycle. b) Open circuit potentials (OCP) that were recorded after each discharge process. c) Open circuit potentials that were recorded after each charge process. d) Theoretical Nernst-potential of the negative half-cell (black curve) is correlated to the theoretical SOC and compared to the measured potentials during both cycling experiments. The solid black lines represent the OCPs of the first 50 cycles of the 1.65V experiment and the solid blue line stands for the 52nd cycle with exchanged electrolyte. The dashed red lines represent the OCPs of the first 50 cycles of the 1.8 V experiment and the dashed blue line stands for the 52nd cycle with exchanged electrolyte. [62].

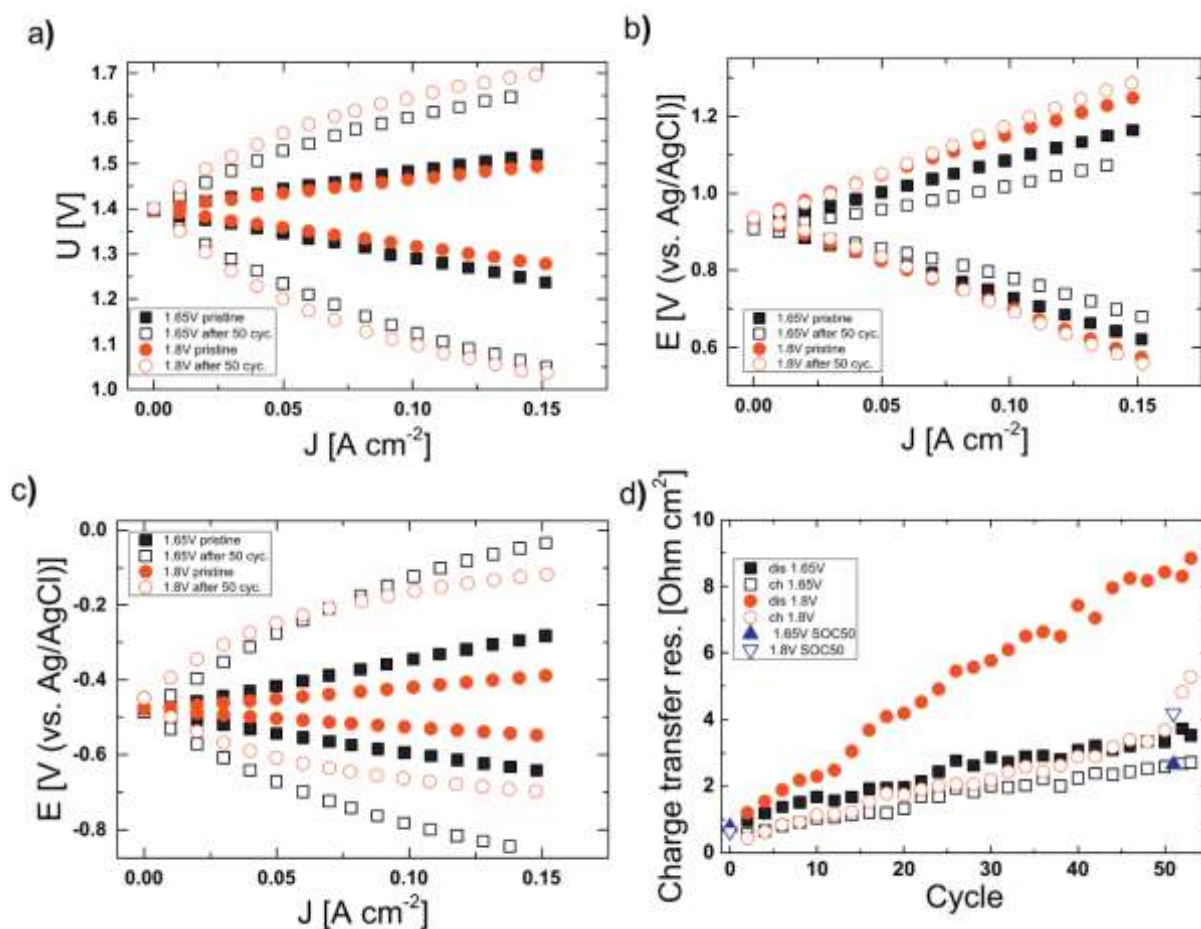


**Fig. 2.21.** Electrochemical characterization of the electrodes with polarization curves and electrochemical impedance spectroscopy. a) IR compensated polarization curves in fresh electrolyte before and after cycling for both experiments. The polarization curves were recorded at a SOC of 50 % (OCV = 1.4V) and an electrolyte flow rate of  $100\ mL\ cm^{-1}$ . b) Uncompensated positive half-cell potentials of the polarization curves from **Fig. 2.19** a) before and after the experiment. c) Uncompensated negative half-cell potentials of the polarization curves from **Fig. 2.19** a) before and after the experiment. d) Charge transfer resistances (CRT) after each charge and discharge process with 10 mV AC voltage and 0 mV DC voltage in a frequency range from 10 kHz to 0.1 Hz. [62].

## 2.4 Concluding remarks

Through the above literature survey, we summarize the influencing factors of various situations on the capacity of vanadium redox flow batteries, and some solutions. It has laid a

good foundation for the follow-up research. Through these investigations, we also formulate important directions for our future research. Avoid some of these problems.

## 2.5 References

1. TLiu, H. T., Yang, L. W., Sun, X., Cheng, H. F., Wang, C. Y., Mao, W. G., & Molina-Aldareguia, J. M. (2016). Enhancing the fracture resistance of carbon fiber reinforced SiC matrix composites by interface modification through a simple fiber heat-treatment process. *Carbon*, 109, 435–443. doi:10.1016/j.carbon.2016.08.047
2. Qiu, L., Zheng, X. H., Zhu, J., Su, G. P., & Tang, D. W. (2013). The effect of grain size on the lattice thermal conductivity of an individual polyacrylonitrile-based carbon fiber. *Carbon*, 51, 265–273. doi:10.1016/j.carbon.2012.08.052
3. McDonald-Wharry, J., Manley-Harris, M., & Pickering, K. (2013). Carbonisation of biomass-derived chars and the thermal reduction of a graphene oxide sample studied using Raman spectroscopy. *Carbon*, 59, 383–405. doi:10.1016/j.carbon.2013.03.033
4. Cançado, L. G., Takai, K., Enoki, T., Endo, M., Kim, Y. A., Mizusaki, H., ... Pimenta, M. A. (2006). General equation for the determination of the crystallite size  $L_a$  of nanographite by Raman spectroscopy. *Applied Physics Letters*, 88(16), 163106. doi:10.1063/1.2196057
5. Fitzer, E. (1989). Pan-based carbon fibers—present state and trend of the technology from the viewpoint of possibilities and limits to influence and to control the fiber properties by the process parameters. *Carbon*, 27(5), 621–645. doi:10.1016/0008-6223(89)90197-8
6. Windhorst, T., & Blount, G. (1997). Carbon-carbon composites: a summary of recent developments and applications. *Materials & Design*, 18(1), 11–15. doi:10.1016/s0261-3069(97)00024-1
7. Iwashita, N., Park, C. R., Fujimoto, H., Shiraishi, M., & Inagaki, M. (2004). Specification for a standard procedure of X-ray diffraction measurements on carbon materials. *Carbon*, 42(4), 701–714. doi:10.1016/j.carbon.2004.02.008

8. Wang, K., Huo, B., Liu, F., Zheng, Y., Zhang, M., Cui, L., & Liu, J. (2020). In situ generation of carbonized polyaniline nanowires on thermally-treated and electrochemically-etched carbon fiber cloth for high efficient solar seawater desalination. *Desalination*, 481, 114303. doi:10.1016/j.desal.2019.114303
9. Buijnsters, J. G., Gago, R., Jiménez, I., Camero, M., Agulló-Rueda, F., & Gómez-Aleixandre, C. (2009). Hydrogen quantification in hydrogenated amorphous carbon films by infrared, Raman, and x-ray absorption near edge spectroscopies. *Journal of Applied Physics*, 105(9), 093510. doi:10.1063/1.3103326
10. Ahmadijokani, F., Shojaei, A., Dordanihaghighi, S., Jafarpour, E., Mohammadi, S., & Arjmand, M. (2020). Effects of hybrid carbon-aramid fiber on performance of non-asbestos organic brake friction composites. *Wear*, 452-453, 203280. doi:10.1016/j.wear.2020.203280
11. He, P., Jia, D., Lin, T., Wang, M., & Zhou, Y. (2010). Effects of high-temperature heat treatment on the mechanical properties of unidirectional carbon fiber reinforced geopolymer composites. *Ceramics International*, 36(4), 1447–1453. doi:10.1016/j.ceramint.2010.02.012
12. Lin, T., Jia, D., He, P., Wang, M., & Liang, D. (2008). Effects of fiber length on mechanical properties and fracture behavior of short carbon fiber reinforced geopolymer matrix composites. *Materials Science and Engineering: A*, 497(1-2), 181–185. doi:10.1016/j.msea.2008.06.040
13. Zhou, G. H., Wang, S. W., Guo, J. K., & Zhang, Z. (2008). The preparation and mechanical properties of the unidirectional carbon fiber reinforced zirconia composite. *Journal of the European Ceramic Society*, 28(4), 787–792. doi:10.1016/j.jeurceramsoc.2007.07.005 .
14. Nibel, O., Taylor, S. M., Pătru, A., Fabbri, E., Gubler, L., & Schmidt, T. J. (2017). Performance of Different Carbon Electrode Materials: Insights into Stability and Degradation under Real Vanadium Redox Flow Battery Operating Conditions. *Journal of The Electrochemical Society*, 164(7), A1608–A1615. doi:10.1149/2.1081707jes .

15. Kim, K. J., Kim, Y.-J., Kim, J.-H., & Park, M.-S. (2011). The effects of surface modification on carbon felt electrodes for use in vanadium redox flow batteries. *Materials Chemistry and Physics*, 131(1-2), 547–553. doi:10.1016/j.matchemphys.2011.10.022
16. Vallerot, J.-M., Bourrat, X., Mouchon, A., & Chollon, G. (2006). Quantitative structural and textural assessment of laminar pyrocarbons through Raman spectroscopy, electron diffraction and few other techniques. *Carbon*, 44(9), 1833–1844. doi:10.1016/j.carbon.2005.12.029
17. H.R. Jiang, W. Shyy, M.C. Wu, R.H. Zhang, T.S. Zhao A bi-porous graphite felt electrode with enhanced surface area and catalytic activity for vanadium redox flow batteries. *Applied Energy*. Volumes 233–234, 1 January 2019, Pages 105-113
18. H.R. Jiang, J. Sun, L. Wei, M.C. Wu, W. Shyy, T.S. Zhao A high power density and long cycle life vanadium redox flow battery. *Energy Storage Materials* Volume 24, January 2020, Pages 529-540
19. Y.Wang, D.C Alsmeyer and R. McCreery, “Raman Spectroscopy of Carbon Materials: Structural Basis Of Observed Spectra”, *Chem.Matter*, 2, 1990.
20. A. K. Geim and K. S. “The Rise of Graphene”, Novoselov, *Nature Materials*, 6, 183 (2007).
21. M. S. “Perspectives on Carbon Nanotubes and Graphene Raman Spectroscopy », *Dresselhaus Nano Lett.*, 10 (3), 751–758 (2010)
22. Peng Li, Lin Zhu, Chao Ma, Lixia Zhang, Lin Guo, Yawen Liu, Hao Ma, Bing Zhao. Plasmonic Molybdenum Tungsten Oxide Hybrid with Surface-Enhanced Raman Scattering Comparable to that of Noble Metals. *ACS Applied Materials & Interfaces* 2020, 12 (16) , 19153-19160
23. Mohammad Tavakkoli, Emmanuel Flahaut, Pekka Peljo, Jani Sainio, Fatemeh Davodi, Egor V. Lobiak, Kimmo Mustonen, Esko I. Kauppinen. Mesoporous Single-Atom-Doped Graphene–Carbon Nanotube Hybrid: Synthesis and Tunable Electrocatalytic Activity for Oxygen Evolution and Reduction Reactions. *ACS Catalysis* 2020, 10 (8) , 4647-4658.
24. Omid Akbarzadeh Pivehzhani Amir Kordijazi Suresh Sagadevan Seyedehmaryam Moosavi Arman Amani Babadi Yasmin Abdul Wahab Nor Aliya Hamizi Zaira Zaman Chowdhury . *Syngas to Green Fuel Conversion: Nanocatalysis Approach*. 2020,545-579.

25. Shida Liu, Haiyan Wang, Robertus Dhimas Dhewangga Putra, Chang Soo Kim, Kevin J. Smith. Impact of Carbon Properties on Mo<sub>2</sub>C/Carbon Catalysts for the Hydrodeoxygenation of 4-Methylphenol. *Energy & Fuels* 2019, 33 (5) , 4506-4514.
26. B.Sun , M.Skayllas-Kazakos *Electrochimica Acta* 37(1992)1253.
27. Yarlagadda, V.; Lin, G.; Chong, P.Y.; Van Nguyen, T. High Surface Area Carbon Electrodes for Bromine Reactions in H<sub>2</sub>-Br<sub>2</sub> Fuel Cells. *J. Electrochem. Soc.* 2016, 163, 5126–5133.
28. Yarlagadda, V.; Lin, G.; Chong, P.Y.; Van Nguyen, T. High Active Surface Area and Durable Multi-Wall Carbon Nanotube-Based Electrodes for the Bromine Reactions in H<sub>2</sub>-Br<sub>2</sub> Fuel Cells. *J. Electrochem. Soc.* 2016, 163, 5134-5143.
29. Jiang, H.R.; Shyy, W.; Wu, M.C.; Zhang, R.H.; Zhao, T.S. A bi-porous graphite felt electrode with enhanced surface area and catalytic activity for vanadium redox flow batteries. *Appl. Energy* 2019, 233–234, 105–113.
30. Jiang, H.R.; Sun, J.; Wei, L.; Wu, M.C.; Shyy, W.; Zhao, T.S. A high power density and long cycle life vanadium redox flow battery. *Energy Storage Mater.* 2020, 24, 529–540.
31. Igor Derr, Michael Bruns, Joachim Langner, Abdulmonem Fetyan, Julia Melke, Christina Roth. Degradation of all-vanadium redox flow batteries (VRFB) investigated by electrochemical impedance and X-ray photoelectron spectroscopy: Part 2 electrochemical degradation. *J. Power Sources* 325(2016)351.
32. Igor Derr, Daniel Przyrembel, Jakob Schweer, Abdulmonem Fetyan, Joachim Langner, Julia Melke, Martin Weinelt, Christina Roth. Electroless chemical aging of carbon felt electrodes for the all-vanadium redox flow battery (VRFB) investigated by Electrochemical Impedance and X-ray Photoelectron Spectroscopy . *Electrochimica Acta* 246(2017)783.
33. Igor Derr, Abdulmonem Fetyan, Konstantin, Konstantin Schutjajew, Christina Roth. Electrochemical analysis of the performance loss in all vanadium redox flow batteries using different cut-off voltages. *Electrochimica Acta* 224(2017)9.
34. Jiang, H. R., Sun, J., Wei, L., Wu, M. C., Shyy, W., & Zhao, T. S. (2019). A high power density and long cycle life vanadium redox flow battery. *Energy Storage Materials*. doi:10.1016/j.ensm.2019.07.005 .

35. Hiroko Kaneko, Ken Nozaki, Yutaka Wada, Takamichi Aoki, Akira Negishi, Masayuki Kamimoto, Vanadium redox reactions and carbon electrodes for vanadium redox flow battery, *Electrochimica Acta*, Volume 36, Issue 7, 1991, Pages 1191-1196.
36. Kazacos M, Skyllas-Kazacos M, *J. Electrochem. Soc.*, 1989, 136(9), 2759-2760.
37. Aaron A. Shinkle, Timothy J. Pomaville, Alice E.S. Sleightholme, Levi T. Thompson, Charles W. Monroe, Solvents and supporting electrolytes for vanadium acetylacetonate flow batteries, *Journal of Power Sources*, Volume 248, 2014, Pages 1299-1305, 34.
38. Li L Y, Kim S, Wang W, Vijayakumar M, Nie Z M, Chen B W, Zhang J L, Xia G G, Hu J Z, Grsff G, Liu J, Yang Z G, *Adv. Energy mater.*, 2011, 1(3), 394-400.
39. Wen Yuehua, Zhang Huamin, Qian Peng, et al. Research on all-vanadium redox flow battery with ion exchange membrane[D]. , 2005.
40. Gab-Jin Hwang, Sang-Won Kim, Dae-Min In, Dae-Yeop Lee, Cheol-Hwi Ryu, Application of the commercial ion exchange membranes in the all-vanadium redox flow battery, *Journal of Industrial and Engineering Chemistry*, Volume 60, 2018, Pages 360-365,
41. M. Skyllas-Kazacos, M. Rychcik, R.G. Robins, and A.G. Fane , New all-vanadium Redox Flow Cell, *Journal of the Electrochemical Society* 133(1986)1057.
42. M. Rychcik and M. Skyllas-Kazacos , Evaluation of electrode materials for vanadium redox cell, *Journal of Power Sources* 19(1987)45.
43. M. Skyllas-Kazacos and F. Grossmith , Efficient Vanadium Redox Flow Cell, *Journal of Electrochemical Society* 134(1987)2950.
44. M. Kazacos and M. Skyllas-Kazacos , Performance Characteristics of Carbon Plastic Electrodes in the All Vanadium Redox Cell, *Journal of The Electrochemical Society* 136(1989)2759.
45. Q. Wang, Z.G. Qu, Z.Y. Jiang, W.W. Yang, Numerical study on vanadium redox flow battery performance with non-uniformly compressed electrode and serpentine flow field, *Applied Energy*, Volume 220, 2018, Pages 106-116.
46. Gundlapalli, R., Kumar, S. & Jayanti, S. Stack. Design Considerations for Vanadium Redox Flow Battery. *INAE Lett* 3, 149–157 (2018).

47. Q. Xu, T.S. Zhao, P.K. Leung, Numerical investigations of flow field designs for vanadium redox flow batteries, *Applied Energy*, Volume 105, 2013, Pages 47-56.
48. Doug Aaron, Zhijiang Tan, Alexander B. Papandrew, Thomas A. Zawodzinski. Polarization curve analysis of All-vanadium redox flow batteries, *Journal of the Applied Electrochemistry* 41(2011)1175-1182.
49. Xiangkun Ma, Huanmin Zhang, Chenxi Sun, Yi Zou, Tao Zhang, An optimal strategy of electrolyte flow rate for vanadium redox flow battery, *Journal of Power Sources* 203(2013)153-158.
50. Ao Tang, Joe Bao, Maria Skyllas-Kazacos, Studies on pressure losses and flow rate optimization in vanadium redox flow battery, *Journal of Power Sources* 248(2014)154.
51. S. Kumar, S. Jayanti, Effect of flow field on the performance of an all-vanadium redox flow battery, *Journal of Power Sources* 307(2016)782-787.
52. Ki Hyun Kim, Bu Gi Kim, Dai Gil Lee, Development of carbon composite bipolar plate for vanadium redox flow battery, *Composit Structures* 109(2014)253
53. Jihai Zhang, Tao Zhou, Liping Xia, Canyao Yuan, Weidong Xiang and Aiming Zhang, Polyporopylene elastomer composite for the VRFB current collector materials, *Journal of Materials Chemistry A* 3(2015)2387.
54. Se-Kook Park, Joonmok Shim, Jung Hoon Yang, Chang-Soo Jin, Bum Suk Lee, Young-Seak Lee, Kyoung-Hee Shin, Jae-Deok Jeon, The influence of compressed carbon felt electrodes on the performance of a vanadium redox flow battery, *Electrochimica Acta*, Volume 116, 2014, Pages 447-452.
55. Hsieh C L, Tsai P H, Hsu N Y, et al. Effect of compression ratio of graphite felts on the performance of an all-vanadium redox flow battery[J]. *Energies*, 2019, 12(2): 313.
56. Faizur Rahman, Maria Skyllas-Kazacos, Vanadium redox battery Positive half-cell electrolyte studies, *J. Power Sources* 189(2009)1212.
57. Maria Skyllas-Kazacos, Liuyue Cao, Michael Kazacos, Nadeem Kausar, and Asem Mousa, Vanadium electrolyte Studies for the Vanadium Redox Battery A Review, *Chemoschem* 9(2016)1521.

58. Shuibo Xiao, Lihong Yu, Lantao Wu, Le Liu, Xinping Qiu, Jingyu Xi, Broad temperature adaptability of vanadium redox flow battery—Part 1: Electrolyte research, *Electrochimica Acta*, Volume 187, 2016, Pages 525-534.
59. P.Mazur, J.Mrlik, J.Pocedic, J.Vrana, J.Dundalek, J.Kosek, T.Bystron, Performance evaluation of thermally treated graphite felt electrodes for VRFB and their four-point single cell characterization, *J.Power Sources* 360(2018)105.
60. P.Mazur, J.Mrlik, J.Benes, J.Pocedic, J.Vrana, J.Dundalek, J.Kosek, Effect of graphite felt properties on the long-term durability of negative electrode in VRFB, *J.Power Sources* 414(2019)354.
61. Liu Shuaizhou, Li Juntao, Shi Xiaohu. Research on the capacity decay mechanism of all-vanadium redox flow batteries [J]. *Power Technology*, 2019, 043(008):1381-1383.
62. Igor Derr, Abdulmonem Fetyan, Konstantin Schutjajew, Christina Roth, Electrochemical analysis of the performance loss in all vanadium redox flow batteries using different cut-off voltages, *Electrochimica Acta*, Volume 224, 2017, Pages 9-16.

## Chapter 3 Research and development of high output vanadium redox flow battery

All-vanadium redox flow batteries have obvious advantages and become one of the preferred technologies in the field of large-capacity energy storage. Compared with other energy storage technologies, the all-vanadium redox flow battery has obvious advantages: First, it is safe and environmentally friendly. The energy storage medium of the all-vanadium redox flow battery is a dilute sulfuric acid aqueous solution containing vanadium ions, which is not easy to explode and burn, and the vanadium electrolyte can be recycled repeatedly. Second, the cycle life is long. The number of charge and discharge cycles of the battery is more than 15,000 times, and the service life is 15 to 20 years. The third is high energy conversion efficiency and good charge and discharge characteristics. The energy efficiency is about 80%, the response speed is fast, it can be deeply discharged, and it is suitable for high current fast charging and discharging. Fourth, the capacity is large. The energy storage capacity ranges from hundreds of kilowatt hours to hundreds of megawatt hours, which is especially suitable for large-capacity fixed energy storage occasions.

Although all-vanadium flow batteries have many advantages, their most important disadvantage is their low energy density [1.2], which makes them bulky and expensive to manufacture [3.4]. As people pay more attention to energy storage and meet the needs of the current energy storage market, the efficiency of energy storage will be improved. The current all-vanadium redox flow battery technology needs further improvement. How to improve the charging and discharging performance of the all-vanadium redox flow battery, reduce the volume of the battery, and reduce the manufacturing cost of the battery. It has become the main target of vanadium redox flow battery research in recent years [5.6]. There are many factors that affect the charging and discharging performance of all-vanadium redox flow batteries, such as the design of the flow path, the concentration of the electrolyte, and the surface activity of the carbon fiber electrode[7.8].

According to the calculations of Sumitomo Electric Corporation of Japan, only when the current density is  $200\text{mA}/\text{cm}^2$  and the energy efficiency is above 80%, the vanadium redox flow

battery is expected to be greatly reduced to achieve real miniaturization. Therefore, many studies are currently aimed at this.

This chapter mainly introduces the surface modification of battery electrodes. The electrodes are treated by heat treatment and CNT coating to improve their specific surface area and degree of graphitization. Thereby improving the charging and discharging performance of the battery.

### **3.1 Carbon fiber electrode heat treatment**

#### ***3.1.1 Introduction***

In this study, the carbon fibers were analyzed by Raman spectroscopy mainly through heat treatment at different temperatures. The spectra of three carbon fibers were compared at six different temperatures of 1000°C, 1500°C, 2400°C, 2700°C, and 3000°C. The results showed that the higher the heat treatment temperature, the higher the D peak near 1360 cm<sup>-1</sup> and the 1580 cm<sup>-1</sup> peak. The results showed that the higher the heat treatment temperature, the smaller the integral area ratio (ID/IG) of the two characteristic peaks: the D peak near 1360 cm<sup>-1</sup> and the G peak near 1580 cm<sup>-1</sup>. Moreover, the characteristic peak of graphite layer number appears at 2700 cm<sup>-1</sup> in the spectrum when the heat treatment temperature is above 1500°C, and the intensity of the characteristic peak increases with higher temperature. When the temperature reaches 3000°C, the D peak tends to smooth out, G etc. decreases compared to 2700°C, and the G' peak reaches the maximum.

#### ***3.1.2 Experimental methods***

This experiment focuses on the analysis of two PAN-based carbon fiber materials after heat treatment by Raman spectroscopy. The differences of each characteristic peak in the spectra of carbon fibers after heat treatment at different temperatures were compared.

This experiment with PAN system of carbon fiber for two kinds of commercially available materials, the parameters are shown in **Table 3-1**. Vacuum high temperature heat treatment temperature 800°C-1500°C, vacuum degree 10<sup>-2</sup>-10<sup>-3</sup>pa, protective gas is argon, heat treatment

time 1 hour, with the furnace cooling to room temperature. 2000°C-3000°C heat treatment due to equipment, commissioned enterprises processing, the experimental conditions are the same. Raman device for the Japanese spectroscopy company NRS-4100, measurement range 0-4000cm<sup>-1</sup>. The number of measurements was 2 times, and the stabilization time was 60s.

The temperature ranges and variations of carbonation and graphitization of organic compounds are shown in **Fig. 3.1**. When an organic compound is heated, non-carbon atoms such as oxygen, hydrogen, and nitrogen leave the compound and become carbonized, and when heating continues, they become graphitized.

Raman spectroscopy has proven to be a simple and reliable technique for the determination of carbon materials. Due to its high structural capability, non-destructive analysis, high spectral and spatial resolution, Raman spectroscopy has become a standard technique in the rapidly developing field of carbon materials. The Raman spectra of carbon materials The Raman spectra of typical carbon materials are shown in **Fig. 3.2**. The Raman spectra of carbon materials have three main characteristic peaks, Dband near the central wavelength of 1270-1450 cm<sup>-1</sup>, Dband near the central wavelength of 1580 cm<sup>-1</sup> and 2Dband near 2700 cm<sup>-1</sup> (also known as G'band).

**Table 3-1.** Two carbon material specifications

	Dulk density	Fiber diameter	Thermal conductivity	Tensile strength	Density
	[g/l]	[um]	[W/m·K]	[MPa]	[g/cm <sup>3</sup> ]
A	>430	11	20	2350	2.0
B	>380	13	25	2540	2.7

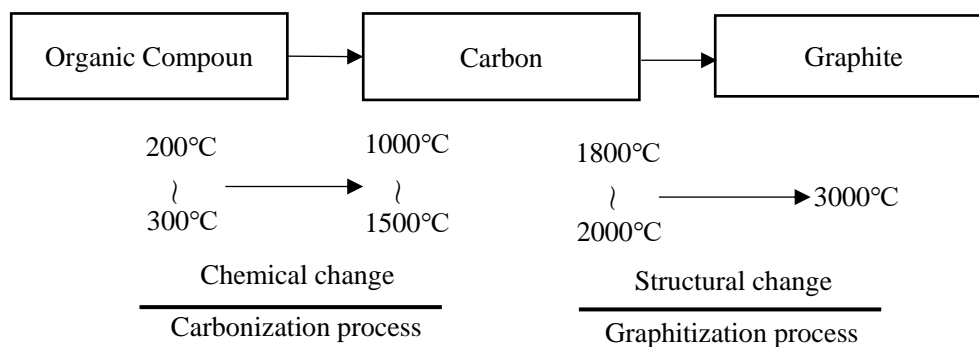


**Fig. 3.1.** Change in organic compound by ,heat treatment at the different temperature.

One of the D peaks is known as the disorder band due to structural perturbations and defect formation. The presence of this peak between  $1270$  and  $1450\text{ cm}^{-1}$  (depending on the excitation wavelength) due to lattice motion away from the center of the region indicates the presence of defects or edges in the carbon material sample.

The G band is one of the characteristic peaks of carbon materials, originating from the in-plane motion of carbon atoms and appearing near  $1580\text{ cm}^{-1}$ . The G-band varies due to the effect of aberrations.

The 2D peak, also known as the G' peak, appears at about  $2700\text{ cm}^{-1}$  and is also used to determine the integrity of the graphitized layer of the carbon material. Its properties are more complex than the frequency shift observed in the G band. As the number of layers increases, the number of double resonance processes also increases and the shape of the spectrum converges to that of graphite.

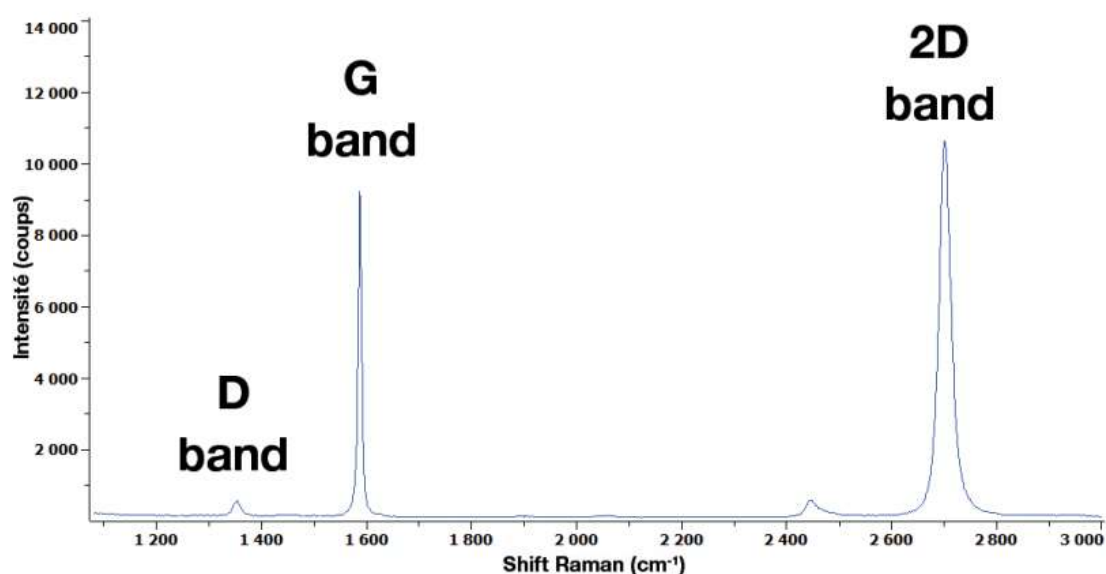


**Fig. 3.2.** Raman spectra of carbon materials Typical Raman spectra of carbon

In the process of Raman spectroscopy, researchers often use the ratio of the integrated areas of the D and G peaks,  $I_D/I_G$ , to characterize the structural integrity of the carbon material.

### 3.1.3 Experimental results

As shown in **Fig. 3.3**, the Raman spectra of the two carbon materials untreated with  $1000^\circ\text{C}$  heat treatment and  $1500^\circ\text{C}$  heat treatment are shown. From the Raman spectra of **Fig. 3.3.a** and

**Fig. 3.3.b**, it can be seen that the characteristic peaks D and G of the two materials are not separated next to each other. The spectra were divided by Origin software and the integral area ratio ID/IG of the D and G peaks were calculated.

The Raman spectra of the two carbon materials after heat treatment at 1000°C are shown in **Fig. 3.3. c** and **Fig. 3.3.d**. The spectra after heat treatment at 1000°C show that along with the separation of the D and G peaks, the half-height width of the D peak starts to narrow. And the G' peak starts to be prominent. This indicates that the organic compounds are gradually carbonized by removing the small amount of impurities in the materials through heat treatment.

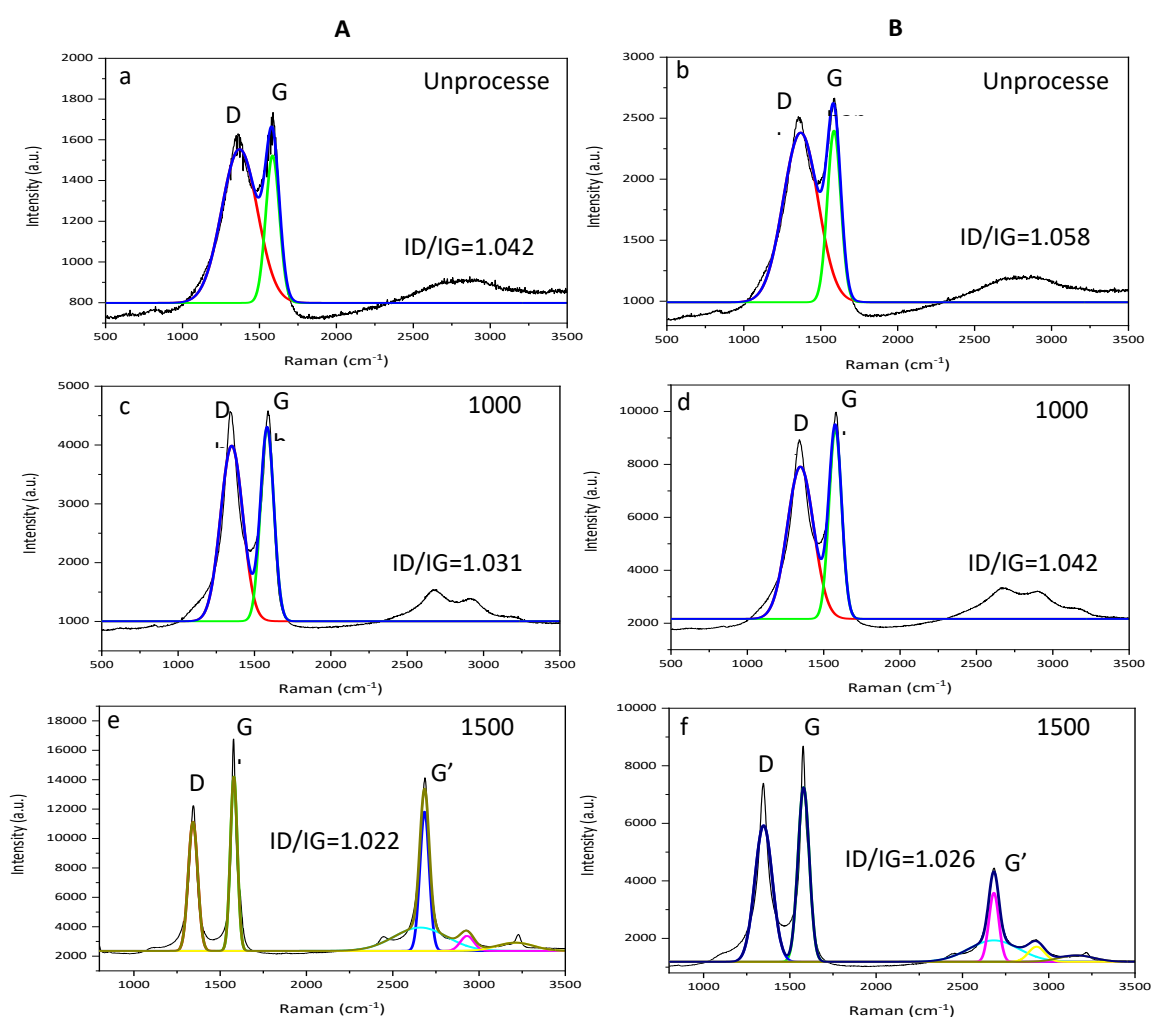


**Fig. 3.3.** Unprocessed 1000°C and 1500°C heat treatment Raman spectra of two materials

**Fig. 3.3 e** and **Fig. 3.3 f** show the Raman after heat treatment at 1500°C. From the figure, it can be seen that with the increase of heat treatment temperature, the D and G peaks have been completely separated, the height of the D peak gradually decreases and the half-value amplitude

decreases, and the intensity of the G' peak increases significantly. This indicates that the magazines are gradually removed from the material as the heat treatment temperature increases, and the material starts to graphitize gradually along with carbonization.

The Raman spectra of the two materials after heat treatment at 2400°C-3000°C are shown in **Fig. 3.4**. **Fig. 3.4.a** and **Fig. 3.4b** show the Raman spectra of the two materials after heat treatment at 2400°C. It can be seen from the figures that the D and G peaks have been completely separated, the height of the D peak has been significantly reduced, and the intensity of the G' peak has been significantly increased. The materials have entered the graphitization stage.

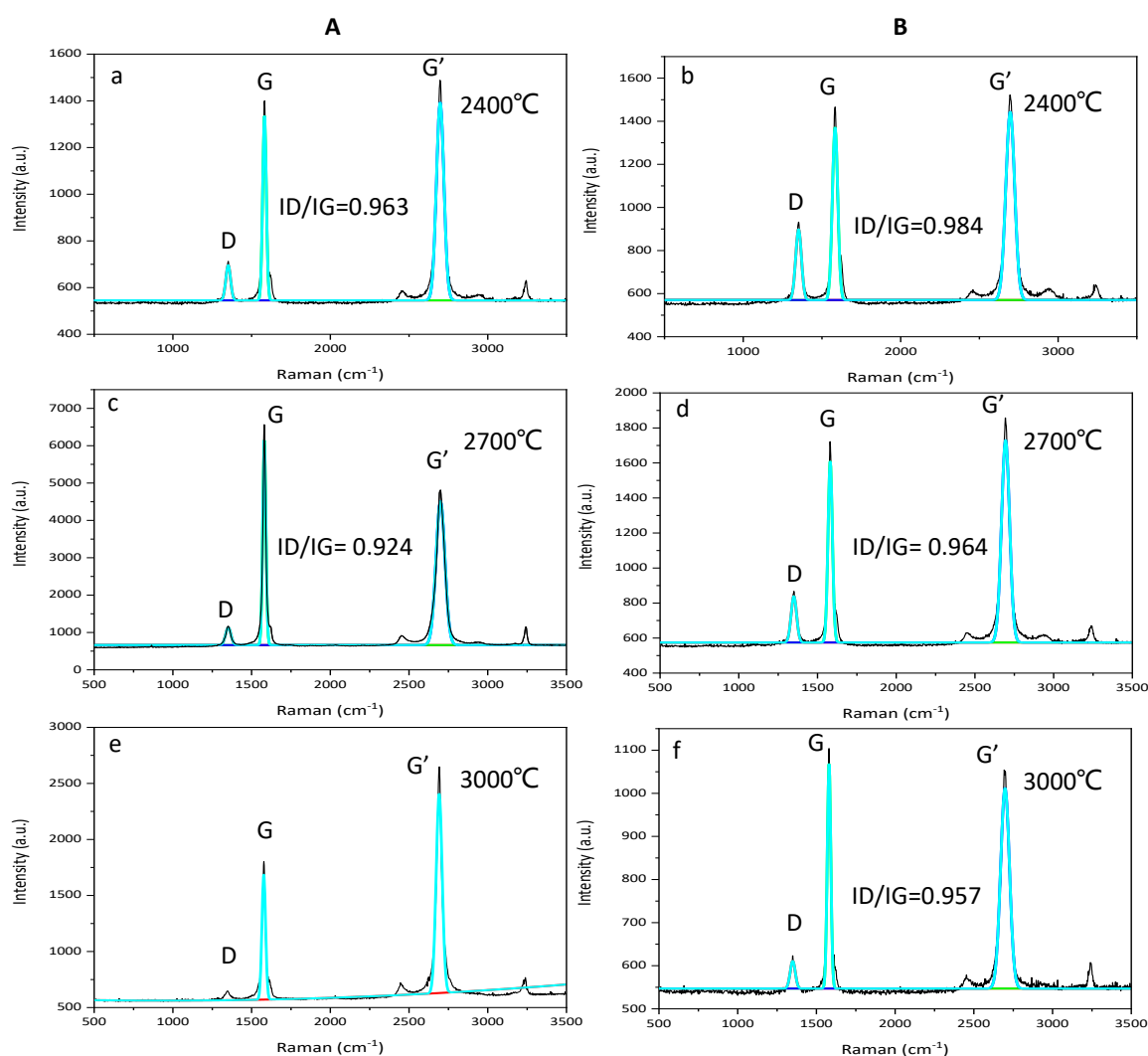


**Fig. 3.4.** Raman spectra of two materials of two materials at heat treatment temperatures of 2400°C ,2700°C and 3000°C

**Fig. 3.4c** and **Fig. 3.4d** show the Raman spectra of heat treatment at 2700°C. Compared with 2400°C, the D peak is reduced by more than half, and the half-value amplitude of the G

peak is also reduced. Figures e and f show the Raman spectra at 3000°C, where the D-peak of material A has tended to smooth out and the intensity of the G' peak is higher than that of the G-peak, indicating that the material in question has been completely graphitized.

**Table 3-2** Calculated data of Raman spectra

Sample	D peak		G peak		ID/IG (Area)	
	Raman shift (cm <sup>-1</sup> )	FWHM (cm <sup>-1</sup> )	Raman shift (cm <sup>-1</sup> )	FWHM (cm <sup>-1</sup> )		
Unprocesse	A	1365	407.7	1546	162.5	1.042
	B	1347	443.8	1591	171.3	1.058
1000°C	A	1356	215.9	1587	126.7	1.031
	B	1341	263.7	1581	120.3	1.042
1500°C	A	1349	152.4	1587	143.7	1.022
	B	1351	108.8	1588	113.0	1.026
2400°C	A	1351	54.3	1582	44.5	0.963
	B	1352	75.4	1584	66.7	0.984
2700°C	A	1351	18.6	1581	25.8	0.924
	B	1350	56.4	1580	47.6	0.964
3000°C	A	1350	—	1580	15.6	—
	B	1348	53.2	1578	45.5	0.957

The data calculated after applying origin software to the Raman spectra for peak splitting are shown in **Table 3-2**. It can be seen from **Table 3-2** that the central wavelengths of the D and G peaks are almost unchanged. The Full width at half maximum (FWHM) of the D and G peaks decreases as the heat treatment temperature increases, and the ratio of ID/IG also decreases. Comparing the two materials A,B, material A is more prone to carbonization and graphitization than material B under the same conditions.

### 3.1.4 Conclusion

By heat treating the two materials and comparing the Raman spectra at different temperatures, we proved that the D peak decreases with the increase of temperature, and the D

peak and G peak gradually separate at 1500°C and begin to graphitize. When the temperature reaches 2400°C, the D band gradually disappears, indicating that the other elements in the material gradually disappear and the material gradually carbonizes as the temperature of the heat treatment increases. When the temperature continues to increase, the G' peak front gradually increases, and the material gradually graphitizes. When the temperature reaches 3000°C, the D peak of material A disappears, the G' peak reaches the highest value, and the material is completely graphitized. Comparing the integrated area ratio of D and G peaks, ID/IG decreases with the increase of temperature, which further proves that the carbonization of the material is more complete when the heat treatment temperature increases.

## 3.2 CNT surface modification of carbon felt

### 3.2.1 Introduction

Carbon fiber, as an electrode material, has been widely used in all-vanadium liquid flow batteries. In order to further reduce the size of the all-vanadium storage system, it is imperative to increase the current density of the battery and to achieve high conductivity and large electrostatic capacitance. The graphitization of the electrode material and the improvement of the specific surface area of the electrode surface also greatly affect the performance of all-vanadium redox liquid flow batteries. Therefore, in this paper, carbon nanotubes (CNTs) with small diameter and large specific surface area were coated on the electrode surface of the VRFB system by dispersion method to improve the cell performance. The performance of the surface modified electrode was also verified by Raman spectroscopy, XRD and SEM surface observation and charge/discharge experiments.

Positive electrode reaction:



Negative electrode reaction:



### ***3.2.2 Experimental methods***

As an energy storage battery, the all-vanadium liquid flow battery has been widely used in various energy storage fields, including large power stations, photovoltaic power generation, wind power generation, etc. [10-13]. However, the disadvantages of low energy density and large size need to be further addressed [14-16]. Therefore, reducing the size of all-vanadium liquid flow battery and increasing the energy density and current density of the battery are the main objectives of current research and development [16-18]. This goal is achieved mainly through two ways, one is to improve the performance of the battery component materials, and the other is to optimize the design of the battery frame and flow path [19,20]. One of them is about the battery component materials, which mainly includes the electrode materials, diaphragm materials of the battery. Electrode materials are improved mainly by means of heat treatment and surface modification [20-24]. The heat treatment process can improve the carbonization of the electrode to reduce the resistance of the electrode [25,26]. But while improving the carbonization, we believe that for aqueous solution batteries. The hydrophilicity of the electrode should be improved at the same time, excessive heat treatment will reduce the hydrophilicity of the electrode [27], thus reducing the charge and discharge performance. The surface modification of the electrode is mainly done by increasing the specific surface area of the carbon ballast [28-30], which increases the contact area between the carbon ballast and the electrolyte, thus improving the reaction rate and reducing the charge mobility resistance [31-34].

In order to further improve the performance of carbon electrodes in VRFB systems, in this paper a method is proposed to dispersively coat carbon nanotubes (CNTs) with small diameters and large specific surface areas on the surface of carbon electrode fibres in VRFB systems. Furthermore, the carbon electrodes were heat-treated at various temperature conditions and the optimum heat treatment conditions were found to improve the electrode performance. The performance of the surface-modified electrodes was verified by Raman spectrum, XRD and SEM surface observations and charge/discharge experiments, which also proved that the method proposed in this thesis is effective.

In this study, the dispersion of multi-walled carbon nanotubes was processed by different dispersion solutions, and the dispersed solutions were analyzed using a ZC-3000 ZETA potential device from Kyowa Interface Science Co. The dispersed CNTs solution was coated on the electrode surface and heated and dried. The VRFB for the charge-discharge test was a homemade spiral pump-driven cell with an electrode area of  $5 \text{ cm} \times 10 \text{ cm}$ . For the data of charge-discharge experiments, SEM-EDS observation analysis, Raman spectroscopic analysis and XRD surface crystallographic analysis were performed on the electrode surface. The obtained analysis data were calculated, and the calculated results were compared to summarize the experimental results.

The CNTs used in this experiment were multi-walled carbon nanotubes produced by WACO Chemical Company, commercially available multi-walled CNTs with an average diameter of 10 nm and an average length of 1  $\mu\text{m}$ . The dispersion medium mainly contained deionized water and ethanol solution, and the surfactant was SDBS (sodium dodecylbenzene sulfonate). Here, 0.006 g of CNTs were placed in three different solvents, stirred for 15 min, sonicated for 20 min and left for 1 h. The stability of the dispersed solution was determined by measuring the ZETA potential as shown in **Fig. 3.5**.

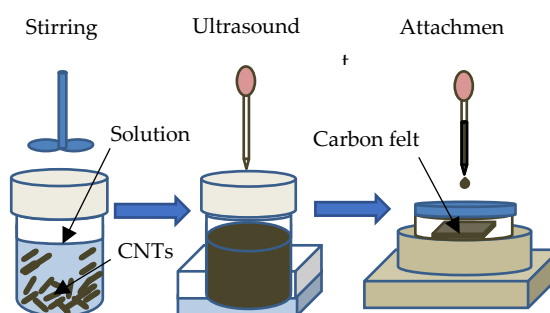


**Fig. 3.5** CNTs dispersion and carbon fiber modification

The charge/discharge experiment was performed with a constant current charge/discharge, an electrolyte flow rate of  $2.4 \text{ mlmin}^{-1}\text{cm}^{-2}$ , and a carbon felt compression ratio of 30%. The charge/discharge experiments were carried out on untreated carbon felt and treated carbon felt, and the charge/discharge data results were calculated to compare the experimental results. The charge and discharge internal resistance (IR), voltage efficiency (EV), coulombic efficiency (EC), energy efficiency (EE), energy density (ED) and output density (OD) of the battery were

calculated based on the constant current charge and discharge curves. The calculation equations are shown in (3-3)-(3-8).

$$I_R = \frac{U_{avg.charge} - U_{avg.discharge}}{2C_D} \quad (3-3)$$

$$E_V = \frac{U_{avg.discharge}}{U_{avg.charge}} \times 100\% \quad (3-4)$$

$$E_C = \frac{\int i_{discharge}(t) dt}{\int i_{charge}(t) dt} \times 100\% \quad (3-5)$$

$$E_E = E_V \times E_C \quad (3-6)$$

$$O_D \left( \frac{W}{L} \right) = \frac{I \times U_{avg.discharge}}{V_1} \quad (3-7)$$

$$E_D \left( \frac{Wh}{L} \right) = \frac{I \times T_d \times U_{avg.discharge}}{V_1} \quad (3-8)$$

### 3.2.3 Experimental results

The dispersions of the three dispersions at different concentrations were compared by measuring the ZETA potential. The results showed that 80% ethanol solution, 0.1 mol/L SDBS aqueous solution and 0.1 mol/L (SDBS+80% ethanol) solution had the best dispersion. The measurement results are shown in **Fig. 3.6**. Since the SDBS ethanol solution produced a large number of bubbles after sonication, the solution started to solidify after 2 hours of standing, and the precipitation was obvious after 6 hours of standing. Therefore, 80% ethanol solution was used in this experiment.

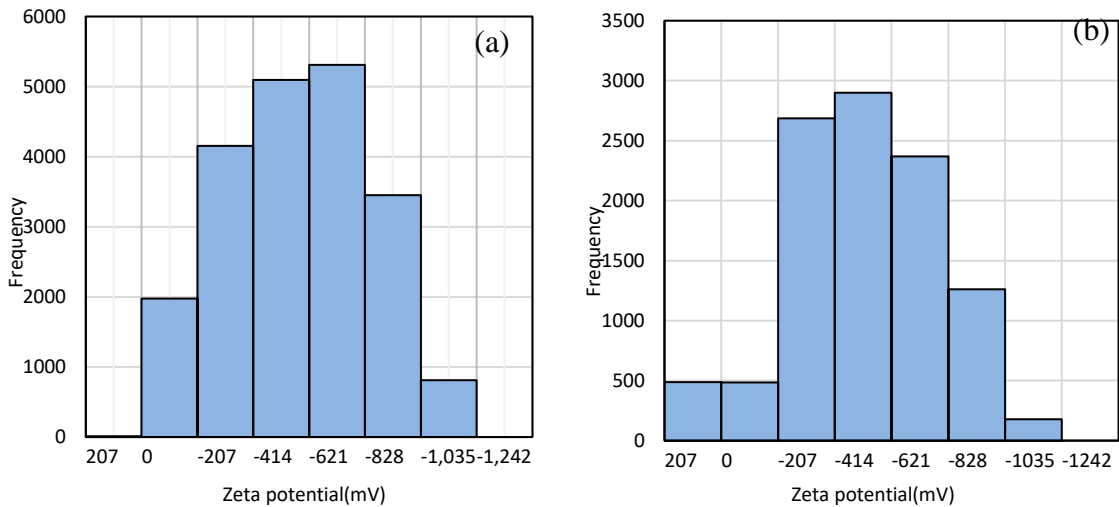


**Fig. 3.6** The ZETA potential;(a) 80% ethanol solution,(b)0.1 mol/L (SDBS + 80% ethanol)

The 100ml of dispersed solution was heated and dried after being dropped into the carbon felt electrode in several times. The surface state and elements of the carbon fiber electrodes were observed and analyzed by SEM-EDS. The SEM images of the untreated electrode (a1.a2.a3.) and the treated electrode (b1.b2.b3.) are shown in **Fig. 3.7**. The SEM comparison shows that the dispersed CNTs have completely adhered to the surface of the carbon felt fibers. The results of the EDS elemental analysis are shown in **Table 3-3** and **Fig. 3.8**. It can be seen from the elemental analysis results that the carbon element percentage of the treated carbon felt has increased by 4.25%.

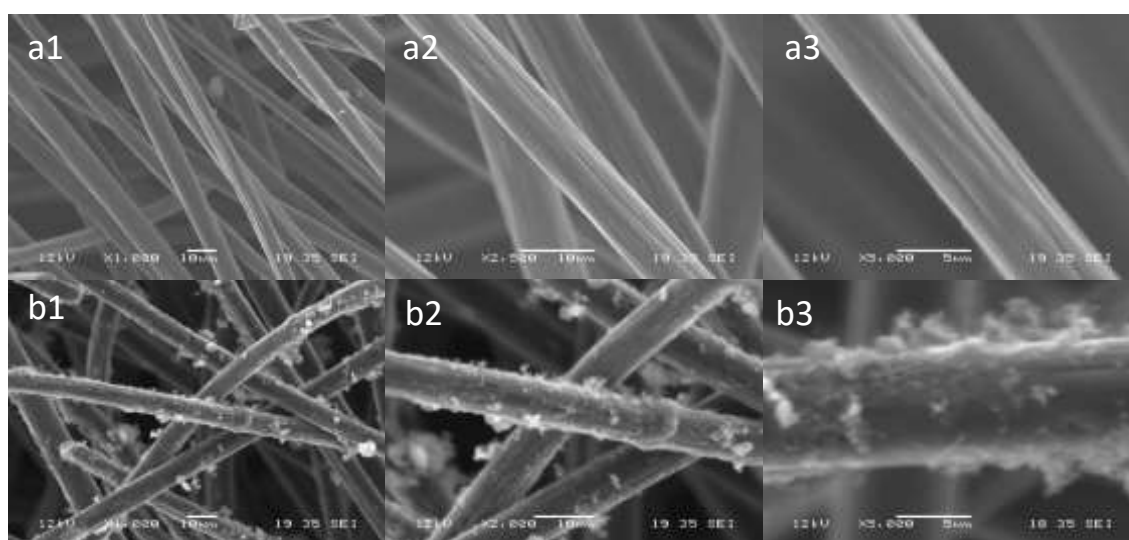


**Fig. 3.7** Comparison of SEM images of untreated carbon felts (top) and treated carbon felts (bottom)

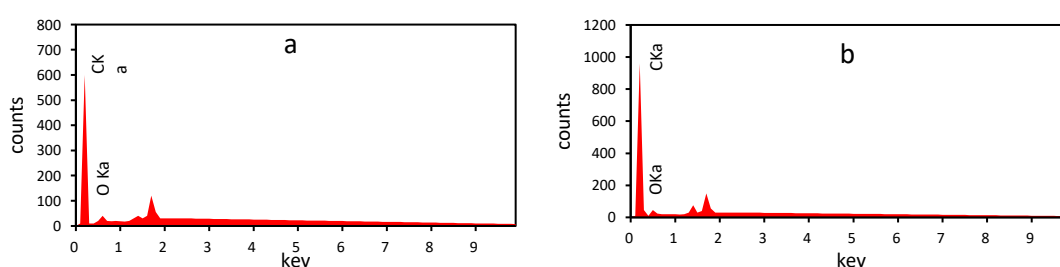


**Fig. 3.8** EDS surface elemental analysis results (a: untreated carbon felt b: carbon felt after attachment treatment)

**Table 3-3.** EDS surface element analysis results comparison.

	C Ka(%)	O Ka (%)	O/C
a	87.23	12.77	0.14
b	91.48	8.52	0.09

The experimental results are shown in **Fig. 3.9** (a: untreated carbon felt, b: treated carbon felt) by conducting a constant current charge/discharge experiment on a single cell with a current density of 100mA/cm<sup>2</sup>-500mA/cm<sup>2</sup>. The maximum power density of the untreated carbon felt electrode is 300mA/cm<sup>2</sup> and the charging voltage is 1.8V. The treated carbon felt electrode can reach 400mA/cm<sup>2</sup> and the charging voltage is 1.6V. The charging and discharging data are calculated according to equations (3)-(8) as shown in **Table 3-4**. It can be seen from **Table 3-4** that the IR of the treated carbon felt is 2 times lower than that of the untreated carbon felt, and the EV and EE are increased by about 15%. This is because the surface coating of carbon felt with CNT improves the conductivity of the electrode and increases the specific surface area, thus reducing the charge/discharge internal resistance.

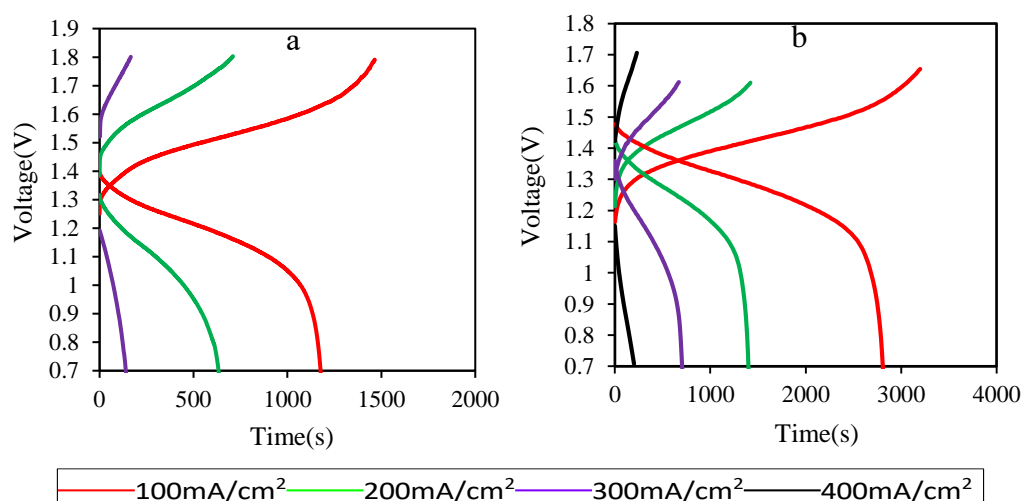


**Fig. 3.9** Charge and discharge data

**Table 3-4.** Constant current charge and discharge data (A: untreated carbon felt, B: treated carbon felt)

	100mA/cm <sup>2</sup>		200mA/cm <sup>2</sup>		300mA/cm <sup>2</sup>		400mA/cm <sup>2</sup>	
	A	B	A	B	A	B	A	B
IR (Ω)	1.715	0.65	1.34	0.56	1.25	0.61	-	0.68
EV(%)	77.63	90.95	66.02	84.72	58.03	82.61	-	75.35
EC(%)	82.73	88.13	96.47	92.50	92.17	82.61	-	88.31
OD(W/L)	297.5	326.5	270.5	314.75	246.5	23750	-	283.5
ED(Wh/L)	100.16	255.76	49.29	129.40	10.48	1253.47	-	53.55
EE(%)	64.22	80.15	63.69	78.37	53.49	68.24	-	66.54

For the charge/discharge experimental data, the AC Impedance of the battery was measured, and the results (Nyquist plot) are shown in **Fig. 3.10** for the test range of  $10^5 \text{ Hz} \rightarrow 0.1 \text{ Hz}$ . The intersection of the starting position of the curve with the x-axis is the on-state resistance (RL) of the battery itself. In the figure, the half-circle part is the charge-movement resistance (RP) in the high-frequency region, and the diagonal part is the material-movement resistance (RD) in the low-frequency region.  $\sigma$  is called the Warburg coefficient,  $\omega$  is the frequency, and Cd is the double layer capacitance. The calculation equation is shown in (3-9) and (3-10).

$$Z' = R_L + \frac{\frac{\sigma}{\sqrt{\omega}} + R_P}{(1 + \sigma\sqrt{\omega}C_d)^2 + \omega^2 C_d^2 \left(\frac{\sigma}{\sqrt{\omega}} + R_P\right)^2} \quad (3-9)$$

$$Z'' = \frac{\frac{\sigma}{\sqrt{\omega}}(1 + \sigma\sqrt{\omega}C_d)^2 + \omega C_d \left(\frac{\sigma}{\sqrt{\omega}} + R_P\right)^2}{(1 + \sigma\sqrt{\omega}C_d)^2 + \omega^2 C_d^2 \left(\frac{\sigma}{\sqrt{\omega}} + R_P\right)^2} \quad (3-10)$$

The main purpose of this experiment is to review the charge movement resistance RP in the high frequency region and the matter movement resistance RD in the low frequency region. from the measured Nyquist diagram, it can be calculated that  $RP=0.7\Omega$  and  $RD=1\Omega$  for the untreated carbon felt and  $RP=0.025\Omega$  and  $RD=0.035\Omega$  for the treated carbon felt. it can be seen that the charge and discharge impedance of the coated carbon felt is reduced by about 5 times.

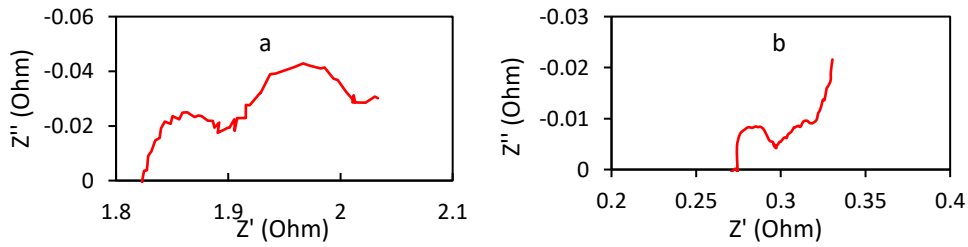


**Fig. 3.10** Single battery cell Nyquist figure

For the results of constant current charging and discharging, we performed Raman spectroscopy and XRD surface crystallographic analysis on two carbon felts.

In this paper, we use the common method of Raman spectroscopy to analyze carbon materials. There are two characteristic peaks in the Raman spectrum of carbon materials: the G peak near  $1580 \text{ cm}^{-1}$  and the D peak near  $1360 \text{ cm}^{-1}$  [36]. Researchers usually go through the D and G peaks. The integrated area ratio ID/IG is used to determine the integrity of the carbon material. the larger the ID/IG ratio, the lower the structural integrity of the carbon material. the

smaller the ID/IG ratio, the higher the structural integrity of the carbon material [37,38]. In this study, the treated carbon fiber electrodes were tested by Raman spectroscopy using NRS-4100 from JASCO. The measured Raman spectra are shown in **Fig. 3.11**, and the measured data are shown in **Table 3-5**. Combining the Raman spectra and the measured data, it can be seen that the peak shapes of the D and G peaks of the coated treated carbon felt became relatively sharp and obvious, and the integrated area ratio and half-height width of the peaks also became smaller, and the characteristic peak G' appeared near 2700 cm<sup>-1</sup> of the carbon felt, and the ratio of ID/IG decreased by 0.068.

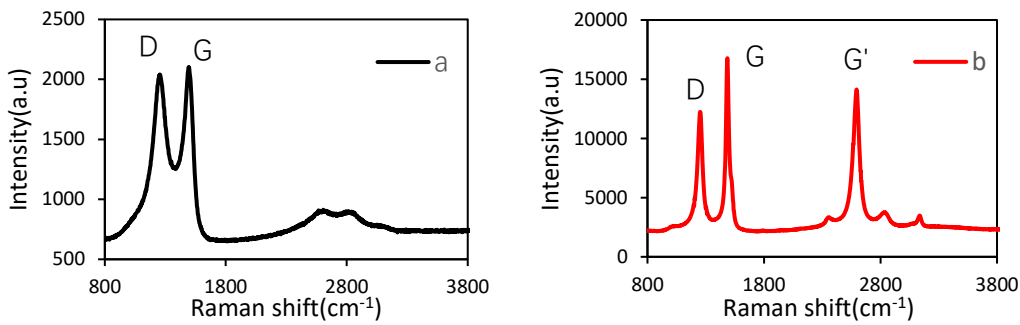


**Fig. 3.11** Structural analysis result by Raman spectroscopy

**Table 3-5.** Calculated results of Raman analysis

Sample	D peak		G peak		ID/IG (Area)
	Raman shift (cm <sup>-1</sup> )	FWHM (cm <sup>-1</sup> )	Raman shift (cm <sup>-1</sup> )	FWHM (cm <sup>-1</sup> )	
a	1252	307.33	1487	147.81	1.038
b	1255	71.90	1491	52.01	0.97

For the surface crystal structure, untreated and treated carbon fibers were analyzed using the RINT 2500 VHF from RIGAKU Corporation, Japan, under the following test conditions: Voltage: 40 kV: 30 mA (Cu). The measurement results are shown in **Fig. 3.12**. It can be seen that the shape of the (002) diffraction peak for 2θ=25° is basically the same. However, the intensity of the peak increases after the coating treatment. There is no significant difference in the (100) diffraction peak at 2θ = 43°.

$$d_{002} = \frac{\lambda}{2\sin\theta} \quad (3 - 11)$$

$$L = \frac{K\lambda}{\beta\cos\theta} \quad (3 - 12)$$

According to formula (3-11) and formula (3-12), the layer spacing  $d_{002}$  of the carbon fiber graphite crystallites and the thickness of the crystallite stack  $L_c$  can be calculated[39]. The (100) peak in the XRD spectrum can be used to calculate the direction of the graphite crystallite along the axis. The crystal plane width  $L_a$ . The diffraction angle of the  $\theta$  crystal plane diffraction peak;  $\lambda$  is the wavelength ( $\lambda = 0.1541\text{nm}$ );  $K$  is the shape factor,  $K = 0.94$  when  $L_c$  is calculated, and  $K = 1.84$  when  $L_a$  is calculated;  $\beta$  is the measured full width at half maximum. The calculation results are shown in **Table 3-6**.

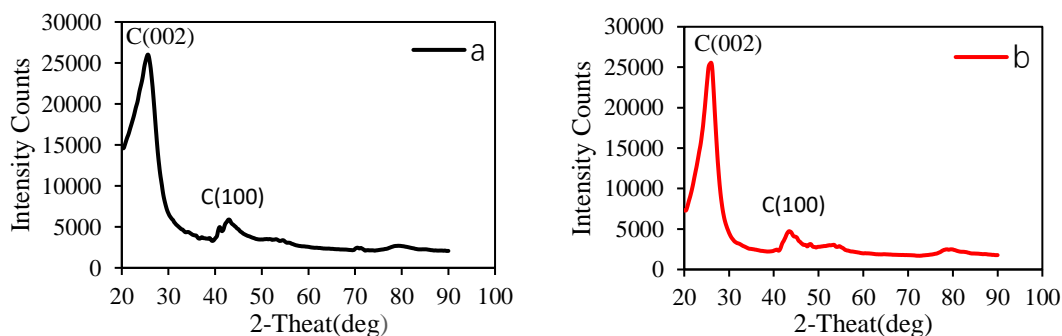


**Fig. 3.12.** Results of crystal structure analysis by XRD (a: unprocessed, b: processed).

From the comparison of the calculated results in **Table 3-6**, it can be found that there is no significant difference between the crystal spacing  $d_{002}$  and the crystal spacing  $d_{100}$  of the untreated and treated electrodes; the radial size  $L_c$  and the axial size  $L_a$  of the crystals of the treated carbon fiber electrodes become larger. The larger crystallite size indicates a more complete development and a higher degree of graphitization [40]. Therefore, it was theoretically demonstrated that the performance of the treated carbon cellulose electrodes was higher than that of the untreated electrodes.

**Table 3-6.** XRD patterns of untreated and treated carbon felts (a: untreated, b: treated carbon felts)

CF	C(002) crystallographic plane				C(100) crystallographic plane			
	$2\theta /^\circ$	$d/\text{nm}$	$\beta/\text{rad}$	$L_c / \text{nm}$	$2\theta /^\circ$	$d/\text{nm}$	$\beta/\text{rad}$	$L_a / \text{nm}$
a	25.6	0.356	0.141	1.054	42.8	0.228	1.385	0.221
b	25.8	0.354	0.100	1.488	43.4	0.224	1.237	0.246

### 3.2.4 Conclusion

In this paper, we improve the VRFB system by proposing a method for dispersion coating of CNT on the surface of carbon electrodes. The following results were obtained from this study.

1. The performance of the existing carbon felt is improved by the CNT surface coating method. Charge and discharge data show that the current density of VRFB can reach up to  $400\text{mA/cm}^2$ . At a current density of  $200\text{mA/cm}^2$ , the energy efficiency is close to 80%, which is about 15% higher than that of untreated carbon felt.

2. AC Impedance data surface, the treated carbon felt reduces the RP by  $0.68\Omega$  and the RD by  $0.96\Omega$  during charging and discharging so that the charge and discharge internal resistance of VRFB is reduced by 3 times.

3. Raman and XRD analyses of the two carbon felts were performed, and the experimental results showed that the ID/IG of the treated carbon felts decreased by 0.068, while the XRD calculation data showed that the crystal radial size  $L_c$  and axial size  $L_a$  of the treated carbon fiber electrode became larger.

4. In this study, the performance of the coated treated carbon felts was tested, but the durability of the treated carbon felts needs further study.

### 3.3 Concluding remarks

Through the above research, we summarize the optimum temperature of carbon fiber heat treatment and obtain electrodes with excellent performance through CNT coating experiments, and the performance is improved by about 3 times. However, the durability of the coated electrodes needs further verification.

### 3.4 Nomenclature

C	concentration ( $\text{molm}^{-3}$ )
D	density(*L)
d	discharge
E	efficiency (%) / energy
K	mass transfer coefficient ( $\text{ms}^{-1}$ )
L	length (m)

O	output density (W/L)
R	area specific resistance ( $\Omega\text{cm}^2$ )
t	thickness (m)
T	temperature (K)/Time(s)
U	charge and discharge voltage(V)
V	cell voltage (V)

Greek Symbols

$\sigma$	Warburg factor
$\lambda$	wavelength ( $\lambda = 0.1541$ nm)
$\theta$	angle ( $^\circ$ )
$\beta$	rad
$\Omega$	frequency
$\Omega$	ohm

Superscripts and Subscripts

avg	average charge charge process
discharge	discharge process

### 3.5 References

1. Álvaro Cunha , Jorge Martins , Nuno Rodrigues , F. P. Brito. Vanadium Redox Flow Batteries: a Technology Review. International Journal of Energy Research 39(7).
2. S.S. Hosseiny, M. Wessling, Ion exchange membranes for vanadium redox flow batteries. Advanced Membrane Science and Technology for Sustainable Energy and Environmental Applications 2011.
3. Ravendra Gundlapalli. Sanjay Kumar. Sreenivas Jayanti. Stack Design Considerations for Vanadium Redox Flow Battery. INAE Letters · June 2018
4. Y.K.Zeng,T.S.Zhao,L.An,X.L.Zhou,L.Wei. A comparative study of all-vanadium and iron-chromium redox flow batteries for large-scale energy storage. Journal of Power Sources Volume 300, 30 December 2015, Pages 438-443
5. Gareth Kear .Akeel A. Shah .Frank C. Walsh. Development of the all-vanadium redox flow battery for energy storage: a review of technological, financial and policy aspects. International Journal of Energy Research 36(11).
6. Christian Blanc .Alfred Rufer. Understanding the Vanadium Redox Flow Batteries. Paths to Sustainable Energy. December 30th 2010.Pages.333-358
7. Q. H. Liu, G. M. Grim, A. B. Papandrew, A. Turhan, T. A. Zawodzinski and M. M. Mench. High Performance Vanadium Redox Flow Batteries with Optimized Electrode

- Configuration and Membrane Selection. *Journal of The Electrochemical Society*, Volume 159, Number 8.
8. M.R.Mohamed, P.K.Leung, M.H.Sulaiman. Performance characterization of a vanadium redox flow battery at different operating parameters under a standardized test-bed system. *Applied Energy*. Volume 137, 1 January 2015, Pages 402-412.
  9. Kear, G.; Shah, A.A.; Walsh, F.C. Development of the all-vanadium redox flow battery for energy storage: A review of technological, financial and policy aspects. *Int. J. Energy Res.* 2012, 36, 1105–1120.
  10. Holzman, D.C. The Vanadium Advantage: Flow Batteries Put Wind Energy in the Bank. *Environ. Health Perspect.* 2007, 115, A358–A361.
  11. Shigematsu, T. Redox Flow Battery for Energy Storage. *SEI Tech. Rev.* 2011, 73, 4–13.
  12. Liu, X.; Li, K. Energy storage devices in electrified railway systems. *Transp. Saf. Environ.* 2020, 2, 183–201.
  13. Jiang, H.; Wei, L.; Fan, X.; Xu, J.; Shyy, W.; Zhao, T. A novel energy storage system incorporating electrically rechargeable liquid fuels as the storage medium. *Sci. Bull.* 2019, 64, 270–280.
  14. Ortiz-Martínez, V.M.; Gómez-Coma, L.; Perez, G.; Ortiz, A.; Ortiz, I. The roles of ionic liquids as new electrolytes in redox flow batteries. *Sep. Purif. Technol.* 2020, 252, 117436.
  15. Doetsch, C.; Pohlig, A. The Use of Flow Batteries in Storing Electricity for National Grids. In *Future Energy—Improved: Sustainable and Clean Options for Our Planet*, 3rd ed.; Elsevier: Amsterdam, The Netherlands, 2020; pp. 263–277.
  16. Zhu, Z.; Meng, Y.; Wang, M.; Yin, Y.; Chen, W. A high-performance aqueous iron–hydrogen gas battery. *Mater. Today Energy* 2021, 19, 100603.
  17. Larcher, D.; Tarascon, J.M. Towards greener and more sustainable batteries for electrical energy storage. *Nat. Chem.* 2015, 7, 19–29.
  18. Gür, T.M. Review of electrical energy storage technologies, materials and systems: Challenges and prospects for large-scale grid storage. *Energy Environ. Sci.* 2018, 11, 2696–2767.

19. Skyllas-Kazacos, M.; Rychcik, M.; Robins, R.G.; Fane, A.G.; Green, M.A. New all-vanadium redox flow cell. *J. Electrochem. Soc.* 1986, 133, 1057.
20. Wu, Q.; Zhang, X.; Lv, Y.; Lin, L.; Liu, Y.; Zhou, X. Bio-inspired multiscale-pore-network structured carbon felt with enhanced mass transfer and activity for vanadium redox flow batteries. *J. Mater. Chem.* 2018, 6, 20347–20355.
21. Wu, X.; Xu, H.; Shen, Y.; Xu, P.; Lu, L.; Fu, J.; Zhao, H. Treatment of graphite felt by modified Hummers method for the positive electrode of vanadium redox flow battery. *Electrochim. Acta* 2014, 138, 264–269.
22. Jiang, H.R.; Shyy, W.; Wu, M.C.; Wei, L.; Zhao, T.S. Highly active, bi-functional and metal-free B4C-nanoparticle-modified graphite felt electrodes for vanadium redox flow batteries. *J. Power Sources* 2017, 365, 34–42. *Coatings* 2021, 11, 736 11 of 11
23. Zhang, J.; Jiang, G.; Xu, P.; Kashkooli, A.G.; Mousavi, M.; Yu, A.; Chen, Z. An all-aqueous redox flow battery with unprecedented energy density. *Energy Environ.* 2018, 11, 2010–2015.
24. Kim, S.; Choi, J.; Choi, C.; Heo, J.; Kim, D.W.; Lee, J.Y.; Hong, Y.T.; Jung, H.T.; Kim, H.T. Pore-Size-Tuned Graphene Oxide Frameworks as Ion-Selective and Protective Layers on Hydrocarbon Membranes for Vanadium Redox-Flow Batteries. *Nano Lett.* 2018, 18, 3962–3968.
25. Zhu, H.Q.; Zhang, Y.M.; Yue, L.; Li, W.S.; Li, G.L.; Shu, D.; Chen, H.Y. Graphite–carbon nanotube composite electrodes for all vanadium redox flow battery. *J. Power Sources* 2008, 184, 637–640.
26. Saha, A.; Basiruddin, S.K.; Ray, S.C.; Roy, S.S.; Jana, N.R. Functionalized graphene and graphene oxide solution via polyacrylate coating. *Nanoscale* 2010, 2, 2777–2782. [PubMed]
27. Pezeshki, A.M.; Clement, J.T.; Veith, G.M.; Zawodzinski, T.A.; Mench, M.M. High performance electrodes in vanadium redox flow batteries through oxygen-enriched thermal activation. *J. Power Sources* 2015, 294, 333–338.
28. So, S.; Cha, M.S.; Jo, S.W.; Kim, T.H.; Lee, J.Y.; Hong, Y.T. Hydrophilic Channel Alignment of Perfluorinated Sulfonic-Acid Ionomers for Vanadium Redox Flow Batteries. *ACS Appl. Mater. Interfaces* 2018, 10, 19689–19696. [PubMed]

29. Zeng, L.; Sun, J.; Zhao, T.S.; Ren, Y.X.; Wei, L. Balancing the specific surface area and mass diffusion property of electrospun carbon fibers to enhance the cell performance of vanadium redox flow battery. *Int. J. Hydrogen Energy* 2020, 45, 12565–12576.
30. Di Blasi, A.; Busacca, C.; Di Blasi, O.; Briguglio, N.; Antonucci, V. Synthesis and characterization of electrospun nickel-carbon nanofibers as electrodes for vanadium redox flow battery. *J. Electrochem. Soc.* 2018, 165, 1478–1485.
31. Maharjan, M.; Bhattarai, A.; Ulaganathan, M.; Wai, N.; Oo, M.O.; Wang, J.Y.; Lim, T.M. High surface area bio-waste based carbon as a superior electrode for vanadium redox flow battery. *J. Power Sources* 2017, 362, 50–56.
32. Ulaganathan, M.; Jain, A.; Aravindan, V.; Jayaraman, S.; Ling, W.C.; Lim, T.M.; Srinivasan, M.P.; Yan, Q.; Madhavi, S. Bio-mass derived mesoporous carbon as superior electrode in all vanadium redox flow battery with multicouple reactions. *J. Power Sources* 2015, 274, 846–850.
33. Wei, G.J.; Gao, Z.G.; Wei, Z.F.; Fan, X.Z.; Liu, J.G.; Yan, C.W. Coupling effect between the structure and surface characteristics of electrospun carbon nanofibres on the electrochemical activity towards the VO<sub>2</sub><sup>+</sup>/VO<sub>2</sub><sup>3+</sup> redox couple. *Phys. Chem. Chem. Phys.* 2015, 17, 20368–20375.
34. Zeng, L.; Zhao, T.; Wei, L. Revealing the performance enhancement of oxygenated carbonaceous materials for vanadium redox flow batteries: Functional groups or specific surface area? *Adv. Sustain. Syst.* 2018, 2, 1700148.
35. Estevez, L.; Reed, D.; Nie, Z.; Schwarz, A.M.; Nandasiri, M.I.; Kizewski, J.P.; Wang, W.; Thomsen, E.; Liu, J.; Zhang, J.G.; et al. Tunable oxygen functional groups as electrocatalysts on graphite felt surfaces for all-vanadium flow batteries. *Chemsuschem* 2016, 9, 1455–1461.
36. Tuinstra, F.; Koenig, J.L. Characterization of graphite fiber surfaces with Raman spectroscopy. *J. Compos. Mater.* 1970, 4, 492–499.
37. Nakamizo, M.; Honda, H.; Inagaki, M. Raman spectra of ground natural graphite. *Carbon* 1978, 16, 281–283.
38. Nemanich, R.J.; Solin, S.A. First and second-order Raman scattering from finite-size crystals of graphite. *Phys. Rev. B* 1979, B20, 39240.

39. Zhu, B.; Cao, W.; Wu, Y.; Cai, X.; Zhao, W. Effect of high temperature heat treatment on RMS spectrum property of carbon felt. *Heat Treat. Metals* 2011, 36, 8.
40. Min, J. Comparison of the Microstructure of Toray T800H and T800S Carbon Fibers. *Mater. Sci. Technol.* 2015, 23, 45–52.

## Chapter 4 Optimal design of battery structure and battery pack test experiment

All-vanadium redox flow batteries have been researched for more than 30 years since 1985. Battery technology is also maturing [1-4]. At the beginning of research on vanadium redox flow batteries, researchers mainly paid attention to the performance of battery components. With the progress of research, people began to study the various components of the stack [5-8]. For example, the electrolyte flow path of the battery has been developed from the original DC type, and has gradually developed a serpentine flow path, a comb-shaped flow path, and the like. Each electrolyte flow path has a different effect on battery performance [9-12].

While studying the electrolyte flow path, factors such as the flow rate of the electrolyte and the compression ratio of the electrodes also play a crucial role in the performance of the battery [13-15].

This chapter mainly introduces the influence of electrolyte flow path and electrolyte flow rate and electrode compression ratio on battery performance. The self-made single cells were evaluated through simulation and charge-discharge experiments to find the most suitable conditions.

According to the characteristics of the all-vanadium redox flow battery, we have mainly improved the battery from the following three aspects.

2. The optimal design of the existing battery frame, through simulation and charging and discharging experiments, verify the charging and discharging performance of the battery under different inlet and outlet flow paths.

3. Adjust the flow rate of the electrolyte of the battery and the compression ratio of the carbon fiber electrode to find the most suitable relationship between the compression ratio of the carbon felt and the flow of the electrolyte.

## 4.1 Optimum design of battery frame

### 4.1.1 Introduction

In this study, the flow of electrolyte in three different inlet and outlet widths of VRFB cell frames with frame size of 5 cm (x) × 10 cm (y) and flow direction in y direction was simulated by Fluent software. The flow uniformity of the simulated electrolyte is analyzed for the same compression ratio, the same electrolyte flow rate, and different inlet and outlet widths. And the effect of electrolyte flow characteristics on the battery performance in three cases is verified experimentally. The three kinds of frames are frame 1. 1.5mm×4 inlet and 2mm×5 outlet. Frame 2. 2mm×5 for inlet and 1.5mm×4 for outlet. Frame 3. 1.5mm×4 for inlet and outlet. It is proved that the charge/discharge internal resistance of frame 1 is minimum 0.4Ω, frame 2 is minimum 0.6Ω, and frame 3 is minimum 0.5Ω under the electrolyte flow rate of 240mL/min. It is proved by simulation and charge/discharge comparison experiments that the inlet width is smaller than the outlet width can improve the charge/discharge performance of VRFB in the case of common flow path.

### 4.1.2 Experimental conditions

The main purpose of this experiment is to simulate three different VRFB frame flow path designs and analyze how the characteristics of electrolyte flow inside the battery assembled by the three frames differ under the same conditions. For the different flow characteristics of the electrolyte, charge and discharge experiments are conducted on the battery to compare the experimental results, thus demonstrating the effect of the flow characteristics on the battery performance.

The VRFB cell used in this experiment is a single cell with a homemade electrode area of 50 cm<sup>2</sup> (5 cm × 10 cm). The cell structure is shown in **Fig. 4.1**. The experimental cell diaphragm is a proton exchange membrane (Nafion211), the bipolar plate is a 5mm thick carbon plate, and the collector plate is a 0.6mm thick copper plate with gold plated surface. The electrolyte is 1.6

mol/L vanadium sulfate electrolyte made by LE SYSTEM. The flow pump for the test is a screw pump, which is easier to achieve large scale than most experimental peristaltic pumps.

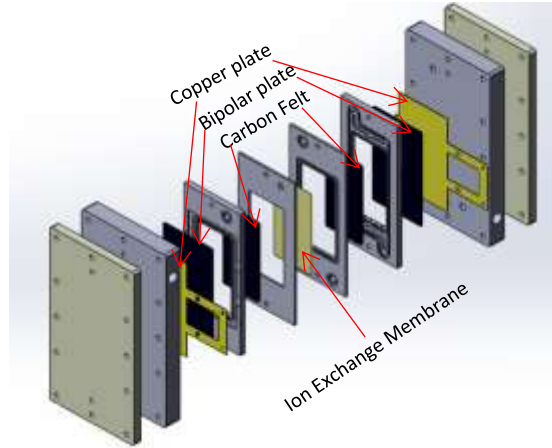


**Fig. 4.1.** Internal structure of the battery

A three-dimensional mathematical model is used to simulate the electrolyte flow with different inlet and outlet methods. The model is mainly divided into three parts (1) electrolyte inlet part, (2) intermediate porous media material part, and (3) electrolyte outlet part. The parameters of the porous media material are mainly, porosity, permeability, and specific surface area. In this study, we mainly study the flow of electrolyte in carbon felt, so only the porosity of carbon felt is considered. Porosity is the ratio of the volume of all voids in the porous medium per unit volume to the total volume. As shown in equation (4-1).  $\phi_a$  in the formula is the porosity,  $V_r$  is the volume of pores, and  $V$  is the total volume.

$$\phi_a = \frac{V_r}{V} \times 100\% \quad (4 - 1)$$

Two different flow frames were simulated by Fluent software to analyze the flow characteristics of the electrolyte in the frame. The simulation conditions are porous system material. The electrolyte viscosity was set to 1.3 times of who, and the initial flow velocity was 0.3m/s. The charge/discharge experiments were performed for constant current charge/discharge with an electrolyte flow rate of  $2.4\text{mlmin}^{-1}\text{cm}^{-2}$  and a carbon felt compression ratio of 30%. The charge/discharge data results were calculated by conducting charge/discharge experiments for two batteries with different electrolyte flow paths and comparing the experimental results. The charge and discharge internal resistance (IR), voltage efficiency (EV), coulombic efficiency (EC), energy efficiency (EE), energy density (ED) and output density

(OD) of the battery were calculated based on the constant current charge and discharge curves. The calculation equations are shown in (4-2)-(4-7).

$$I_R = \frac{U_{avg.charge} - U_{avg.discharge}}{2C_D} \quad (4-2)$$

$$E_V = \frac{U_{avg.discharge}}{U_{avg.charge}} \times 100\% \quad (4-3)$$

$$E_C = \frac{\int i_{discharge}(t) dt}{\int i_{charge}(t) dt} \times 100\% \quad (4-4)$$

$$E_E = E_V \times E_C \quad (4-5)$$

$$O_D \left( \frac{W}{L} \right) = \frac{I \times U_{avg.discharge}}{V_1} \quad (4-6)$$

$$E_D \left( \frac{Wh}{L} \right) = \frac{I \times T_d \times U_{avg.discharge}}{V_1} \quad (4-7)$$

### 4.1.3 Experimental results

The flow patterns of electrolyte in different flow paths were analyzed by simulating four different frames. The simulation results are shown in **Fig. 4.2**.

The comparison in **Fig. 4.2** shows that for the frame without flow path, the electrolyte flows diagonally inside with higher pressure in the inlet and outlet parts and higher flow rate, and the pressure at the remaining two diagonal parts is small. The electrolyte does not flow uniformly inside the battery, which reduces the utilization rate of the electrolyte and the charging performance.

The electrolyte in the frame of the comb type flow path enters perpendicular to the direction of the carbon felt, and then diffuses out to both sides. The internal electrolyte flow uniformity is the

best, and the utilization rate of carbon homburg is the highest. The comparison between the two ways shows that the electrolyte can flow out smoothly inside the battery with a small inlet and a large outlet, but with a large inlet and a small outlet, the electrolyte has a high pressure at the outlet, and the electrolyte cannot flow out of the battery in time after charging and discharging, which can easily cause local voltage increase.

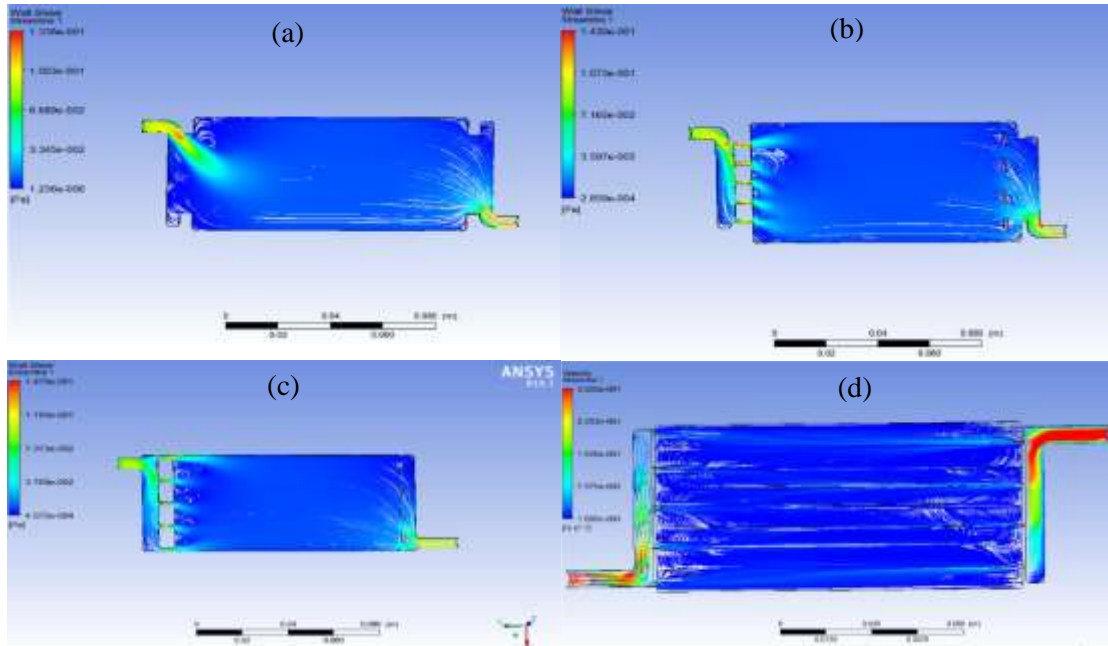


**Fig. 4.2.** Simulation results of electrolyte flow in the bipolar plate;(a) No flow path;(b) Parallel flow path, large inlet and small outlet;(c) Parallel flow path, small inlet and large outlet;(d) Comb-type flow path

For the simulation results,  $100\text{mA}/\text{cm}^2$  charge/discharge experiments were conducted for four different frames of batteries with carbon felt compression ratio of 30%. The flow rate of electrolyte was controlled by changing the voltage of the flow pump. The flow rate was about  $63\text{ml}/\text{min}$  at  $PV=2\text{V}$ ,  $125\text{ml}/\text{min}$  at  $PV=3\text{V}$ ,  $190\text{ml}/\text{min}$  at  $PV=4\text{V}$  and  $290\text{ml}/\text{min}$  at  $PV=5\text{V}$ . The charging and discharging curves are shown in **Fig.4.3** and the calculation results are shown in **Table 4-1**.

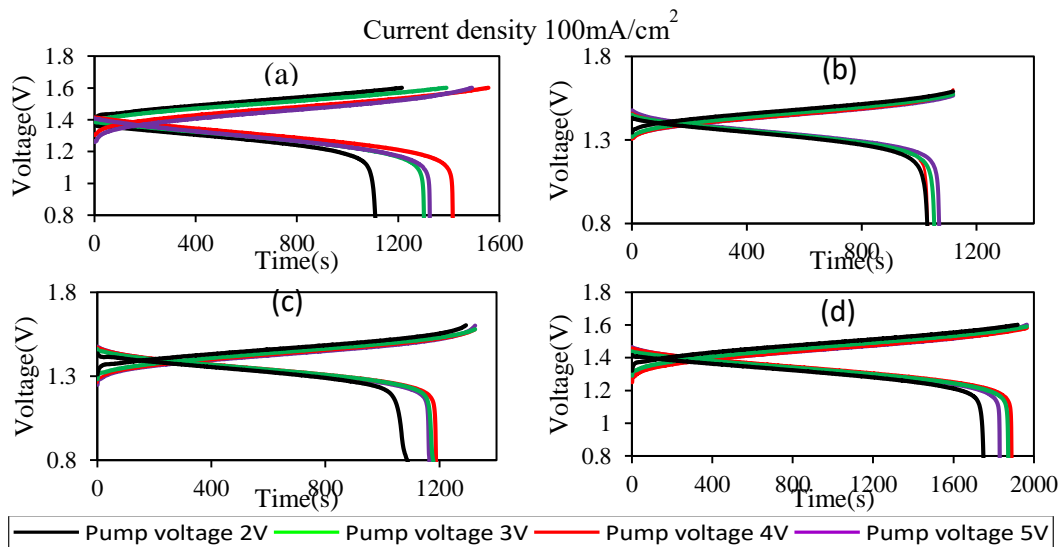


**Fig. 4.3** Charge and discharge experiments of three different flow path batteries

**Table 4-1** The calculation results

CD		100mA/cm <sup>2</sup>					
PV	IR	EV	EE	EC	OD	ED	
(V)	(Ω/cm <sup>2</sup> )	(%)	(%)	(%)	(W/L)	(Wh/L)	
a	2	1.17	84.57	74.84	88.5	320.5	99.8
	3	1.04	85.65	77.21	90.15	322.25	116.73
	4	0.89	87.96	81.01	92.1	325	128.01
	5	0.84	88.46	80.67	91.2	323	118.78
	2	0.76	89.73	82.16	91.56	332	96.10
b	3	0.64	91.26	83.32	91.31	334	98.44
	4	0.56	92.19	85.60	92.85	333.5	96.25
	5	0.56	92.29	85.84	93.01	335.00	100.31
	2	0.66	90.98%	77.90%	85.61%	333	102.40
c	3	0.54	92.53%	83.88%	90.65%	334.5	113.54
	4	0.475	93.37%	84.14%	90.11%	334.5	112.62
	5	0.465	93.50%	83.34%	89.13%	334.50	109.73
	2	0.76	89.73%	82.16%	91.56%	332	96.10
d	3	0.64	91.26%	83.32%	91.31%	334	98.44
	4	0.565	92.19%	85.60%	92.85%	333.5	96.25
	5	0.56	92.29%	85.84%	93.01%	335.00	100.31

The charging and discharging curves show that the frame without flow path in **Fig. 4.3a** is most severely affected by the electrolyte flow. The comb-type flow path has almost no effect on the cell flow rate. The remaining two frames have lower discharge performance, when the electrolyte flow rate is lower than 125 ml/min, and the performance has no effect after the flow rate is greater than 125 ml/min. Combined with the simulation, it can be analyzed that the electrolyte of the no-flow path frame flows diagonally, the flow distance is farther, and the internal electrolyte flow is not uniform, which leads to the poor charging and discharging performance. The electrolyte in the comb type flow path enters perpendicular to the surface of the carbon felt and then diffuses out to both sides, with the shortest flow distance and the best

uniformity. The other two frames are parallel to the surface of the carbon felt, and the flow distance is small compared to the diagonal flow distance, and the uniformity is good. However, the effect of the width of the inlet outlet on the electrolyte can be seen in **Fig.4.3. c** and **Fig. 4.3d**. When the flow rate is less than 125 ml/min, the discharge performance of frame 3 decreases. The reason for the analysis is that when the outlet width is smaller than the inlet width, the electrolyte cannot flow out of the inside of the cell in time, resulting in the degradation of the cell performance.

For the above charging and discharging experiments, the comb type flow path has the most outstanding performance, but at the same time, the processing cost is also much higher than other frames, so it is not conducive to cost saving when the cell size is expanded. So we think that the same performance can be achieved by the ordinary flow path when the flow rate is greater than 190ml/min.

To analyze the effect of the inlet and outlet widths on the cells with normal flow paths after cell size expansion, we conducted high current density charging and discharging experiments for frames 3 and 4 with current densities of 100mA/cm<sup>2</sup>-800mA/cm<sup>2</sup>. the results are shown in **Fig. 4.4** and **Table 4-2**. **Fig. 4.4 a** shows frame 3 and **Fig. 4.4 b** shows frame 4.

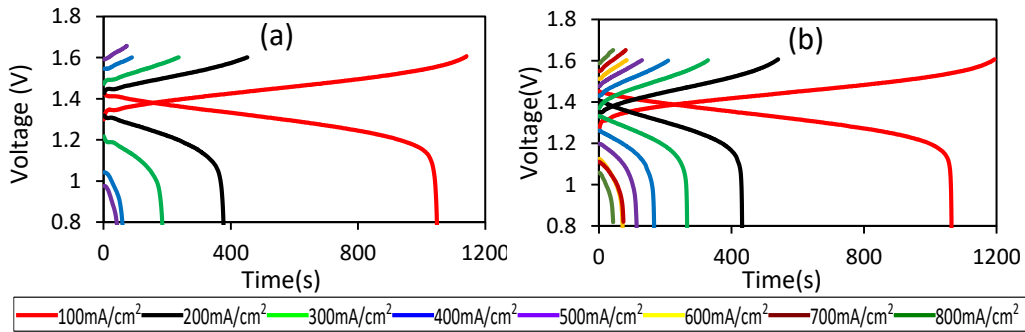


**Fig. 4.4** Comparison of charge and discharge of two electrodes

**Table 4-2** Calculation results

	$C_D$ (mA/cm <sup>2</sup> )	$I_R$ (Ω/cm <sup>2</sup> )	$E_V$ (%)	$E_E$ (%)	$E_C$ (%)	$O_D$ (W/L)	$E_D$ (Wh/L)
a	100	0.76	89.62	85.30	95.18	326	98.34
	200	0.71	81.14	68.57	84.51	613	65.05
	300	0.69	73.15	58.89	80.51	843.75	44.53
	400	0.76	61.55	47.72	77.53	967.00	18.53
	500	0.73	55.17	41.57	75.34	1120.0	17.11
b	100	0.61	91.59	81.80	89.31	332.25	98.42

200	0.55	85.58	68.49	80.03	647	108.88
300	0.43	82.97	68.09	82.07	931.5	69.86
400	0.42	77.76	64.37	82.78	1182.00	56.80
500	0.42	72.86	67.26	92.31	1406.2	46.88
600	0.49	63.03	57.76	91.64	1491	44.48
700	0.40	65.42	59.76	91.36	1834	37.70
800	0.39	61.64	57.34	93.02	1996	22.18

The high current density charge/discharge curve shows that the highest current density of frame 3 is 500mA/cm<sup>2</sup> and the EE of the battery is below 60% when the current density is 300mA/cm<sup>2</sup>. The highest current density of frame 4 can reach 800mA/cm<sup>2</sup> and the EE tends to 70% at 500mA/cm<sup>2</sup>. The IR comparison shows that the charge/discharge internal resistance IR of frame 4 is smaller than that of frame 3. This further indicates that the uniformity of electrolyte flow in frame 4 is higher than that in frame 3.

#### **4.1.4 Conclusion**

In this study, the different flow patterns of electrolyte in the four flow paths were analyzed by simulating the four frames. And the effect of the four different flow paths on the battery performance was further confirmed by charging and discharging experiments.

The simulation analysis shows that the comb type flow path has the best homogeneous flow performance for electrolyte among the four feeding methods, and the frame electrode solution without flow path has the worst homogeneous flow performance. The uniform flow performance of electrolyte in the two common flow paths is higher than that in the frame without flow path.

The simulation results were further demonstrated by 100mA/cm<sup>2</sup> constant current charge/discharge experiments. The electrolyte flow rate has the greatest effect on the performance of the cell without flow path. The comb-type flow path is least affected by electrolyte flow rate. The discharge performance of the cells with two common type flow paths decreased when the electrolyte flow rate was lower than 190 ml/min. No effect when the flow rate is higher than 190 ml/min.

For the two common type of flow path for high current density charging and discharging of the battery, the experiment proves that the framework of small inlet and large outlet is more conducive to the performance of the battery, the reason for analysis is that the electrolyte after charging and discharging can pass through the internal battery faster, avoiding the phenomenon of voltage increase caused by the accumulation of electrolyte.

## **4.2 Adjustment of electrolyte flow and velocity**

### ***4.2.1 Introduction***

All vanadium flow batteries (VRFB) are used in the field of energy storage due to their long service life and high safety [16-19]. In order to further improve the charge-discharge performance of VRFB, this study mainly used the comparative evaluation of VRFB's carbon fiber electrode compression ratio and electrolyte flow rate. Charge and discharge the battery under different current density, different compression ratio and different flow rate. The results show that increasing the compression ratio at different current densities can reduce the internal resistance of the battery, but an excessive compression ratio will accelerate the transfer of vanadium ions, increase the deviation of the electrolyte, and reduce the coulombic efficiency of the battery. The performance of the battery tends to be balanced when the compression ratio is 30%. At the same time, in the case of the same compression ratio, increasing the flow rate of the electrolyte can reduce the internal reaction resistance of the battery. When the flow reaches a certain value, the influence on the internal resistance will be smaller.

### ***4.2.2 Experimental method***

This experiment mainly studies the influence of the compression ratio and flow/velocity of carbon fiber on the charge and discharge performance of the vanadium redox flow battery under the same conditions. The experimental single cell bipolar plate is 0.6mm, one kinds of carbon fiber, the thickness is 4mm, and the area is  $5\text{cm}\times 10\text{cm}=50\text{cm}^2$ . The experimental method is to determine the charge and discharge performance of the battery by changing the compression

ratio of the carbon dioxide electrode and the flow rate of the electrolyte. According to the measured data, choose the most suitable plan.

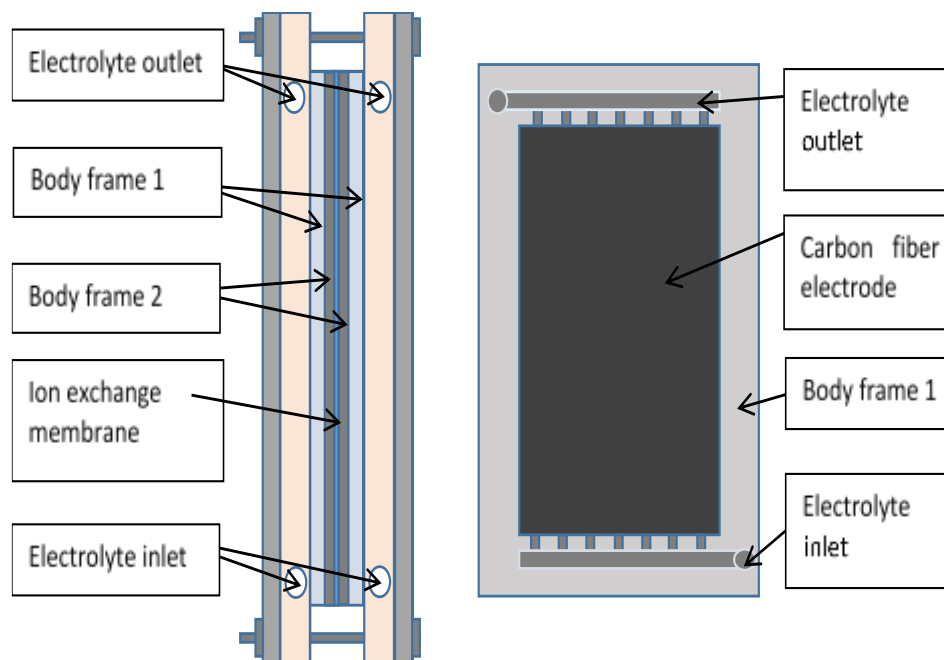


**Fig. 4.5.** Self-made VRFB framework for experiment

Due to the small electrode area of the vanadium redox battery on the market (about  $4\text{cm}\times 4\text{cm}$ ), the electrolyte flow distance in the carbon fiber electrode is very short, and it is easy to achieve a uniform speed. The obtained data cannot fully explain the effect of electrolyte flow rate on battery charging and discharging. Therefore, the battery used in this experiment is a self-designed single cell battery with an electrode area of  $50\text{cm}^2$  ( $10\text{cm}\times 5\text{cm}$ ). The flow path is shown in **Fig.4.5**. The compression ratio of carbon fiber is controlled by changing the thickness of the body frame 2. This experiment uses a variable flow screw pump, which tends to be more practical than a hose peristaltic pump. Peristaltic hose pumps are better in controlling flow and velocity, but large energy storage equipment cannot be used. Many experimental results obtained by using a hose peristaltic pump cannot be fully realized after the battery pack is expanded into a high-power variable-frequency pump. In this experiment, the battery diaphragm used proton exchange membrane (Nafion211), the bipolar plate was SGL 0.6mm thick, and the collector plate was 0.6mm thick gold-plated copper plate. The electrolyte is 1.6mol/L vanadium sulfate electrolyte manufactured by LE SYSTEM.

Conduct constant current (I=, 3A, 4A, 5A) charging and discharging experiments on the assembled battery through a constant current output power supply. A constant current (I=3A,4A,5A) charge and discharge experiment (CD current density : 60mA/cm<sup>2</sup>, 80mA/cm<sup>2</sup>,100mA/cm<sup>2</sup>) is performed on the assembled battery through a constant current output power supply. The charging and discharging voltage is 1.6V-0.8V. The flow rate of the electrolyte is controlled by changing the voltage of the flow pump. Carbon fiber compression ratio CR calculation formula is shown in (8) (carbon fiber thickness: d thickness after compression: d0) according to the constant current charge and discharge curve to calculate the battery's charge and discharge internal resistance (IR), voltage efficiency (EV), Coulomb efficiency (EC), energy efficiency (EE), energy density (ED) and output density (OD). The calculation formula is shown in (2)-(7), (pump voltage: PV. ,charge and discharge voltage: U, discharge time: Td, carbon fiber electrode volume: V1). In addition, the flow and velocity of the electrolyte are measured by external measuring equipment.

$$C_R = \frac{d - d_0}{d} \times 100\% \quad (4 - 8)$$

### 4.2.3 Experimental results

The influence of compression/flow ratio on the internal resistance of battery charge and discharge

As shown in **Fig. 4.7**, The different current density charge and discharge curves of the flow pump voltage of 2V-5V under different compression ratios. It can be seen from the comparison in **Fig. 4.7** that the charging and discharging curves appear to cross when the compression ratio increases. The initial charge voltage becomes lower, the initial discharge voltage becomes higher, and the charged battery OCV becomes larger. According to formula (2), the internal resistance IR of the battery can be calculated. , The results are shown in **Table 4-3**.

**Table 4-3.** IR changes under different CR and PV

$C_D(\text{mA}/\text{cm}^2)$	$C_R(\%)$	$P_V=2V$	$P_V=3V$	$P_V=4V$	$P_V=5V$
		$I_R(\Omega/\text{cm}^2)$	$I_R(\Omega/\text{cm}^2)$	$I_R(\Omega/\text{cm}^2)$	$I_R(\Omega/\text{cm}^2)$
60	10	3.25	2.80	2.16	1.90
	20	2.06	1.58	1.38	1.35
	30	1.68	1.10	1.05	0.98
	60	0.88	0.85	0.81	0.75

80	10	3.26	2.48	2.03	1.79
	20	1.91	1.72	1.52	1.51
	30	1.80	1.41	1.13	0.99
	60	1.01	0.92	0.76	0.70
100	10	2.91	2.18	1.93	1.70
	20	1.32	1.08	0.94	0.90
	30	1.17	1.04	0.89	0.84
	60	1.10	0.74	0.66	0.65

According to the data in **Table 4-3**, when the CD is the same, the battery's charge and discharge internal resistance IR decreases with the increase of PV, and decreases with the increase of CR. This is because the pore size of the carbon felt is also the same under the same CR. After the flow rate increases, the flow rate of the electrolyte in the carbon felt is faster, the charge-discharge reaction is faster, and the charge transfer resistance is smaller. In the case of the same PV, increasing the compression ratio can effectively reduce the contact resistance between carbon, bipolar plate and diaphragm. whilst, increase the compression ratio and reduce the pore size of the carbon. Under the same pressure, the smaller the pores, the faster the electrolyte flow rate flowing through the surface of the carbon, the faster the charge and discharge reaction, and the smaller the charge transfer resistance.

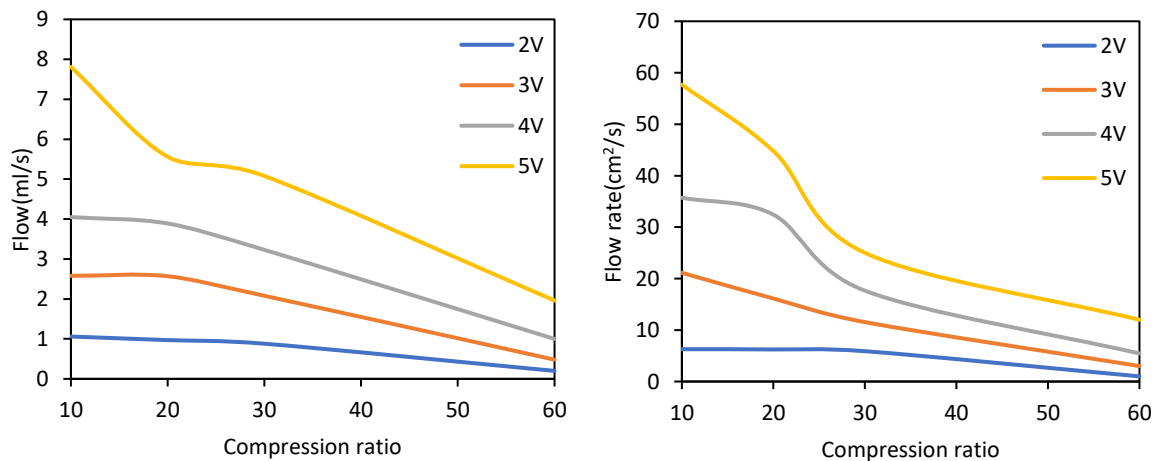


**Fig.4.6** The relationship between pump input voltage and flow rate with different compression ratios of 4mm carbon fiber.

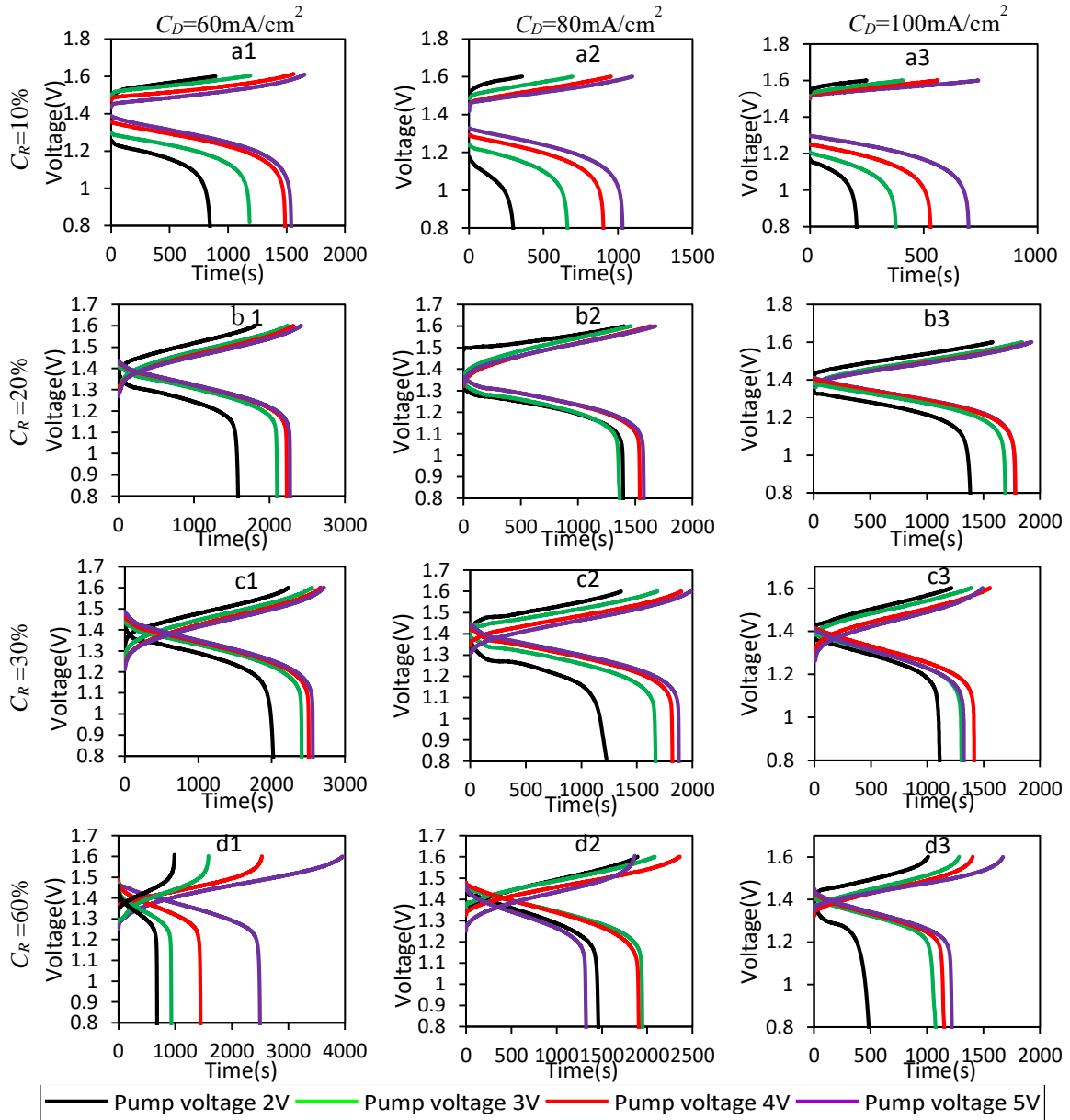


**Fig.4.7.** Charge and discharge data with different current densities, different compression ratios, and different electrolyte flow rates.

Simultaneously, it can be seen from **Fig.4.7** that under the same compression ratio, changing the supply flow rate of the electrolyte can effectively reduce the internal resistance of the battery during charge and discharge. The principle is the same as the previous explanation. When the flow rate of the pump reaches 4V-5V, the charge and discharge curves of the battery tend to coincide. This shows that when the flow rate of the electrolyte reaches a certain level, it will no longer affect the internal resistance of the battery in charge and discharge. **Fig.4.6.** shows the relationship between pump input voltage and electrolyte flow rate under different

compression ratios. It can be seen from the comparison in the **Fig.4.6.** that the compression ratio increases, the flow rate of the electrolyte decreases.

According to the different constant current charging and discharging data and formula 3 to formula 7, the battery charging and discharging data can be calculated as shown in **Table 4-4.** According to the data in **Table 4-4,** the relationship between the variable flow charging and discharging data under different compression ratios is summarized in **Fig. 4.8.** As shown, the comparison between **Table 4-4** and **Fig.4.8** shows that when the CR is the same, the battery's charge and discharge performance (EV, EE, OD, ED) Increase with the increase of PV. But EC is maximum at PV=3V-4V, the PV continues to increase and EC decreases instead. This is because the diaphragm used this time is N211, the thickness of the diaphragm is thin, and the electrolyte offset is serious, which affects the cullen efficiency of the battery. When CR=60% PV=2V, the EE, EC and ED of the battery are reduced by 50%. It can be seen from **Fig.4.6** that when PV=2V, the electrolyte flow rate is only 0.48ml/s. Because the electrolyte flow rate is too low, the reaction speed between the electrolyte and the carbon dioxide becomes low, and the voltage changes excessively during charge and discharge.

When the PV is the same, the CR is below 60%, EV, EE, OD and ED increase with the increase of CR. EC decreases as CR increases. When CR is 60%, the overall charge and discharge performance decreases. The overall performance is reduced by about 50%. This is because carbon dioxide is over-compressed at 60%, the specific surface area of the fiber is greatly reduced, the reaction speed of the electrolyte is reduced, and the charge and discharge performance is also reduced. Simultaneously, excessive compression makes the electrolyte drift more serious.

The long service life of the vanadium flow battery is its main feature. In this research works, the 50 times repeated experiments on the battery under different current densities, different compression ratios and different flow rates were carried out, and the changes in battery performance under different charge and discharge times were calculated. As the results of the first two charging and discharging experiments are unstable, the calculation results start from the third time. The experimental results are shown in **Fig. 4.8.** EC increases with the increase in the number of charging and then tends to balance. EV and EC decrease as the number of charging increases. When CR =10% PV=3V, the current density is 60 mA/cm<sup>2</sup>, EE drops by

0.33% after 50 cycles of charge and discharge, and EE drops by 0.43%. When the current density is increased by 100mA/cm<sup>2</sup>, EE decreases by 0.14%, and EV decreases by 0.18%. When CR =30% PV =5V, the current density is 60mA/cm<sup>2</sup>, EE drops by 0.13% after 50 cycles of charge and discharge, and EV drops by 0.25%. When the current density is increased by 100mA/cm<sup>2</sup>, the EE drops by 0.22% and the EV drops by 0.28%. In summary, in the case of low compression ratio and low electrolyte flow, increasing the current density can reduce the degradation of the battery's charge and discharge performance. When the compression ratio and electrolyte flow are increased, the battery charge and discharge performance deteriorates seriously.

**Table 4-4.** 4mm carbon fiber charge and discharge settlement results with different compression ratio

<i>C<sub>D</sub></i>	60mA/cm <sup>2</sup>						80mA/cm <sup>2</sup>					100 mA/cm <sup>2</sup>				
	<i>P<sub>V</sub></i> (V)	<i>E<sub>V</sub></i> (%)	<i>E<sub>E</sub></i> (%)	<i>E<sub>C</sub></i> (%)	<i>O<sub>D</sub></i> (W/L)	<i>E<sub>D</sub></i> (Wh/L)	<i>E<sub>V</sub></i> (%)	<i>E<sub>E</sub></i> (%)	<i>E<sub>C</sub></i> (%)	<i>O<sub>D</sub></i> (W/L)	<i>E<sub>D</sub></i> (Wh/L)	<i>E<sub>V</sub></i> (%)	<i>E<sub>E</sub></i> (%)	<i>E<sub>C</sub></i> (%)	<i>O<sub>D</sub></i> (W/L)	<i>E<sub>D</sub></i> (Wh/L)
10%	2	75	73	97	292	70	66	63	95	264	25	63	54	85	250	29
	3	78	77	99	305	100	74	72	9	289	54	65	62	94	258	55
	4	82	79	95	316	130	89	67	73	329	124	68	65	95	269	80
	5	84	79	93	320	137	90	70	78	331	137	71	67	94	279	109
	2	83	74	89	315	142	91	85	94	336	184	82	74	90	314	124
20%	3	87	83	95	325	193	92	74	81	335	179	86	80	93	322	154
	4	88	86	97	327	206	88	85	96	325	162	87	81	93	325	162
	5	89	84	94	327	208	89	86	95	326	163	87	82	93	326	163.
	2	86	79	91	321	183	81	78	97	307	112	84	74	88	320	99
30%	3	91	86	94	331	222	84	84	99	319	149	85	77	90	322	11
	4	91	86	94	330	231	87	84	96	324	165	87	81	92	325	128
	5	91	86	94	331	236	89	84	94	326	171	88	80	91	323	118
	2	92	53	57	331	64	89	67	73	329	124	85	43	50	318	45
60%	3	93	65	70	333	89	90	70	78	331	137	89	75	84	329	98
	4	93	59	64	337	136	91	85	94	336	184	90	77	84	330	109
	5	92	56	60	338	239	92	74	81	335	179	90	67	74	331	115

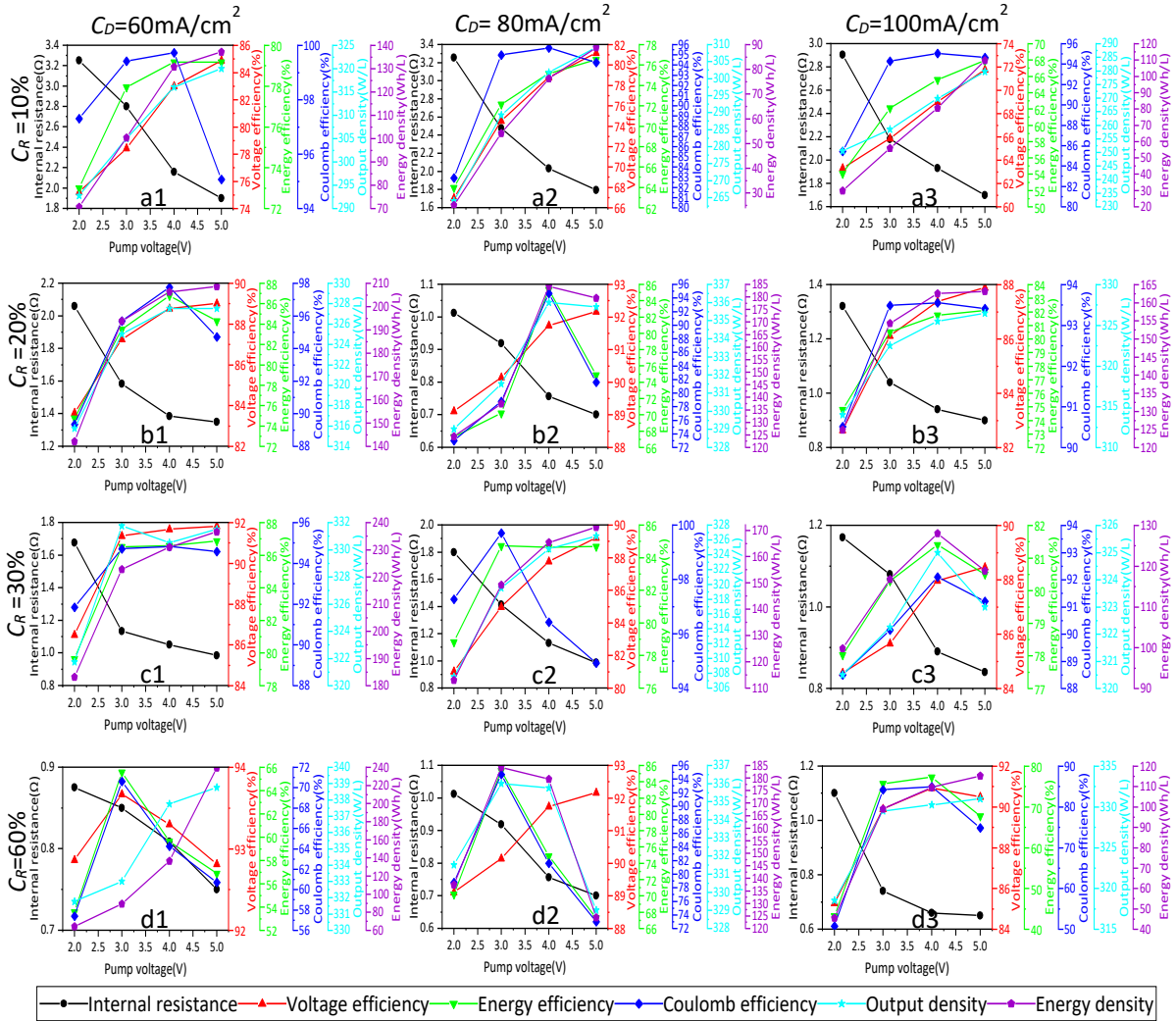


**Fig.4.8.** Comparison of battery charge and discharge performance at different flow rates at the same compression ratio

When the carbon fiber electrode is compressed, the fiber volume becomes smaller and the density becomes larger. The porosity and cross-sectional area of the electrode flow direction decrease, and the flow velocity increases under the same flow rate. The increase in speed promotes the flow of the electrolyte, enhances the convection of the electrolyte on the surface of the carbon fiber electrode, and causes the concentration overpotential ( $E_{con}$ ) to decrease. The calculation formula of the concentration overpotential is shown in formula (4-9)-(4-13).[ 20]

Where  $R$  is the general gas constant  $R$ ,  $T$  is the experimental temperature,  $F$  is the Faraday constant,  $i$  is the charge and discharge current density,  $i_{lim}$  is the limiting current density,  $C$  is

the volume concentration,  $K$  is the mass transfer coefficient[21], and  $V$  is the average velocity of the electrode solution.  $Q$  is the flow rate of the electrolyte,  $A_{felt}$  is the cross-sectional area,  $\rho$  is the electrode porosity,  $L_{avg}$  is the average length of the electrolyte flow path,  $L_{felt}$  is the length of the carbon fiber electrode, and  $\varepsilon$  is the porosity after compression[22].

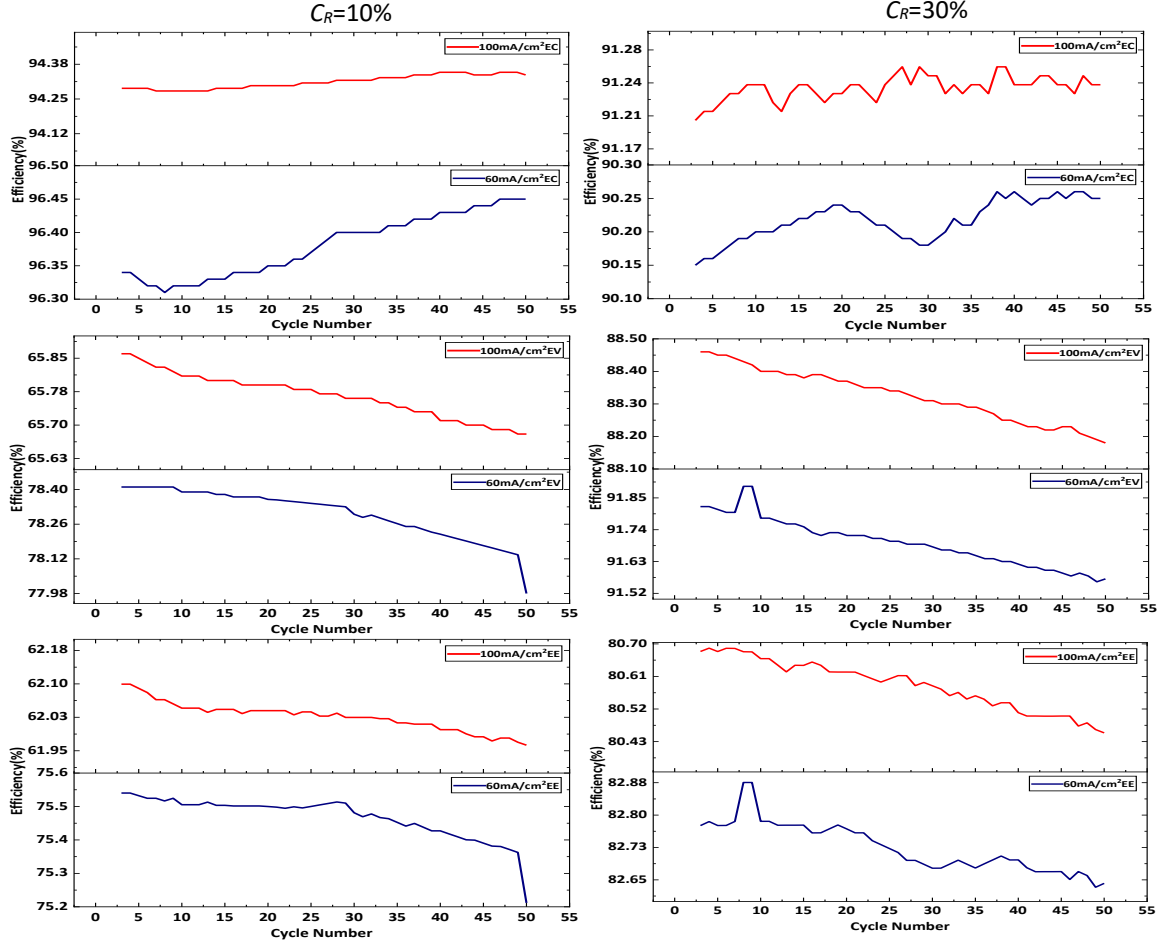


**Fig.4.9.** Current density of 60mA/cm<sup>2</sup> and 100mA/cm<sup>2</sup>, the changes of battery  $E_V$ ,  $E_C$ ,  $E_E$  under different  $C_R$  and  $P_V$  conditions.

$$E_{con} = \frac{\bar{R}T}{F} \ln\left(\frac{i_{lim}}{i_{lim} - i}\right) \quad (4-9)$$

$$i_{lim} = FKC \quad (4-10)$$

$$K = 1.6 \times 10^{-4} v^{0.4} \quad (4-11)$$

$$v = \frac{QL_{avg}}{A_{felt}\varepsilon L_{felt}} \quad (4-12)$$

$$\varepsilon = \frac{\rho_{fiber} - \rho_{felt}}{\rho_{fiber}} \quad (4-13)$$

Equation (4-11)-(4-13) calculates the concentration overpotential of the battery at different flow rates and different compression ratios. The calculation results are shown in **Table 4-5**. It can be seen from the data comparison that when the compression ratio is the same, increasing the flow rate can effectively reduce the concentration overpotential of the battery. The overpotential pair at PV=2V and PV=5V is reduced by 70%.

But when the flow rate is the same, the CR of the carbon fiber is increased. When the CR exceeds 30%, the concentration overpotential of the battery will be increases. Therefore, an excessive compression ratio is not conducive to the concentration overpotential of the battery.

**Table 4-5.** The influence of compression ratio and flow rate on battery overpotential

$C_R$ (%)	$P_V$ (V)	$\varepsilon$	$L_{avg}/L_{felt}$	$Q$ ( $m^3s^{-1}$ )	$V$ ( $ms^{-1}$ )	$K$ ( $ms^{-1}$ )	$i_{lim}$ ( $Am^{-2}$ )	$E_{con}$ (mV)	$R_{\Omega}$ ( $\Omega cm^2$ )
10	2	1.052	1.10	$1.06 \times 10^{-7}$	$6.15 \times 10^{-4}$	$8.32 \times 10^{-6}$	1292	38.23	1.91
	3	1.052	1.10	$2.58 \times 10^{-7}$	$1.50 \times 10^{-3}$	$1.19 \times 10^{-5}$	1844	20.08	1.615
	4	1.052	1.10	$4.05 \times 10^{-7}$	$2.35 \times 10^{-3}$	$1.42 \times 10^{-5}$	2208	15.49	1.465
	5	1.052	1.10	$7.81 \times 10^{-7}$	$4.54 \times 10^{-3}$	$1.85 \times 10^{-5}$	2872	11.00	1.36
20	2	0.976	1.08	$0.97 \times 10^{-7}$	$6.71 \times 10^{-4}$	$8.61 \times 10^{-6}$	1337	35.42	1.32
	3	0.976	1.08	$2.57 \times 10^{-7}$	$1.78 \times 10^{-3}$	$1.27 \times 10^{-5}$	1974	18.15	1.08
	4	0.976	1.08	$3.89 \times 10^{-7}$	$2.69 \times 10^{-3}$	$1.50 \times 10^{-5}$	2330	14.41	0.94
	5	0.976	1.08	$5.56 \times 10^{-7}$	$3.85 \times 10^{-3}$	$1.73 \times 10^{-5}$	2688	11.95	0.9
30	2	0.944	1.06	$0.88 \times 10^{-7}$	$7.06 \times 10^{-4}$	$8.78 \times 10^{-6}$	1364	33.93	1.17
	3	0.944	1.06	$2.08 \times 10^{-7}$	$1.67 \times 10^{-3}$	$1.24 \times 10^{-5}$	1924	18.84	1.04
	4	0.944	1.06	$3.23 \times 10^{-7}$	$2.59 \times 10^{-3}$	$1.48 \times 10^{-5}$	2295	14.70	0.89
	5	0.944	1.06	$5.08 \times 10^{-7}$	$4.07 \times 10^{-3}$	$1.77 \times 10^{-5}$	2751	11.61	0.84
60	2	0.794	1.02	$0.20 \times 10^{-7}$	$3.21 \times 10^{-4}$	$6.41 \times 10^{-6}$	996	-	1.1
	3	0.794	1.02	$0.48 \times 10^{-7}$	$7.70 \times 10^{-4}$	$9.10 \times 10^{-6}$	1413	31.60	0.74
	4	0.794	1.02	$1 \times 10^{-7}$	$1.60 \times 10^{-3}$	$1.22 \times 10^{-5}$	1895	19.27	0.66
	5	0.794	1.02	$1.96 \times 10^{-7}$	$3.14 \times 10^{-3}$	$1.60 \times 10^{-5}$	2481	13.26	0.65

Through the data of 50 times of charge and discharge, we also compared the influence of battery discharge capacity under different conditions (as shown in **Fig.4.10**). The experimental results show that under the same compression ratio, increasing the flow rate of the electrolyte reduces the discharge capacity. At the same flow rate, increasing the compression ratio will also reduce the discharge capacity of the battery. Since the thickness of the N211 diaphragm is

thinner and the permeability of vanadium ions is higher, increasing the flow rate promotes the transfer of vanadium ions, which lowers the discharge capacity. When the compression ratio is increased at the same time, the pressure between the electrolyte and the diaphragm increases, which further accelerates the penetration of vanadium ions.

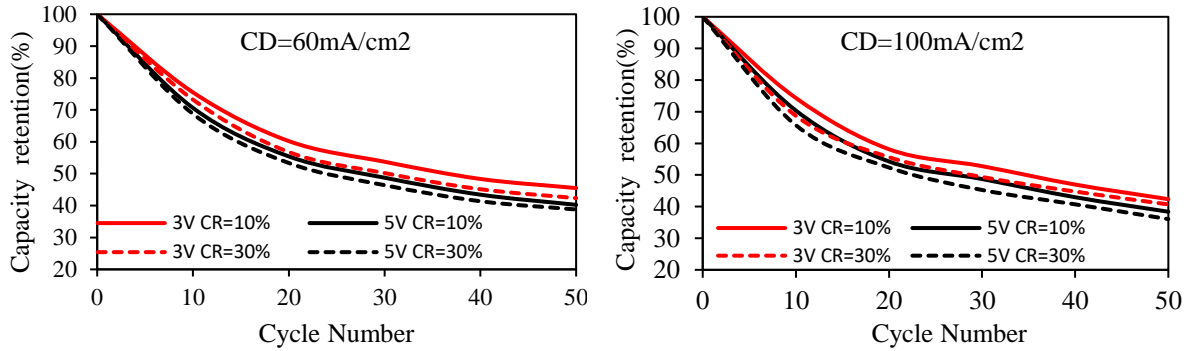


**Fig.4.10.** The effect of compression ratio and flow rate on discharge capacity retention

#### 4.2.4 Conclusion

Through the charge and discharge experiment of the battery under different compression ratio and different electrolyte flow rate, the following conclusions are obtained by comparing the experimental data.

In the case of the same compression ratio, increasing the electrolyte flow rate can reduce the internal resistance of the battery during charge and discharge. When the flow rate reaches a certain value, the charge and discharge resistance does not change. In the case of the same electrolyte flow, slightly compressing the carbon fiber electrode can also reduce the charge and discharge resistance of the battery.

In the case of the same compression ratio, increasing the electrolyte flow rate can improve the charge and discharge performance of the battery. When the flow rate reaches a certain value, the electrolyte offset will increase and the battery EC will decrease accordingly. Therefore, the thickness of the ion membrane should be selected according to the actual situation. In the case of the same electrolyte flow, slightly compressing the carbon fiber electrode can also improve the charge and discharge performance of the battery. But when CR is too large, the performance of the battery will be offset.

By comparing multiple charge and discharge data analysis, since this experiment uses N211 diaphragm, the permeability of vanadium ions is relatively high, so the compression rate and

flow rate have a great influence on the battery discharge capacity. Therefore, choosing a separator with low vanadium ion permeability can increase the discharge capacity of the battery.

In the case of the same compression ratio, increasing the flow rate of the electrolyte can effectively offset the concentration overpotential of the battery. In the case of the same electrolyte flow, the compression ratio is below 30%, which can reduce the concentration overpotential of the battery, and excessive compression will increase the concentration overpotential of the battery.

### **4.3 Evaluation of performance of all-vanadium redox flow battery pack**

#### ***4.3.1 Introduction***

In recent years, research on all-vanadium redox flow batteries has been increasing, but many researches use small single cells (electrode area of about 2\*2cm) [23-26], and the circulating pump used is a constant flow hose pump[27]. This combination can achieve high current density charging and discharging in the laboratory, but it is difficult to achieve the original performance after the battery is enlarged. The main reason is that the flow of electrolyte inside the battery after expansion is more difficult to control than that of small single cells. In addition, after the battery is expanded into a battery pack, a fixed-flow hose pump cannot be used, and only a three-phase variable frequency pump can be used. This also increases the grasp of the electrolyte flow.

#### ***4.3.2 Experimental method***

The battery pack used in this experiment is a self-made battery pack, and the electrode area of the single cell is 5\*10cm<sup>2</sup> and the thickness is 3mm. The electrolyte is 1.6mol electrolyte provided by LE Company. The test temperature is room temperature (about 25°C). The electrolyte circulating pump used in the experiment is a variable voltage screw pump. The calculation of this experiment is based on the formulas (4-2)-(4-7) described in 4.1.2.

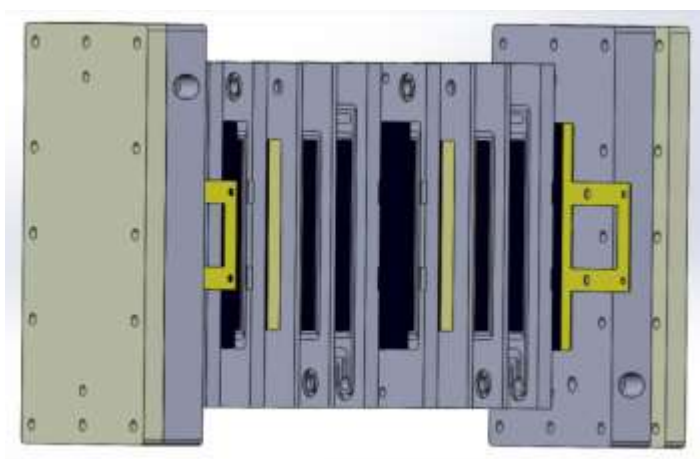


Fig. 4.11 Three battery structure

### 4.3.3 Experimental results

Based on the experimental data in Chapter 3(Fig. 4.11), we assembled a battery pack of three cells. The performance of each single cell was compared through charge and discharge experiments, and the battery pack was continuously charged and discharged to verify the stability of the battery pack under multiple operations.

Our research this time uses a single cell with an electrode area of 5\*10cm, and uses a variable frequency pump for experiments, so commercial mass production can be achieved after this single cell is expanded.

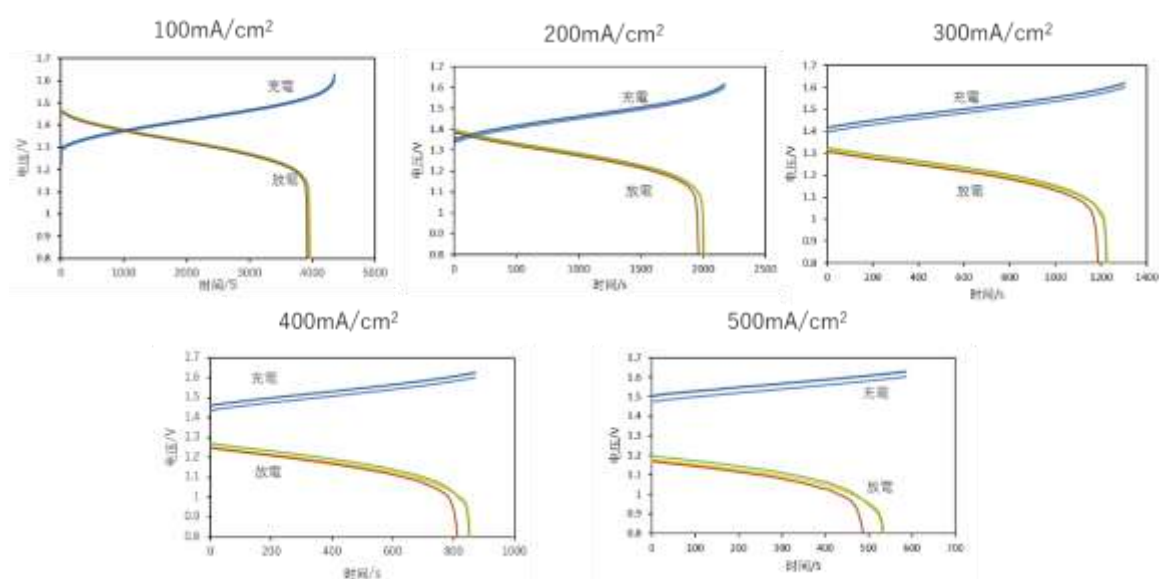


Fig. 4.12 The charge-discharge curve

The voltage difference between the individual cells of the battery pack is also an important data for evaluating the stability of the battery pack, so we fabricated three battery packs and evaluated the charge-discharge performance of each single cell. The charge-discharge curve is shown in **Fig. 4.12**. The calculated data are shown in **Table 4-6**.

**Table 4-6** The calculated data

	100mA/cm <sup>2</sup>			200mA/cm <sup>2</sup>			300mA/cm <sup>2</sup>			400mA/cm <sup>2</sup>			500mA/cm <sup>2</sup>		
	1	2	3	1	2	3	1	2	3	1	2	3	1	2	3
IR(Ω)	0.52	0.47	0.54	0.47	0.43	0.49	0.47	0.43	0.48	0.4	0.41	0.4	0.46	0.41	47
EV(%)	92	93	92	87	88	86	81	82	80	76	78.3	75	70.	73.0	69
EC(%)	91	91	91	92	92	92	94	94	94	98	98	98	91	91	91
CD(W/L)	331	332	330	319	321	318	305	308	303	292	296	290	275	280	273
ED(Wh/L)	365	366	364	178	179	177	104	105	103	69	70	69	41	42	40
EE(%)	84	85	84	80.	81	80	76	78	76	75	77	74	64	67	64

It can be seen from the charge and discharge data of the current density of 100mA/cm<sup>2</sup>-500mA/cm<sup>2</sup> that the energy density of the battery pack exceeds 80% when the current density is 200mA/cm<sup>2</sup>. And the current density reaches about 75% when the current density is 400mA/cm<sup>2</sup>. Compared with the current commercial stack, this battery pack has reached the world's advanced level.

At the same time, with the increase of current density, a voltage difference is generated among the three groups of cells, as shown in **Fig. 4.13**. When the current density is 100mA/cm<sup>2</sup>, the voltage difference is below 0.01V. The cause of the voltage difference is that both ends of the battery pack are connected to the collector plate. Part of the impedance of the collector plate is included in the single cells at both ends, so a voltage difference is generated.

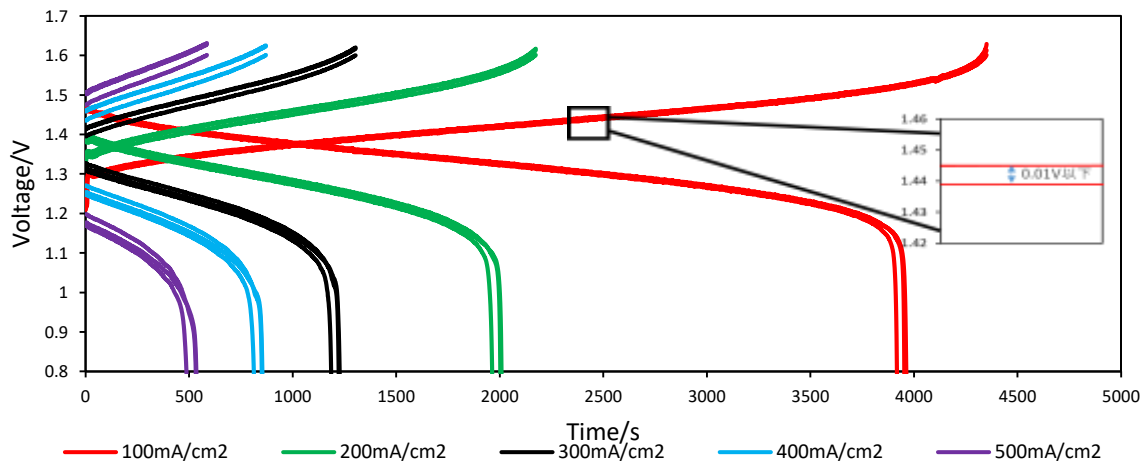


**Fig. 4.13** Charge and discharge voltage difference comparison

The operation stability of the battery pack is also one of the important methods to evaluate the battery performance. We continuously charge and discharge the battery pack at a constant current of 200 mA/cm<sup>2</sup> and 300 mA/cm<sup>2</sup>. The performance of the battery pack in operation was evaluated. The charge-discharge curve is shown in Fig. 4.14, and the charge-discharge data is shown in Table 4-7 and Table 4-8.

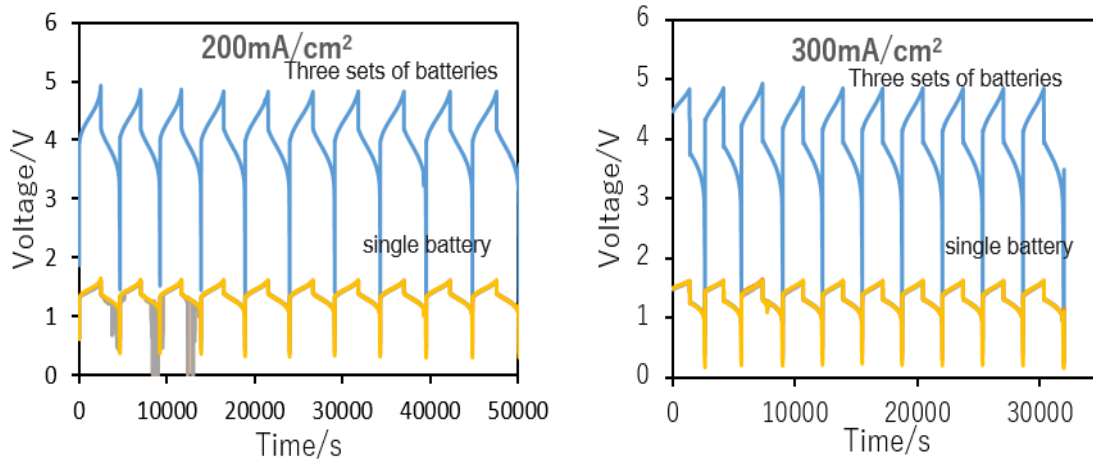


Fig. 4.14 200 mA/cm<sup>2</sup> and 300 mA/cm<sup>2</sup> continuous charge and discharge

Table 4-7 200mA/cm<sup>2</sup> continuous charge and discharge data (a: the second time, b: the tenth time)

	a	1	2	3	b	1	2	3
$I_R(\Omega/cm^2)$		0.567	0.537	0.507		0.525	0.467	0.525
$E_V(\%)$		84.48	85.18	86.22		85.77	87.23	85.77
$E_C(\%)$		92.86	92.86	92.86		95.84	95.80	95.84
$O_D(W/L)$		309	309	317.5		316.5	319.25	316.5
$E_D(Wh/L)$		186.43	186.43	191.56		222.96	224.81	222.87
$E_E(\%)$	78.45	79.10	80.06	82.21	83.57	82.21		

Table 4-8 300 mA/cm<sup>2</sup> continuous charge and discharge data (c: the second time, d: the tenth time)

	c	1	2	3	d	1	2	3
$I_R(\Omega/cm^2)$		0.561	0.521	0.573		0.501	0.441	0.498
$E_V(\%)$		78.00	79.33	77.53		79.96	82.11	80.09
$E_C(\%)$		96.46	96.46	96.46		93.83	93.83	93.83
$O_D(W/L)$		298.75	300.25	296.75		300.25	304	300.75
$E_D(Wh/L)$		117.76	118.35	116.97		130.61	132.24	130.83
$E_E(\%)$	75.25	76.52	74.79	75.03	77.04	75.15		

Since the battery needs to start the electrolyte when starting the first charge, the calculation starts from the second charge and discharge. Through the continuous charging and discharging

data, it can be seen that the charging and discharging performance of the battery pack is improved. The reason for the analysis is that when the battery is continuously charged and discharged, the temperature of the battery pack system increases, and the viscosity of the electrolyte decreases, so the charging and discharging performance is improved.

#### **4.3.4 Conclusion**

By combining the above studies, a 3-cell stack was assembled, and the following conclusions were obtained by charging and discharging experiments of the cell stack.

1. With a current density of  $200\text{mA} / \text{cm}^2$ , the energy efficiency of the 3-cell stack is maintained above 80%. At the same time, the internal resistance of charge and discharge is less than  $0.5\Omega$ , reaching the world's top class level.

2.3 Comparing the charge and discharge of the 3-cell stack, the voltage difference between the cells on both sides and the cell in the middle is about  $0.01\text{V}$ . The cause was that the cells on both sides had gold-plated copper plates, so there was resistance from the copper plates, and the internal voltage of the cells on both sides rose.

3. The charge / discharge performance of continuous charge / discharge was higher than that of the 10th and 2nd data. The reason is that the temperature of the electrolytic solution rises during continuous charging / discharging, the viscosity decreases, and the reactivity of the electrolytic solution improves. Therefore, it is necessary to maintain a constant temperature during operation.

#### **4.4 Concluding remarks**

Through the above research, The optimal design of the inlet and outlet flow paths of the stack, through simulation and charge-discharge experiments, verified the fluidity of the electrolyte inside the stack, and tested the charge-discharge performance of different flow paths. The optimal design of the electrolyte flow rate and the compression ratio of the carbon fiber electrode, by testing the performance of the battery under different thicknesses and different flow rates, the optimal compression ratio and optimal flow rate of the 3mm thick carbon felt were obtained.

## 4.5 Nomenclature

A	area (m <sup>2</sup> )
C	concentration (molm <sup>-3</sup> )
D	density(*L)
d	discharge
E	efficiency (%)/energy
F	Faraday constant (96485 Cmol <sup>-1</sup> )
i	current density (Am <sup>-2</sup> )
K	mass transfer coefficient (ms <sup>-1</sup> )
L	length (m)
O	output density (W/L)
Q	flow rate (m <sup>3</sup> s <sup>-1</sup> )
$\bar{R}$	universal gas constant (8.314 kJ kg <sup>-1</sup> K <sup>-1</sup> )
R	area specific resistance ( $\Omega$ cm <sup>2</sup> )
t	thickness (m)
T	temperature (K)/Time(s)
U	charge and discharge voltage(V)
v	velocity (ms <sup>-1</sup> )
V	cell voltage (V)
V	volume(L)

### Greek Symbols

$\varepsilon$	porosity
$\rho$	density (gcm <sup>-3</sup> )
$\Omega$	ohm

### Superscripts and Subscripts

avg	average charge charge process
con	concentration
discharge	discharge process
felt	felt
fiber	fiber
lim	limiting

## 4.6 References

1. Alotto P, Guarnieri M, Moro F. Redox flow batteries for the storage of renewable energy: A review[J]. Renewable and sustainable energy reviews, 2014, 29: 325-335.
2. Ye R, Henkensmeier D, Yoon S J, et al. Redox flow batteries for energy storage: a technology review[J]. Journal of Electrochemical Energy Conversion and Storage, 2018, 15(1).

3. Winsberg J, Hagemann T, Janoschka T, et al. Redox-flow batteries: from metals to organic redox-active materials[J]. *Angewandte Chemie International Edition*, 2017, 56(3): 686-711.
4. Dunn B, Kamath H, Tarascon J M. Electrical energy storage for the grid: a battery of choices[J]. *Science*, 2011, 334(6058): 928-935.
5. Ghimire P C. Electrode modification and in-situ studies to enhance the performance of vanadium redox flow batteries[J].
6. Roy A, Patra S. Development of An All Vanadium Redox Flow Battery For Efficient Utilization of Renewable Energy[J]. 2018.
7. Fan L, Ru Y, Xue H, et al. Vanadium-Based Materials as Positive Electrode for Aqueous Zinc-Ion Batteries[J]. *Advanced Sustainable Systems*, 2020, 4(12): 2000178.
8. Daugherty M C. Enhanced kinetics and modeling of PAN-based carbon felt anodes in vanadium redox flow batteries[J]. 2020.
9. Zhang K, Yan C, Tang A. Unveiling electrode compression impact on vanadium flow battery from polarization perspective via a symmetric cell configuration[J]. *Journal of Power Sources*, 2020, 479: 228816.
10. Houser J, Clement J, Pezeshki A, et al. Influence of architecture and material properties on vanadium redox flow battery performance[J]. *Journal of Power Sources*, 2016, 302: 369-377.
11. Kumar S, Jayanti S. Effect of flow field on the performance of an all-vanadium redox flow battery[J]. *Journal of Power Sources*, 2016, 307: 782-787.
12. Wang Q, Qu Z G, Jiang Z Y, et al. The numerical study of vanadium redox flow battery performance with different electrode morphologies and electrolyte inflow patterns[J]. *Journal of Energy Storage*, 2021, 33: 101941.
13. Y.K.Zeng,T.S.Zhao,L.An,X.L.Zhou,L.Wei. [A comparative study of all-vanadium and iron-chromium redox flow batteries for large-scale energy storage]. *Journal of Power Sources* Volume 300, 30 December 2015, Pages 438-443

14. Sankaralingam R K, Seshadri S, Sunarso J, et al. Overview of the factors affecting the performance of vanadium redox flow batteries[J]. *Journal of Energy Storage*, 2021, 41: 102857.
15. Ke X, Prahl J M, Alexander J I D, et al. Redox flow batteries with serpentine flow fields: Distributions of electrolyte flow reactant penetration into the porous carbon electrodes and effects on performance[J]. *Journal of Power Sources*, 2018, 384: 295-302.
16. Zeng Y K, Zhao T S, An L, et al. A comparative study of all-vanadium and iron-chromium redox flow batteries for large-scale energy storage[J]. *Journal of Power Sources*, 2015, 300: 438-443.
17. Huang Z, Mu A, Wu L, et al. Vanadium redox flow batteries: Flow field design and flow rate optimization[J]. *Journal of Energy Storage*, 2021: 103526.
18. Christian Blanc .Alfred Rufer. [Understanding the Vanadium Redox Flow Batteries]. *Paths to Sustainable Energy*. December 30th 2010.Pages.333-358
19. Hu G, Jing M, Wang D W, et al. A gradient bi-functional graphene-based modified electrode for vanadium redox flow batteries[J]. *Energy Storage Materials*, 2018, 13: 66-71.
20. Xiangkun Ma, Huamin Zhang, Feng Xing. [A three-dimensional model for negative half cell of the vanadium redox flow battery].*Electrochimica Acta*.Volume 58, 30 December 2011, Pages 238-24630
21. YifengLi,XinanZhang,JieBao,MariaSkiyllas-Kazacos [Control of electrolyte flow rate for the vanadium redox flow battery by gain scheduling]. *Journal of Energy Storage*.Volume 14, Part 1, December 2017, Pages 125-133
22. Dongjiang,Youa,b,Huamin Zhanga, Jian Chena.[A simple model for the vanadium redox battery].*Electrochimica Acta* 54 (2009) 6827–6836.
23. Chakrabarti M H, Brandon N P, Hajimolana S A, et al. Application of carbon materials in redox flow batteries[J]. *Journal of Power Sources*, 2014, 253: 150-166.
24. Xu J, Zhang Y, Huang Z, et al. Surface Modification of Carbon-Based Electrodes for Vanadium Redox Flow Batteries[J]. *Energy & Fuels*, 2021, 35(10): 8617-8633.

25. Ke X, Alexander J I D, Prah J M, et al. Flow distribution and maximum current density studies in redox flow batteries with a single passage of the serpentine flow channel[J]. *Journal of Power Sources*, 2014, 270: 646-657.
26. Leung P, Li X, De León C P, et al. Progress in redox flow batteries, remaining challenges and their applications in energy storage[J]. *Rsc Advances*, 2012, 2(27): 10125-10156.
27. Pour N, Kwabi D G, Carney T, et al. Influence of edge-and basal-plane sites on the vanadium redox kinetics for flow batteries[J]. *The Journal of Physical Chemistry C*, 2015, 119(10): 5311-5318.
28. Xiao W, Tan L. Control strategy optimization of electrolyte flow rate for all vanadium redox flow battery with consideration of pump[J]. *Renewable Energy*, 2019, 133: 1445-1454.

## Chapter 5 Conclusions

In this study, the constituent materials, battery structure and external factors of the all-vanadium redox flow battery were analyzed. Design and assemble single cells for experimental analysis, and assemble three battery packs for verification tests. The designed vanadium redox flow battery has reached the current world-leading level.

1. Through the heat treatment test and CNT coating test on carbon fiber electrodes, the following conclusions are obtained:

(1). The change in the carbon fiber electrode after the heat treatment was confirmed by the heat treatment experiment and Raman analysis, and the charge / discharge performance of the carbon fiber electrode after the heat treatment was also confirmed in the charge / discharge experiment. Experiments have shown that heat treatment temperature performance between 1500 ° C and 2400 ° C is more suitable for vanadium-based redox flow batteries.

(2). Electrodes with good charge / discharge performance were obtained by CNT coating experiments. The maximum current density for charging and discharging was 400mA / cm<sup>2</sup>. At the same time, energy efficiency has increased to 15%. After coating, the internal resistance of charge and discharge of the electrode was also reduced by 1/3. Charge transfer resistance is reduced to 1/4 of the original.

2. Through the optimal design of the inlet and outlet flow paths of the battery, the following conclusions are obtained:

(1). Judging from the simulation results, whirlpools did not occur due to the flow of the electrolytic solution in the comb tooth flow path, so the flow uniformity of the electrolytic solution is the best. From the viewpoint of charge / discharge performance, the performance of the comb tooth flow path is good when the flow rate of the electrolytic solution is small. When the flow rate is high, the performance is the same as that of the parallel flow path 2.

(2). It is better that the width of the entrance and exit of the two types of parallel flow path frames is adjusted, and as a result, the width of the exit is larger than the entrance. This is because the larger the width of the outlet, the faster the outflow of the reacted vanadium ions. As a result, the charge / discharge performance of the battery is improved.

3. Through the optimal design of electrolyte flow and carbon fiber electrode compression ratio, the following conclusions are obtained:

(1). When the compression ratio is the same, increasing the electrolyte flow rate can improve the charge / discharge performance of the cell. When the flow rate exceeds 2 ml / min / cm<sup>2</sup>, the improvement in performance diminishes. At the same time, when there is a compression ratio, the uniform fluidity of the electrolytic solution is also maintained stably.

(2). When the flow rate of the electrolytic solution is the same, increasing the compression ratio reduces the internal resistance during charging and discharging of the cell. If the compression ratio exceeds 60% for a 3 mm carbon fiber electrode, the charge / discharge performance of the cell will deteriorate.

4. Through the continuous charge and discharge experiments of the three assembled batteries, the constant current charge and discharge experiments were carried out, and the following conclusions were obtained:

(1). With a current density of 200mA/cm<sup>2</sup>, the energy efficiency of the 3-cell stack is maintained above 80%. At the same time, the internal resistance of charge and discharge is less than 0.5Ω, reaching the world's top class level.

(2).3 Comparing the charge and discharge of the 3-cell stack, the voltage difference between the cells on both sides and the cell in the middle is about 0.01V. The cause was that the cells on both sides had gold-plated copper plates, so there was resistance from the copper plates, and the internal voltage of the cells on both sides rose.

(3). The charge / discharge performance of continuous charge / discharge was higher than that of the 10th and 2nd data. The reason is that the temperature of the electrolytic solution rises during continuous charging / discharging, the viscosity decreases, and the reactivity of the electrolytic solution improves. Therefore, it is necessary to maintain a constant temperature during operation.

## Related publications

### Journal Article:

1. **Zhongxu Tai**, Kenzo Hanawa, Dongying Ju , Wenping Luo, Rui Lyu, Kousuke Ishikawa, and Susumu Sato Effects of Carbon Fiber Compression Ratio and Electrolyte Flow Rate on the Electrochemical Performance of Vanadium Redox Batteries. *Journal of Chemistry* Volume 2021, Article ID 6646256, 10 pages 2021.03.11. (Accepted, in press)
2. **Zhongxu Tai**, Dongying Ju , Susumu Sato and Kenzo Hanawa. Discrete Coating of CNT on Carbon Fiber Surfaces and the Effect on Improving the Electrochemical Performance of VRFB Systems. *Coatings*. 2021, 11(6),736. 2021.06.18. (Accepted, in press)

### International Conferences:

1. **Zhongxu Tai**, Dongying Ju. Improvement of charge-discharge performance of vanadium redox flow battery by thermal coating of CNT on the surface of positive electrode carbon material. *The 4th International Conference on New Energy and Future Energy Systems (NEFES 2019)*. July 21-24, 2019 Macau, China
2. **Zhongxu Tai**, Dongying Ju. Improvement of charge-discharge performance of vanadium redox flow battery by thermal coating of CNT on the surface of positive electrode carbon material. *The Applied Energy Symposium and Forum 2020: Low carbon cities and urban energy systems (CUE2020)* on October 10-17, 2020, Tokyo

## Acknowledgements

I would like to express my sincere gratitude to my supervisors, Prof. Dong-Ying Ju and Prof. Susumu Sato, for accepting me as a student and giving me the opportunity to do research at Saitama Institute of Technology. I would like to sincerely thank them for their support, encouragement and guidance during my study. This thesis would not have been possible without their tireless efforts to revise and embellish my drafts. They spent most of their time reading my manuscript and suggesting further revisions. In addition, Professor Dong-Ying Ju has given me a lot of support and generous help in securing research funding, seeking corporate assistance, and in my life, for which I would like to express my sincere gratitude in particular.

During the research process, Prof. Kenzo Hanawa gave me a lot of support and valuable advice. Without guidance of Prof. Hanawa, I might not have been able to carry out this research so smoothly. Therefore, I would like to express my special thanks to Prof. Hanawa. In the meantime, I sincerely thank Prof. Osamu Niwa and Associate Prof. Hiroaki Matsuura for their recognition of my research work during my doctoral studies and for their valuable comments during my defense.

I would also like to express my sincere gratitude to the (late) Professor Osamu Hamamoto, who gave me my initial guidance in learning the basics of electrochemistry and all-vanadium liquid flow battery systems. His guidance enlightened my interest in this research and laid a solid foundation for my work. I wish to dedicate my PhD thesis to Prof. Osamu Hamamoto and to inform him that it was an honor to be supervised by you.

Finally, I would like to thank all the members of Ju Lab for their help and cooperation over the years. I am deeply grateful to my family for their love, support and encouragement during my studies and graduate work

February, 2022

Zhongxu Tai

